University of California
Santa Barbara

Periodic approximations and spectral analysis of the Koopman operator: theory and applications

A dissertation submitted in partial satisfaction
of the requirements for the degree

Doctor of Philosophy
in
Mechanical Engineering

by

Nithin Govindarajan

Committee in charge:

Professor Igor Mezić, Co-Chair
Professor Shivkumar Chandrasekaran, Co-Chair
Professor Bassam Bamieh
Professor Jeffrey Moehlis

December 2018

The Dissertation of Nithin Govindarajan is approved.

Professor Bassam Bamieh

Professor Jeffrey Moehlis

Professor Shivkumar Chandrasekaran, Committee Co-Chair

Professor Igor Mezić, Committee Co-Chair

September 2018

Periodic approximations and spectral analysis of the Koopman operator: theory and applications

by

Nithin Govindarajan

This dissertation is dedicated to my grandfather who sadly passed away during my graduate studies in Santa Barbara.

Acknowledgements

Looking back at these past fours years, it startles me how much I have learned and grown. The opportunity of pursuing graduate studies at UCSB was truly a blessing, both from an academic perspective and personal perspective. I was given the freedom to pursue my own research interests and also given the time to develop my skills in mathematical analysis. I was very fortunate to have great advisors who were very kind and patient with guiding me through my PhD. I really feel lucky to learn from true experts in their respective fields: one in dynamical systems theory, and one in numerical analysis. Igor and Shiv, thank you for everything.

The atmosphere at UCSB was truly amazing. Pretty much every faculty member here is of the highest caliber, but at the same time also very laid back and approachable. I would like to thank my committee members Bassam and Jeff, with whom I also have taken great courses. I also would like to thank my colleagues and fellow students here at UCSB. I became so close with them, that I found it hard to actually concentrate at work due to the constant tendency to socialize with them. Thank you Cory, Abhe, Kristen, Hassan, Ryan, Chris, Allan, Timothy, Bharat, Ljuboslav, Poorva, Gowtam, Emir, and Milan.

Apart from academics, living in Santa Barbara was truly amazing and I am definitely going to miss it: right next to ocean, hills in the backdrop, and amazing sunsets. During my stay I have attempted to do some surfing, but mostly I have learned how to dance to Latin music. Thank you Amber, Genesis, and Jason for being great friends. Also thank you Erika, Marco and ME sabor dance familia for making me a better dancer. Finally, thank you Chris for being an amazing friend, I will never forget the day we went skydiving!

Curriculum Vitæ

Nithin Govindarajan

Education

2018	Ph.D. in Mechanical Engineering, University of California, Santa Barbara, USA
2012	MSc in Aerospace Engineering, Delft University of Technology, Delft, The Netherlands
2009	BSc in Aerospace Engineering, Delft University of Technology, Delft, The Netherlands

Publications

S. Chandrasekaran, N. Govindarajan, A. Rajagopal, "*Fast Algorithms for Displacement and Low-Rank Structured Matrices*", ISSAC 18 in New York.

N. Govindarajan, R. Mohr, S. Chandrasekaran, and I. Mezić, "*On the approximation of koopman spectra for measure preserving flows*", arXiv preprint arXiv:1806.10296 (2018).

N. Govindarajan, R. Mohr, S. Chandrasekaran, and I. Mezić, "*On the approximation of koopman spectra for measure preserving transformations*", arXiv preprint arXiv:1803.03920 (2018). (*Submitted SIAM journal on Applied Dynamical Systems*)

N. Govindarajan, H. Arbabi, L. van Blargian, T. Matchen, E. Tegling, I. Mezić, "*An operator-theoretic viewpoint to non-smooth dynamical systems: Koopman analysis of a hybrid pendulum*", 2016 IEEE 55th Conference on Decision and Control (CDC) in Las Vegas.

Abstract

Periodic approximations and spectral analysis of the Koopman operator: theory and applications

by

Nithin Govindarajan

Modeling complex dynamical systems, with an eye towards accurate reconstruction of individual trajectories, is an inherently difficult proposition. This difficulty, which arises from exponential sensitivity to initial conditions, also makes it nearly impossible to simulate long-term trajectories. Fortunately, in many applications, it is sufficient if a reduced-order model is able to just capture the global invariant and quasiperiodic structures which fall within the resolution of observation.

Koopman operator theory is a mathematical formalism which allows one to extract these global structures. Many geometric notions in the state-space, as well as statistical properties on the attractor, are characterizable in terms of the spectral decomposition of this linear operator. The linearization of a system through the Koopman operator is achieved by lifting the dynamics to the space of observables, making the technique applicable to any system for which the flow map is well defined.

The generality of the Koopman formalism is specifically demonstrated here on a nonsmooth system in which a pendulum is subjected to downward kicks at fixed angles. In the absence of damping, it is shown that the fixed space of the operator yields a characterization of the ergodic partition, whereas the set of limit cycles on the attractor gives rise to a continuous spectrum. Under marginal damping, the continuous spectrum is shown to disintegrate and the appearance of dissipative eigenvalues associated with the transient dynamics of the stable fixed point can be related to a linear system by means

of a semi-conjugacy.

Critical to the wide-scale application of Koopman operator theory are numerical methods which are able to approximate the spectral decomposition of observables. Given that any computational method must reduce the infinite-dimensional Koopman operator to something finite, this dissertation specifically examines how the Koopman operators of finite-state dynamical systems are related to their infinite dimensional counterparts.

A convergence result is proven here in which the class of continuous, measure-preserving automorphisms on compact metric spaces is shown to be approximable by periodic systems on a finite state-space. The Koopman operators of these so-called "periodic approximations" are shown to converge spectrally to that of the original operators in a weak sense. Herein, it is demonstrated that even though the individual rank-one spectral projectors are spurious, smooth weighted sums of these projectors applied to a fixed observable are meaningful and converge to the quantities one would expect for their infinite-dimensional counterparts.

The results are generalizable to handle measure-preserving flows through an intermediate time-discretization. For convergence of the spectra to occur, a sufficient condition is derived requiring the spatial refinements in the periodic approximation to happen at a faster pace than the temporal refinements. Peculiarly, this requirement is somewhat opposite to what the CLF condition dictates for stability of finite difference schemes. Albeit, the periodic approximation may be interpreted as a specific semi-Lagrangian scheme where additional "global" efforts are made to prevent two grid points from collapsing into one.

Given the aforementioned approximation results, numerically convergent methods for computing spectra of observables are formulated. The crucial part of the numerical method is the construction of the periodic map, which in the general case can be done by solving a bipartite matching problem. It is shown that for Lipschitz continuous maps,

this process can be executed in roughly $O(n^{3m/2})$ complexity, where m is the dimension of the state-space and n the size of the partition in each dimension. Since the remainder of the numerical method exploits the structure of permutation matrices and only requires computing Discrete Fourier transforms, the entire scheme is numerically stable and "fast", hence yielding a viable method to compute the spectral decomposition of Koopman operators for the measure-preserving case.

Contents

Chapter 1

Introduction

The classical perspective towards the analysis and modeling of dynamical systems relies on the so-called "state-space" representation. This geometric viewpoint of Poincaré certainly had been very fruitful for the scientific community, and its applications are unquestionable, particularly in the area of control theory. In recent times, an alternative viewpoint to dynamical systems has been receiving a lot of attention. This viewpoint, which is based on the "dynamics of observables" picture, considers the evolutions of functions (i.e. observables) defined on the state-space through the framework of the Koopman operator [1]. A remarkable feature to this approach is that the dynamics are always linear in the space of observables, irrespective of the underlying properties of the dynamical system in the state-space.

Within the state-space formulation, there has always been a "disparity of comprehensibility" when it comes to the analysis of linear systems versus nonlinear ones, with the latter being significantly more complex. Given the tools of spectral operator theory, the Koopman operator allows one to treat nonlinear systems in a linear setting. This fact even holds true for non-smooth systems which are characterized by discontinuous orbits. The associated benefits of Koopman operator theory do however come at the price of

dealing with an infinite-dimensional system. Finite-dimensional approximations of an operator and numerical approximation of its spectra are a delicate issue. Apart from exploring the applicability of Koopman operator theory to nonsmooth/hybrid systems, the main goal of this dissertation is to analyze these issues in greater depth.

1.1 The Koopman operator

Mathematically, the Koopman formalism can be expressed as follows. Let $X \subset \mathbb{R}^N$ denote the state-space and $S^t : X \mapsto X$ a flow map satisfying the (semi-)group properties: $S^t \circ S^s(x) = S^{t+s}(x)$, $S^0(x) = x$. Now consider an observable $g : X \mapsto \mathbb{C}$, for some fixed $t \in \mathbb{R}$, the Koopman operator is defined as the operation:

$$\left(\mathcal{U}^t g\right)(x) := g \circ S^t(\boldsymbol{x}).$$

The Koopman formalism replaces the original system expressed by the tuple (X, S^t, t) with the alternative representation expressed by $(\mathcal{G},\mathcal{U}^t, t)$, where $\mathcal{G}$ denotes the space of observables. It is easily verifiable that $\mathcal{U}^t$ is a *linear operator* on $\mathcal{G}$. This linear description of a nonlinear, and possibly, non-smooth system is obtained through "lifting" of the dynamics on the state-space to a higher, infinite-dimensional space of functions.

The linearity of $\mathcal{U}^t$ allows one to exploit the machinery of spectral operator theory. In particular, eigenfunctions may be defined for the operator. A nonzero function $\phi_\lambda \in \mathcal{G}$ is called a Koopman eigenfunction if it satisfies:

$$\left(\mathcal{U}^t \phi_\lambda\right)(x) = e^{\lambda t}\phi_\lambda(x) \tag{1.1}$$

for some eigenvalue $\lambda \in \mathbb{C}$. Given the infinite-dimensional nature of the operator, $\mathcal{U}^t$ may also contain continuous spectrum. In that case, one can extend the notion of eigenfunc-

tions in an appropriate weak sense using the concept of distributions. These generalized objects, referred to as eigendistributions, satisfy the relation:

$$\int_X \left(\mathcal{U}^t \phi_\lambda\right)(x) w(\boldsymbol{x}) d\mu = e^{\lambda t} \int_X \phi_\lambda(x) w(x) d\mu \tag{1.2}$$

where $w(x)$ is some arbitrary test function on X. Indeed, it follows that all eigenfunctions are eigendistributions, but the converse does not hold true.

From a dynamical systems point of view, the interesting aspect of these eigenfunctions/-distributions is that they are preserved under conjugacy. If $S^t : X \mapsto X$, $R^t : Y \mapsto Y$ are two topologically conjugate dynamical systems under the homeomorphism $h : X \mapsto Y$, i.e. $h \circ S^t(x) = R^t \circ h(x)$, and if ϕ_λ is an eigenfunction/eigendistribution of $\mathcal{U}_R^t$, then so should $\phi_\lambda \circ h$ be an eigenfunction/-distribution of $\mathcal{U}_S^t$. Also, the level sets of Koopman eigenfunctions are directly related to many geometric state-space notions of a dynamical system. That is, let:

$$\Psi_{\phi_\lambda}^c := \{x \in X : \phi_\lambda(x) = c\}$$

denote a specific level-set of an eigenfunction. Then the mapping of the set $\Psi_{\phi_\lambda}^c$ forward under the flow yields the relation:

$$S^t\left(\Psi_{\phi_\lambda}^c\right) = \Psi_{\phi_\lambda}^{c \exp(\lambda t)}. \tag{1.3}$$

The interpretation of (1.3) is that the level-sets of ϕ_λ characterize how specific ensembles of initial conditions are propogated under the flow.

1.2 Koopman analysis of hybrid systems

Analysis of nonlinear flow fields through the spectral properties of the Koopman operator has already been carried out under various settings [1]. These approaches have been particularly useful in describing dynamically relevant modes in fluid flows [2, 3], coherency in power systems [4], and energy efficiency in buildings [5]. The wide-scale applicability of Koopman analysis is primarily because the linearization holds true for any system for which the flow map is well defined. The framework is even applicable piecewise-smooth dynamical systems where the orbits are characterized by smooth evolutions, interrupted by discrete jumps.

This dissertation, explores some applications of Koopman operator theory to hybrid systems. This is done by studying a model problem of a pendulum which receives a downward kick at certain fixed angles. It is shown that eigenfunctions for this system can still be computed using the technique of taking weighted time averages of observable traces [6]:

$$\lim_{t\to\infty} \frac{1}{t} \int_0^t e^{-\lambda\tau} \left(\mathcal{U}^\tau g\right)(\boldsymbol{x}) d\tau \tag{1.4}$$

Many of the connections of Koopman eigenfunctions to geometric quantities (e.g. invariant partitions, isotables, isochrons) that have played a key role in the success of Koopman operator theory for nonlinear systems, seem to naturally extend for this specific example of a hybrid system.

In particular, one can use the eigenfunctions to establish a (semi-)conjugacy with a linear system. As a consequence of the classical Hartman-Grobman theorem, a nonlinear system is conjugate to a linear system around a small neigborhood of a stable fixed point. In [7] it was shown that this conjugacy can be extended to the entire basin of attraction. A remarkable[1] aspect to this fact is that the result also applies to a system

[1] But perhaps unsurprising for those who are familiar with the proof technique of [7].

with discontinuous orbits!

1.3 Numerical methods for Koopman analysis

An important avenue of research is the development of reliable numerical methods to compute the spectral decomposition of the Koopman operator. A lot of work has already been dedicated on this subject. The existing numerical methods can roughly be classified into four categories:

1. Computing time-averages
2. The Krylov subspace approach (e.g. DMD)
3. Galerkin-type methods (e.g. Extended DMD, Ulam approximation)
4. Reconstruction of spectra from moment data

The first approach which involves computing time-averages are straightforward numerical implementations of classical ergodic theorems such as Birkhoff's and Wiener&Wintner's results on measure-preserving systems (see e.g. [8, 9, 10, 11]). Although the classical ergodic theorems apply to only eigenvalues on the unit circle, in [6] it was shown that dissipative eigenfunctions may also be constructed from the generalization of harmonic averages in (1.4).

The second approach which relies on a truncated Krylov sequence to compute eigenvalues goes largely under the name of Dynamic Mode Decomposition (DMD) [3, 12]. Although DMD was originally formulated to extract spatial flow structures that evolve linearly with time, the connections between DMD and Koopman modes were first established in [3]. In [13], it was further shown that the eigenvalues and modes of DMD converge to those of the Koopman operator for the given Krylov subspace.

The third approach is based on classical Galerkin-type approximations of infinite-dimensional operators using a truncated basis. A method which falls within this class is Extended-DMD [14], where the goal is to obtain a finite-dimensional approximation of the Koopman operator from a "dictionary of observables". In [15], it was shown that accumulation points of the spectra converge weakly to eigenvalues and eigenfunctions of the Koopman operator for the Extended-DMD algorithm. Another method of the Galerkin-type is the Ulam approximation which is used for the Perron-Frobenius operator [16, 17], the adjoint of the Koopman operator. This specific kind of approximation has a Markov chain interpretation where indicator functions are used as the dictionary of observables.

The fourth approach one could take is to compute spectra from moment data. This route was advocated in [18] for measure-preserving systems where the Christoffel-Darboux kernel was used to reconstruct the spectral measure. A feature of this approach is that it is capable of distinguishing the atomic and continuous parts of the spectrum.

1.3.1 Periodic approximations

This dissertation introduces a new method for computing the spectral decomposition of the Koopman operator. The philosophy behind the proposed method differs slightly from the Krylov or Galerkin-based approaches, in the sense that, the operator is not approximated directly in the space of observables. Instead, a discrete approximation of the dynamical system itself is seeked, yielding a discretization of the operator indirectly. The method closely recognizes that any computer/numerical implementation of a dynamical system will involve some kind of a reduction to a finite-state model, i.e. a map $T : X \mapsto X$ defined on a state-space $X = \{1, 2, \ldots, N\}$ with finite cardinality.

The main question adressed here is how such finite-state models relate spectrally with

the underlying dynamical system from which they were obtained. The focus in this dissertation is to particularly investigate this matter for the class of measure-preserving dynamical systems on compact domains. For this class of systems, the Koopman operator is unitary in an appropriate Hilbert space. The discrete equivalent of a measure-preserving system on a finite state-space is a bijective map. The trajectories of such a map are periodic and the associated Koopman operator is a permutation. It will be shown that measure preserving systems can be approximated arbitrarily well by periodic discrete maps, and they in turn, may be used to efficiently compute spectra. These so-called periodic approximations are closely related to the Ulam approximation, but instead of assigning transition probabilities, one explicitly enforces a bijection on the state-space partition so that the unitary structure of the operator is preserved.

1.3.2 Inherent challenges of computing spectra

The computation of spectral properties of an infinite-dimensional operators is accompanied with inherent challenges. A classical challenge in this domain is the issue of spurious eigenvalues that may arise in the finite-dimensional truncation. This issue was first discovered in model problems of Hydrodynamic stability [19] where one is faced with eigenvalue problem such as:

$$\Psi_{zzzz} = \lambda \Psi_{zz}, \qquad -1 < z < 1$$

$$\Psi(\pm 1) = \Psi_z(\pm 1) = 0$$

The Chebyshev-tau method converts this infinite-dimensional problem to a generalized eigenvalue problem of the form $Ax = \lambda Bx$. Apart from the close approximations of the true eigenvalues, it was observed that the discretization also generated large positive

eigenvalues. These spurious eigenvalues had nothing to do with those of the original infinite-dimensional system (the true eigenvalues $\lambda = -n^2\pi^2$ were all negative). This specific example shows that one always has to be cautious in the discretization of infinite-dimensional operators.

Another challenge, more specifically related to Koopman operators, is the sensitivity of certain spectral properties of a dynamical systems. For example, the map:

$$T(x) = (x + \omega) \mod 1$$

has isolated eigenvalues if $\omega \in \mathbb{Q}$ and a dense set of eigenvalues if $\omega \notin \mathbb{Q}$. Another example illustrating the sensitivity of the spectra is:

$$T_\epsilon(x) = (x_1, x_2 + \omega + \epsilon \sin(2\pi x_1)).$$

This map has a fully discrete spectrum at $\epsilon = 0$ (and also isolated if $\omega \in \mathbb{Q}$), but an absolutely continuous spectrum when $\epsilon \neq 0$ (see e.g. [20]). From a backward stability analysis point of view, examples of this kind illustrate that the numerical approximation of certain spectral quantities may be ill-posed if not formulated correctly.

1.4 The main contribution of this dissertation

The notion of a periodic approximation of a measure-preserving dynamical system is not new [21, 22, 23, 24, 25, 26, 27]. It is well-known amongst specialists that the set of measure-preserving automorphisms, which forms a group under composition, are densely filled by periodic transformations under various topologies (see e.g. [21]). These earlier periodic approximation results were useful in proving certain claims such as whether an automorphism is "generically" ergodic or mixing. Katok and Stepin [25] also showed

that the rate at which an automorphism admits a periodic approximation can be directly related to properties of ergodicity, mixing, and entropy. Certain spectral results were also proven in [25]. For example, it was shown that if T admits a cyclic approximation by periodic transformations at a certain rate, then the spectrum of the Koopman operator is simple.

Despite of these spectral results, the formulations proposed by ergodic theorists are not suitable for the applications considered in this dissertation. This is because of the difficulty to construct periodic approximations of the kind suggested in [25] from a practical sense. The focus of this earier work was more on answering certain deep theoretical questions concerning global properties of automorphisms, rather than the more engineering oriented applications adressed in [28, 29].

With that stated, the main novelty of this dissertation is really the application of the concept of periodic approximations for the purposes of computing spectral decompositions of observable dynamics.

1.5 Permissions and Attributions

1. The content of chapter 2 is the result of a collaboration with Hassan Arbabi, Louis van Blargian, Timothy Matchen, Emma Tegling, and Igor Mezić. The work originates from the conference paper:

   > N. Govindarajan, H. Arbabi, L. van Blargian, T. Matchen, E. Tegling, I. Mezić, "*An operator-theoretic viewpoint to non-smooth dynamical systems: Koopman analysis of a hybrid pendulum*", 2016 IEEE 55th Conference on Decision and Control (CDC) in Las Vegas.

2. The contents of the remaining chapter is the result of a collaboration with Ryan

Mohr, Shivkumar Chandrasekaran, and Igor Mezić. Most of the work is summarized in the papers:

> N. Govindarajan, R. Mohr, S. Chandrasekaran, and I. Mezić, "*On the approximation of koopman spectra for measure preserving transformations*", arXiv preprint arXiv:1803.03920 (2018). (*Submitted SIAM journal on Applied Dynamical Systems*)

and

> N. Govindarajan, R. Mohr, S. Chandrasekaran, and I. Mezić, "*On the approximation of koopman spectra for measure preserving flows*", arXiv preprint arXiv:1806.10296 (2018).

Chapter 2

A case study: the hybrid pendulum

A considerable number of dynamical systems in engineering practice are essentially hybrid in nature. These systems typically model non-smooth phenomena such as impact, collision, and switching between several discrete modes. Under the hybrid automaton framework, these discontinuities are often expressed in terms of guard conditions, state resets, and switching between several "system modes". The imposition of such conditions result in so-called piecewise-smooth dynamical systems of which the orbits are characterized by smooth evolutions, interrupted by discrete jumps.

This chapter illustrates how Koopman analysis can be applied to certain classes of hybrid systems consisting of a single discrete mode, but are subjected to guard conditions and state resets. The emphasis is on a specific benchmark pendulum system that is subjected to downward "kicks" under fixed angles. Overall, two cases are considered: (i) the undamped case where the continuous part of the system is Hamiltonian, and (ii) a damped case where the pendulum is exposed to viscous damping.

Remark 2.0.1. The notation and variables defined in this chapter are independent of the forthcoming chapters. Some of the variables will be re-used later for different purposes.

2.1 A model of a kicked pendulum

Consider a mathematical pendulum with length l and mass m. In the absence of damping or external forcing, the equations of motion for this system are formed by defining $x := (\theta, \omega) \in \mathbb{S}^1 \times \mathbb{R} =: X$ and $f : X \mapsto \mathbb{R}^2$ such that:

$$\dot{x} = f(x) = \begin{bmatrix} \omega \\ -(g/l)\sin\theta \end{bmatrix}.$$

Now suppose that the pendulum experiences an instantaneous backwards "kick" when passing through the given angles $\pm\theta^*$. This kick is modeled by an instantaneous change in angular velocity $\Delta\omega > 0$. In the hybrid automaton notation, the kick is included in the model as a reset map $\mathcal{R} : X \mapsto X$ defined by,

$$\mathcal{R}(\theta, \omega) = \begin{cases} (-\theta^*, \omega + \Delta\omega) & \text{if } (\theta = -\theta^*) \wedge (\omega < 0) \\ (\theta^*, \omega - \Delta\omega) & \text{if } (\theta = \theta^*) \wedge (\omega > 0) \end{cases},$$

where, for ease of notation,the guard conditions are incorporated as well. Note that the reset only occurs upon passing through $\pm\theta^*$ from below, so that the kick is always directed towards the stable equilibrium point of the pendulum. Note that in this formulation, no resets occur when the pendulum only grazes the "kicking surfaces" at $\pm\theta^*$. The situation is illustrated in fig. 2.1, where also the corresponding hybrid automaton representation and state-space are shown.

Normalized equations

To simplify the analysis, it is convenient to normalize the state x by dividing the angular velocity ω by the kick strength $\Delta\omega$, i.e.

$$\begin{bmatrix} \dot{\theta} \\ \dot{p} \end{bmatrix} = \begin{bmatrix} \mu_1 p \\ -\left(\mu_2^2/\mu_1\right)\sin\theta \end{bmatrix}. \tag{2.1}$$

and

$$\mathcal{R}(\theta, p) = \begin{cases} (-\theta^*, p+1) & \text{if } (\theta = -\theta^*) \wedge (p < 0) \\ (\theta^*, p-1) & \text{if } (\theta = \theta^*) \vee (p > 0) \end{cases}, \tag{2.2}$$

where $p = \omega/\Delta\omega$ denotes the normalized momentum. The equations (2.1), (2.2), are parametrized in terms of $\mu_1 := \Delta\omega > 0$ (the kick strength) and $\mu_2 := \omega_n := \sqrt{g/l} > 0$ (the natural frequency of the linearized pendulum). Note that the continuous part of the (undamped) hybrid pendulum is Hamiltonian. One can verify that the function:

$$\mathcal{H}(\theta, p) := \frac{1}{2}\left(\frac{\mu_1}{\mu_2}p\right)^2 + 1 - \cos\theta \tag{2.3}$$

constitute an invariant for the flow of (2.1). This particularly implies that, in between state resets, the trajectories of the pendulum are confined to level sets of (2.3).

The damped case

The dynamics of the kicked pendulum will also be studied under the effects weak viscous damping on the system. The continuous part of the hybrid system in that case is replaced by

$$\begin{bmatrix} \dot{\theta} \\ \dot{p} \end{bmatrix} = \begin{bmatrix} \mu_1 p \\ -\left(\mu_2^2/\mu_1\right)\sin\theta - kp \end{bmatrix} \tag{2.4}$$

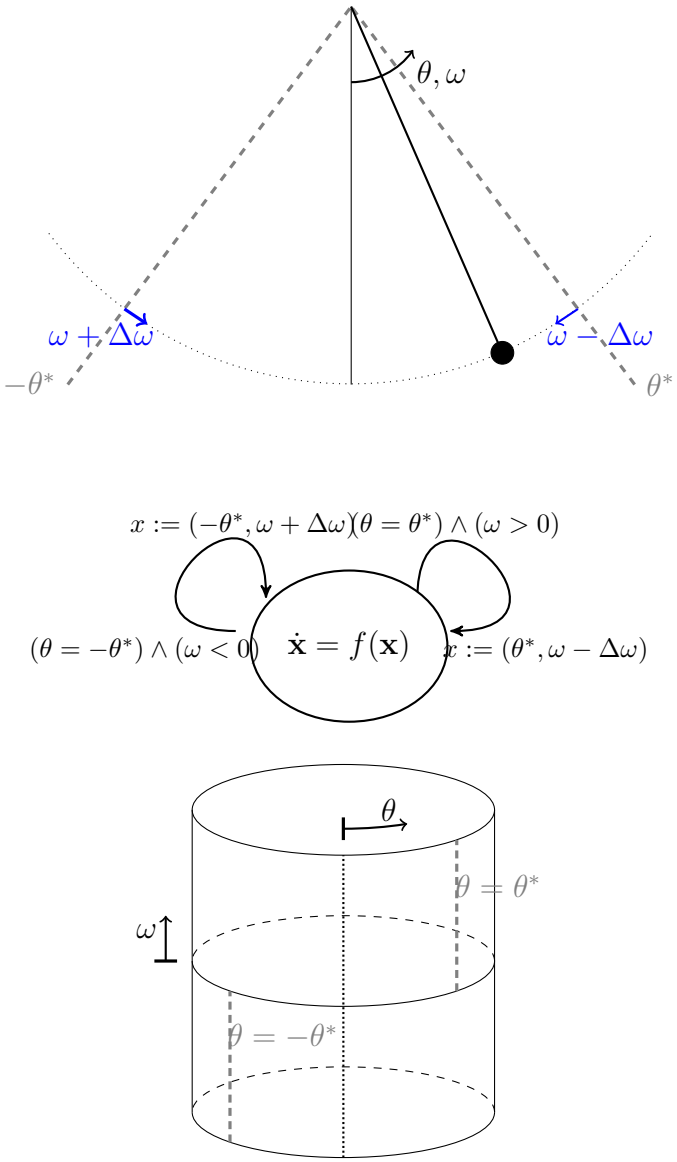

Figure 2.1: The hybrid pendulum: (top) upon passing the angle $\pm\theta^*$ from below the pendulum experiences a change in angular velocity by $\Delta\omega$, (middle) the corresponding hybrid automaton representation, (bottom) the state-space of the system.

where $k > 0$ is the viscous damping coefficient.

2.2 Classic geometric analysis of the kicked pendulum

In this section, the pendulum is analyzed from a geometric perspective using classical tools. The undamped case is covered at first, followed by damped case.

2.2.1 Geometric analysis of the undamped case

The Poincaré map

The trajectories of the freely oscillating pendulum are confined to the level sets of (2.3). Through this observation, it is clear that for initial conditions belonging to the set

$$\mathcal{A}_1 := \{(\theta, p) \in X : \mathcal{H}(\theta, p) < \mathcal{H}(\theta^*, 0)\} \tag{2.5}$$

the behavior of the hybrid pendulum is exactly identical to that of the freely oscillating pendulum.

The more distinctive behavior can be found only in the region: $\mathcal{H}(\theta, p) \geq \mathcal{H}(\theta^*, 0)$. In this part of the state-space, the pendulum gets "kicked" at least once in its orbit for almost any initial condition. The only initial conditions that never get kicked here are those that lie exactly on the homoclinic orbit of the unstable fixed point, and additionally satisfy $\theta > \theta^*$, $p > 0$ or $\theta < -\theta^*$, $p < 0$.

The dynamics of the kicked region can be fully understood from a discrete map defined on the kicking surfaces. Given that the orbits between two consecutive impacts are uniquely determined by the momentum at $\pm\theta^*$, a map can be defined to describe the (normalized) momentum $p\big|_{\theta=\pm\theta^*}$ of the pendulum right *before* the next impact. To do this thoroughly, at first the points on the kicking surfaces that directly get mapped into

the homoclinic orbit are described. Let:

$$p_{cr} := \frac{\mu_2}{\mu_1}\sqrt{2 + 2\cos\theta^*} \tag{2.6}$$

denote the critical momentum required to be on the homoclinic orbit and assign the variable γ to be the state of the pendulum at the unstable fixed point. The Poincaré map $T : \{\mathbb{R} \cup \gamma\} \mapsto \{\mathbb{R} \cup \gamma\}$ is defined by

$$T(p) = \begin{cases} p+1 & p < -(p_{cr}+1) \\ |p+1| & -(p_{cr}+1) < p \leq 0 \\ 0 & p = 0 \\ -|p-1| & 0 < p < p_{cr}+1 \\ p-1 & p_{cr}+1 < p \\ \gamma & p = \gamma \text{ or } p = \pm(p_{cr}+1) \end{cases} \tag{2.7}$$

Asymptotic dynamics of the hybrid pendulum

To fully describe the asymptotic dynamics of the pendulum in the region: $\mathcal{H}(\theta, p) \geq \mathcal{H}(\theta^*, 0)$, the following result about the map (2.7) is stated first.

Lemma 2.2.1. *The map $T : \{\mathbb{R} \cup \gamma\} \mapsto \{\mathbb{R} \cup \gamma\}$ defined by (2.7) has the following asymptotic properties:*

(i) If $p \in D := \{p \in \mathbb{R} : p = \gamma \wedge p = \pm(p_{cr} + k), k \in \mathbb{N}\}$, then there exists $M > 0$, such that:

$$T^n(p) = \gamma, \quad \forall n > M$$

(ii) If $p \notin D$, then there exists a $M > 0$, such that:

$$T^n(p) \in [-1, 1], \quad \forall n > M$$

Proof. (i) can be established by computing the pre-images $T^{-k}(\{\gamma\})$ for $k \in \mathbb{N}$. To show that (ii) is true, observe at first that $T([-1, 1]) = (-1, 1)$, which shows that $[-1, 1]$ is a positively invariant set. Now consider any $p \notin D$ with $|p| > 1$, then $|T(p)| = |p| - 1$. Using induction, it may be shown that:

$$|T^n(p)| = |p| - n, \quad |p| > n$$

from where it follows that $T^n(p)$ enters the interval $[-1, 1]$ in a finite number of iterations. □

Lemma 2.2.1 states that the interval $[-1, 1]$ is an attracting set for (2.7). Furthermore, it states that the trajectories enter the interval $[-1, 1]$ in a finite number of iterations. The interior of the attracting set is composed of:

(i) a fixed point at $p = 0$.

(ii) an uncountable family of period-2 cycles of the form:

$$\{p_1, p_1 - 1\}, \quad p_1 \in (0, 1) \tag{2.8}$$

These results on the map (2.7) are related to the actual hybrid system in the following way. The interval $[-1, 1]$ from Lemma 2.2.1 corresponds to the set

$$\mathcal{A}_2 := \{(\theta, p) \in X : H_- \leq \mathcal{H}(\theta, p) \leq H_+, |\theta| \leq \theta^*\} \tag{2.9}$$

where:

$$H_- := \mathcal{H}(\theta^*, 0), \quad H_+ := \mathcal{H}(\theta^*, 1). \tag{2.10}$$

This set is foliated by an uncountable family of limit cycles. In correspondence with the period-2 cycles of the map (2.7), the limit cycles can as well be parametrized by $\{p_1, p_1 - 1\}$, $p_1 \in (0, 1)$. The following relationship can be obtained between the original coordinates and the limit cycle in which the system is on:

$$p_1(\theta, p) = \begin{cases} \frac{\mu_2}{\mu_1}\sqrt{2(\mathcal{H}(\theta, p) - 1 + \cos\theta^*)} & p \geq 0 \\ 1 - \frac{\mu_2}{\mu_1}\sqrt{2(\mathcal{H}(\theta, p) - 1 + \cos\theta^*)} & p < 0 \end{cases} \tag{2.11}$$

where $(\theta, p) \in \mathcal{A}_2$. In summary, the following result follows.

Theorem 2.2.2. *The trajectories of the hybrid pendulum, starting from almost everywhere in the region': $\mathcal{H}(\theta, p) \geq \mathcal{H}(\theta^*, 0)$, enter into a discontinuous periodic orbit in finite time.*

Proof. Trajectories in the interior of the set (15) are already in a discontinuous periodic orbit. From lemma 1 it follows that almost all other trajectories eventually enter one of these periodic orbits. A measure zero set of trajectories get kicked into the homoclinic orbit, hence the statement almost everywhere. □

Basin of attraction

The basin of a specific limit cycle p_1 can be found by repeatedly computing the pre-images of the map (2.7). fig. 2.2 shows the basin of the limit cycle at $p_1 = 0.7$ for three different values of p_{cr}.

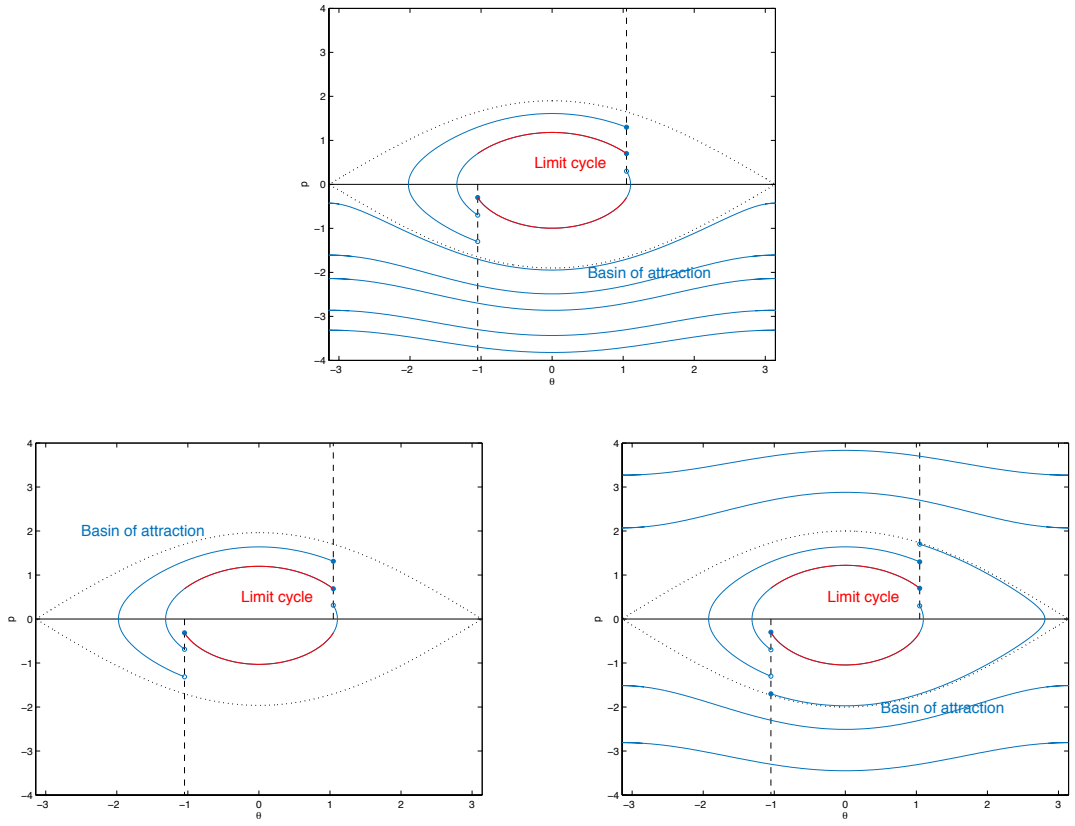

Figure 2.2: Basin of attraction for the limit cycle with $p_1 = 0.7$. $p_{cr} = 1.65$ (top), $p_{cr} = 1.7$ (bottom-left), $p_{cr} = 1.73$ (bottom-right).

Action-angle coordinates

If the pendulum is released at $\theta = -\theta^*$ with an initial momentum $p_1 \in (0, 1)$, then the time required to reach a certain $\theta \in [-\theta^*, \theta^*]$ is determined by the elliptic integral:

$$\Gamma[\theta, p_1] = \int_{-\theta^*}^{\theta} \frac{1}{\mu_2} \left[2 \left(\frac{1}{2} \left(\frac{\mu_1}{\mu_2} p_1 \right)^2 - \cos\theta^* + \cos\xi \right) \right]^{-\frac{1}{2}} \mathrm{d}\xi$$

The function $\Gamma[\theta, p_1]$ permits us to define action-angle coordinates for the set (2.9).

The period of a specific limit cycle $\{p_1, p_1 - 1\}$ is given by the formula:

$$P[p_1] = \Gamma[\theta^*, p_1] + \Gamma[\theta^*, 1 - p_1] \tag{2.12}$$

On every limit cycle $\{p_1, p_1 - 1\}$, a phase coordinate $\psi \in [0, 2\pi)$ can be assigned such that: $\psi = 0$ at $(\theta, p) = (-\theta^*, p_1)$. This is done as follows: let $o(p_1)$ denote the orbit of a specific limit cycle, i.e.

$$o(p_1) := \big\{(\theta, p) \in X : S^t(-\theta^*, p_1) = (\theta, p) \text{ for some } t \geq 0\big\}$$

Then, the phase on $o(p_1)$ can be defined as:

$$\psi = \frac{1}{P[p_1]} \begin{cases} \Gamma[\theta, p_1] & p > 0 \\ \Gamma[\theta^*, p_1] + \Gamma[\theta^* - \theta, 1 - p_1] & p < 0 \end{cases} \tag{2.13}$$

where $(\theta, p) \in o(p_1)$.

The formulas (2.13) together with (2.11) define action-angle coordinates for the interior of the set (2.9). That is, under the coordinate transformation $(I, \psi) = h(\theta, p)$, where:

$$h_1(\theta, p) = p_1(\theta, p) \tag{2.14a}$$

$$h_2(\theta, p) = \frac{1}{P[p_1(\theta, p)]} \begin{cases} \Gamma[\theta, p_1(\theta, p)] & p > 0 \\ \Gamma[\theta^*, p_1(\theta, p)] + \Gamma[\theta^* - \theta, 1 - p_1(\theta, p)] & p < 0 \end{cases} \tag{2.14b}$$

the set $\mathcal{A}_2$ is mapped onto the set

$$Y := (0, 1) \times \mathbb{S}^1 \tag{2.15}$$

under which the flow is simply

$$R^t(I, \psi) = (I, (\Omega[I]t + \psi) \mod 2\pi) \tag{2.16}$$

where $\Omega[I] := 2\pi/P[I]$.

The kicked pendulum has an invariant measure whose support is restricted to the set $\mathcal{A}_2$. In fact, under the bijection (2.14) the dynamics on the set $\mathcal{A}_2$ is conjugate to the Lebesgue measure-preserving system in (2.16). Hence, if μ_Y denotes the Lebesgue measure for the domain (2.15), then

$$\mu_{\mathcal{A}_2} = \mu_Y \circ h \tag{2.17}$$

is an invariant measure for the hybrid system on (2.9).

2.2.2 Geometric analysis of the damped case

In this section, the damped hybrid pendulum is studied from the geometric perspective.

Poincaré map for the damped system

The asymptotic properties of the hybrid pendulum under viscous damping can again be analyzed through the study of some discrete map. Because of dissipation, all trajectories that start at $\mathcal{H}(\theta, p) \geq \mathcal{H}(\theta^*, 0)$ must eventually enter the set (2.9). Given that all trajectories in $\mathcal{A}_1$ spiral into the stable fixed point of the pendulum, the analysis of what happens in $\mathcal{A}_2$ is critical to determining the global properties of the system overall.

The analysis is pursued by viewing the system in terms of its energy state H, which has a one-to-one correspondence with the normalized momentum p if the inherent symmetry

is exploited in the system. The discrete map that characterizes the dynamics inside $\mathcal{A}_2$ is defined in reference to the value of the energy at the condition $(\pm\theta^*, p)$, where $0 \leq p \leq 1$. In the most general sense, the map takes the form:

$$H' = u\,(H) := f \circ d(H) \tag{2.18}$$

Here, u is a composition of two separate functions: d, which represents the energy dissipated due to damping as the pendulum traverses from $\pm\theta^*$ to $\mp\theta^*$, and f, which represents the energy change related to the kicking of the pendulum at $\pm\theta^*$. By knowing the change in momentum that occurs after a kick, and given (2.3), one can derive that:

$$f(H) = H - \left(\frac{\mu_1}{\mu_2}\right)^2 p(H) + \frac{1}{2}\left(\frac{\mu_1}{\mu_2}\right)^2 \tag{2.19}$$

where:

$$p(H) = \frac{\mu_2}{\mu_1}\sqrt{2(H + \cos\theta^* - 1)}$$

The dissipation function d, on the other hand, must be a monotonically increasing function and takes the form $d\,(H) = r\,(H)\,H$ with $0 < r\,(H) < 1$ for all $H > 0$. Based on some numerical simulations (see figure 2.3), it is *assumed* that the dissipation function is linear:

$$d(H) = rH, \quad 0 < r < 1.$$

For the undamped case, the map (2.18) is defined on the domain $[H_-, H_+]$ (see (2.10)) and has a neutrally stable fixed point at $H_{fp,0} = \mathcal{H}(\theta^*, 1/2)$. Furthermore, it has an uncountable family of neutrally stable period-2 cycles , since $f^2 := f \circ f = \mathrm{Id}$. The introduction of damping restricts the domain of the map (2.18) to $[H_0, H_+]$, where $H_0 :=$

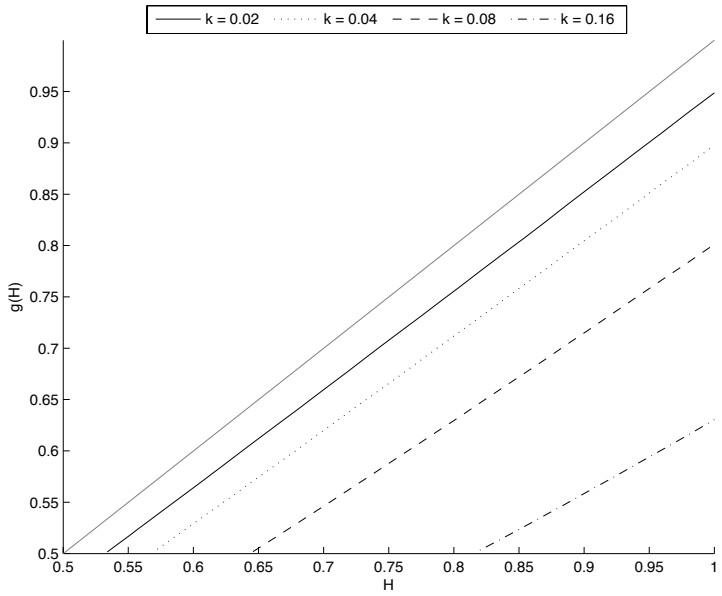

Figure 2.3: The dissipation function d computed for different viscous damping coefficients. The kick angle θ^* is set to $\pi/3$ rad, $\mu_1 = 1$ rad/s, and $\mu_2 = 1$ rad/s.

H_-/r. The range of (2.18) equals $u([H_0, H_+]) = [H_-, H_+]$, hence a subset of initial conditions will eventually get mapped outside the domain of u. The next theorem shows that this subset is, in fact, the entire domain except for one specific point corresponding to the unstable fixed point of u.

Theorem 2.2.3. *Consider the map* (2.18) *and assume that the dissipation function is linear. Furthermore, denote* $r = 1 - \delta$*, with* $\delta > 0$ *sufficiently small. Then:*

(i) there exists a unique fixed point $H_{fp}(\delta) > H_{fp,0}$ *which is unstable.*

(ii) the map $u := f \circ d$*, defined by* (2.18)*, has no period 2-cycles.*

(iii) $\forall H \neq H_{fp}(\delta)$, $\exists n > 0$ *s.t.* $u^n(H) \notin [H_0, H_+]$

Proof. For notational convenience, let us denote $\eta := \frac{\mu_1}{\mu_2}$. To show that the fixed point H_{fp} moves to the right and observe that it must belong to the graph of the implicit

function:

$$s(H;\delta) := \delta H - \eta^2 p((1-\delta)H) + \frac{1}{2}\eta^2 = 0$$

Since,

$$\begin{aligned} \frac{\partial}{\partial \delta} s(H;\delta)\bigg|_{\delta=0, H=H_{fp,0}} &= H_{fp,0}\left(1 + \frac{1}{p(H_{fp,0})}\right) \\ &= 3H_{fp,0} \\ &> 0 \end{aligned}$$

the implicit function theorem guarantees that $H_{fp} = H_{fp}(\delta)$, such that $s(H_{fp}(\delta);\delta) = 0$ for a sufficiently small neighborhood around $\delta = 0$. Furthermore,

$$H_{fp}(\delta) = H_{fp,0} + 3H_{fp,0}\delta + \mathcal{O}(|\delta|^2)$$

which shows that the fixed point moves to the right for $\delta > 0$. The fixed point $H_{fp}(\delta)$, $\delta > 0$ is unstable. To show this, take note that $u(H) = u(H;\delta)$, and:

$$u'(H;\delta) = (1-\delta)\left(1 - \frac{1}{p((1-\delta)H)}\right)$$

Consider $u'(H_{fp}(\delta);\delta)$, the fixed point is unstable if, and only if, $|u'(H_{fp}(\delta);\delta)| > 1$. Given that $u'(H_{fp}(0);0) = -1$, the following needs to be shown:

$$u'(H_{fp}(\delta);\delta) < u'(H_{fp}(0);0) = -1$$

Since,

$$\begin{aligned}\left.\frac{d}{d\delta}u'(H_{fp}(\delta),\delta)\right|_{\delta=0} &= \frac{8}{\eta^2}\left(\cos\theta^* - 1\right)\\ &< 0, \quad \text{if } \theta^* \neq 0\end{aligned}$$

this is indeed the case, which completes the proof for (i).

To prove (ii), consider $u^2(H) := u \circ u(H)$, it will be shown that for a sufficiently small $\delta > 0$,

$$\frac{d}{dH}u^2(H) = u'(u(H))u'(H) \geq 1.$$

Since $u^2(H_{fp}) = H_{fp}$ with $\frac{d}{dH}u^2(H_{fp}) > 1$, the above inequality would imply that $u^2(H)$ has no other fixed points, which proves the non-existence of period-2 cycles. To show that the inequality is valid, observe at first that $u'(H) = u'(H;\delta)$ and that $u'(u(H)) = u'(u(H;\delta);\delta)$. Furthermore,

$$\begin{aligned}u'(H;\delta) &= u'(H;0) + \left.\frac{\partial}{\partial\delta}u'(H;\delta)\right|_{\delta=0}\delta + \mathcal{O}(|\delta|^2)\\ u'(u(H;\delta);\delta) &= \frac{1}{u'(H;0)} + \left.\frac{\partial}{\partial\delta}u'(u(H;\delta);\delta)\right|_{\delta=0}\delta + \mathcal{O}(|\delta|^2)\end{aligned}$$

So that for sufficiently small $\delta > 0$:

$$\frac{d}{dH}u^2(H) = 1 + \left(\left.\frac{\partial}{\partial\delta}u'(H;\delta)\right|_{\delta=0}\delta\right)\left(\frac{1}{u'(H;0)}\right) + \left(\left.\frac{\partial}{\partial\delta}u'(u(H;\delta);\delta)\right|_{\delta=0}\delta\right)u'(H;0) + \mathcal{O}(|\delta|^2)$$

Hence, if it can be shown that:

$$k(H) := \left.\frac{\partial}{\partial\delta}u'(H;\delta)\right|_{\delta=0} \cdot \frac{1}{u'(H;0)} + \left.\frac{\partial}{\partial\delta}u'(u(H;\delta);\delta)\right|_{\delta=0}u'(H;0) \geq 0$$

then $\frac{d}{dH}u^2(H) \geq 1$. And indeed,

$$\begin{aligned}
\left.\frac{\partial}{\partial\delta}u'(H;\delta)\right|_{\delta=0} &= -u'(H;0) - \frac{\eta H}{(\eta p(H))^3} \\
\left.\frac{\partial}{\partial\delta}u'(u(H;\delta);\delta)\right|_{\delta=0} &= -\frac{1}{u'(H;0)} - \frac{\eta u(H;0)}{(\eta(1-p(H)))^3}
\end{aligned}$$

and after some algebraic manipulations:

$$\begin{aligned}
k(H) &= -2 + \frac{\frac{1}{2}\eta^2 p(H)(1-p(H)) + 1 - \cos\theta^*}{\eta^2 p(H)^2(1-p(H))^2} \\
&\geq -2 + \frac{1}{2}\frac{1}{p(H)(1-p(H))} \\
&\geq -2 + \frac{1}{2}\min_{0<p<1}\frac{1}{p(1-p)} \\
&= 0
\end{aligned}$$

which completes the proof for (ii).

The proof of (iii) follows directly from $\frac{d}{dH}u^2(H) \geq 1$. □

Corollary 2.2.4. *For $\delta > 0$ sufficiently small, the trajectories of the hybrid pendulum, starting from almost everywhere, asymptotically reach the fixed at $\theta = 0$.*

2.3 Koopman analysis of the kicked pendulum

In this section, the kicked pendulum is analyzed from the Koopman operator theory perspective. First, the undamped case is studied, followed by the damped case.

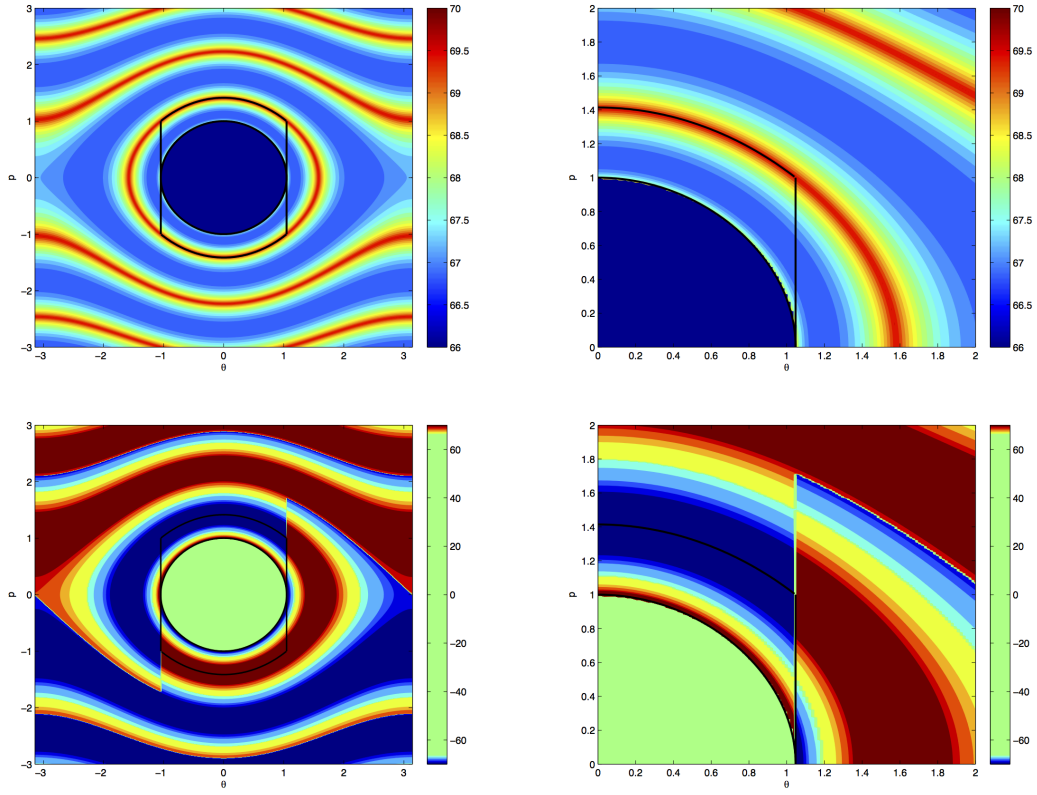

Figure 2.4: Projections of observables onto the eigenspace of Koopman at $\lambda = 0$. The boundaries of the set of limit cycles (2.9) is demarcated in black, $\mu_1 = 1$ rad/s, $\mu_2 = 1$ rad/s, and $\theta^* = \frac{\pi}{3}$ rad. The top two figures are the results obtained with the Hamiltonian function (2.3), whereas the bottom two are those obtained with the signed Hamiltonian function (2.21). The figures on the right show a close up of the results into the region [0,2] x [0,2].

2.3.1 Koopman analysis of the undamped case

Eigenspace of Koopman at $\lambda = 0$

The level sets of Koopman eigenfunctions at $\lambda = 0$ partition the state-space into invariant sets. In fact, the characterization of the eigenspace at $\lambda = 0$ is directly related to the ergodic partition [30, 28].

To describe this partition for the hybrid pendulum, consider at first the dynamics on the invariant set (2.9). In section 2.2.1 it was shown that this set is foliated by an

uncountable family of limit cycles. Given this property, one can verify that[1]

$$\phi_0(\theta, p) = \delta(h_1(\theta, p) - I_0), \quad I_0 \in (0, 1) \tag{2.20}$$

form a collection of eigendistributions at $\lambda = 0$, where h_1 specifically refers to (2.14a). In a certain sense, these distributions are the building blocks of all eigenfunctions at $\lambda = 0$. That is, if $c : (0, 1) \mapsto \mathbb{C}$ denotes a function on the open unit interval, then:

$$\phi_0(\theta, p) = \int_0^1 c(I)\delta(h_1(\theta, p) - I)dI = c(h_1(\theta, p))$$

is an eigenfunction at $\lambda = 0$.

The definition of ϕ_0 can be extended to outside of $\mathcal{A}_2$ if all initial conditions belonging to the basin of a particular limit cycle $\{p_1, p_1 - 1\}$ are assigned the value $c(p_1)$. Clearly, if c is a bijection, the level sets of ϕ_0 describe the orbits of the system.

Eigenfunctions of the Koopman operator can be recovered by computing time-averages of observable traces. These averages are projections of observables $\mathcal{P}^\lambda g$ onto the eigenspace at $\lambda \in \mathbb{C}$. The top two figures in fig. 2.4 depict a high-resolution contour plot of a projection $\mathcal{P}^0 g$, when g is set equal to the Hamiltonian function (2.3). In the figures, initial conditions that have the same color belong to the same level set, and hence, fall under the same equivalence class of long-term dynamical behavior. Note that for this particular eigenfunction, these equivalence classes are not the actual limit cycles themselves, since trajectories that end up in the limit cycles:

$$\{p_1, p_1 - 1\} \text{ and } \{1 - p_1, -p_1\}, \quad p_1 \in (0, 1/2)$$

have exactly the same time-average.

[1] δ denotes here the Dirac delta function

To obtain a more refined partition, one generally needs to consider the product partition of multiple projections conjointly [31]. For the pendulum however, the time-average of the observable:

$$g(\theta, p) = \text{sign}(p)\mathcal{H}(\theta, p) \tag{2.21}$$

can be determined, which gives the Hamiltonian a sign, depending on the direction in which the pendulum is moving. This observable is capable of separating the limit cycles $\{p_1, p_1 - 1\}$ and $\{1 - p_1, -p_1\}$ from each other. The bottom two figures of fig. 2.4 show contour plots of the projections obtained with this observable.

Spectral decomposition on the set of limit cycles

The hybrid pendulum is measure-preserving on the set (2.9). An invariant measure is given by (2.17). Consequently, the Koopman operator is unitary on $L^2(\mathcal{A}_2, \mu_{\mathcal{A}_2})$. This implies that the operator admits a spectral decomposition.

An expression for the spectral decomposition is most conveniently obtained by first deriving the decomposition for the conjugate system (2.16) and then applying the fact that eigendistributions are conserved under conjugacy [1]. The evolution of a square-integrable function $g(I, \psi) \in L^2(Y, \mu_Y)$ under the action of the Koopman operator is given by,

$$\left(\mathcal{U}^t g\right)(I, \psi) = g(I, \psi + \Omega[I]t \mod 2\pi).$$

By expanding the observables in a Fourier series:

$$\begin{aligned}\left(\mathcal{U}^t g\right)(I,\psi) &= \mathcal{U}^t\left(\sum_{j\in\mathbb{Z}} g_j(I)e^{ij\psi}\right)\\ &= \sum_{j\in\mathbb{Z}} g_j(I)e^{ij\Omega(I)t}e^{ij\psi}\\ &= \int_0^1 g_0(I)\delta(s-I)ds + \\ &\quad \sum_{j\in\mathbb{Z},j\neq 0}\int_{\mathbb{R}} e^{ij\rho t}g_j(I)e^{ij\psi}\delta(j\Omega(I)-\rho)d\rho,\end{aligned}$$

the spectral expansion can be written in the form:

$$\left(\mathcal{U}^t g\right)(I,\psi) = g^*(I) + \int_{\mathbb{R}} e^{i\rho t}d\mathcal{S}(\rho)g(I,\psi) \tag{2.22}$$

where the time average g^* only has dependence on I and where the projection-valued measure $d\mathcal{S}(\rho)$ has the explicit expression:

$$d\mathcal{S}(\rho)g(I,\psi) = \sum_{j\in\mathbb{Z},j\neq 0} g_j(I)e^{ij\psi}\delta(j\Omega(I)-\rho)d\rho.$$

Substitution of (2.14) into (2.22) will yield the spectral expansion in the original coordinates. Notice that the spectrum of the operator is continuous.

2.3.2 Koopman analysis of the damped case

Eigenspace of Koopman at $\lambda = 0$

From corollary 2.2.4, it follows that almost all trajectories end up at the stable equilibrium of the pendulum as time approaches infinity. The introduction of damping therefore severely simplifies the eigenspace at $\lambda = 0$, given that the only permissible eigenfunctions are now those which are constant almost everywhere in X.

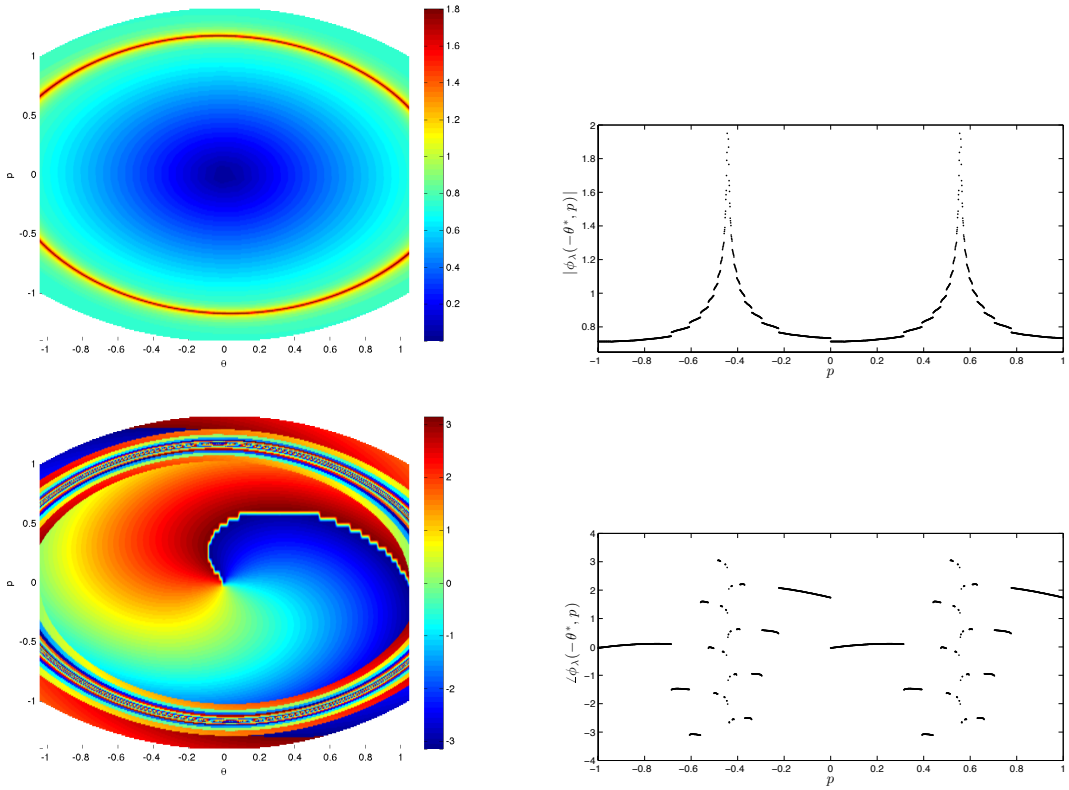

Figure 2.5: The Koopman eigenfunction $\phi_\lambda(x)$ of theorem 2.3.1 shown for the regions (2.5) and (2.9). The figures on the right display the eigenfunction at a cut: $\theta = -\theta^*$, $p \in (-1, 1)$. The viscous damping coefficient is set to $k = 0.03$. Top row: The modulus $|\phi_\lambda(x)|$. The phase $\angle\phi_\lambda(x)$.

Point spectrum of the operator

The addition of viscous damping turns the fixed point at $\theta = 0$ into a spiral sink. In terms of the Koopman operator, these changes give rise to point spectrum in the left-half complex plane. The point spectra are products of the eigenvalues[2] of the linearized pendulum:

$$\dot{y} = \mathrm{A}y, \quad \mathrm{A} = \begin{bmatrix} 0 & 1 \\ -1 & -k \end{bmatrix} \tag{2.23}$$

[2]This follows from the property $\mathcal{U}g_1g_2 = (\mathcal{U}g_1)(\mathcal{U}g_2)$.

where $y = \begin{bmatrix}\theta & p\end{bmatrix}^T$ and whose eigenvalues are given by $\lambda/\bar{\lambda} = -\sigma \pm i\eta$, with $\sigma = \frac{1}{2}k$, $\eta = \sqrt{1 - \frac{1}{4}k^2}$.

Following the concepts discussed in [7, 32], one can show that an eigenfunction at λ and $\bar{\lambda}$ can be computed from the observables:

$$g_1(\theta, p) := \frac{1}{\sqrt{2}} \left\| \begin{bmatrix} v & \bar{v} \end{bmatrix}^{-1} \begin{bmatrix} \theta \\ p \end{bmatrix} \right\|_2, \tag{2.24}$$

$$g_2(y) := \frac{\begin{bmatrix} 1 & 0 \end{bmatrix} \begin{bmatrix} v & \bar{v} \end{bmatrix}^{-1} \begin{bmatrix} \theta \\ p \end{bmatrix}}{g_1(\theta, p)} \tag{2.25}$$

where v, $\bar{v}$ are the right eigenvectors of A.

Theorem 2.3.1. *Consider the damped hybrid pendulum defined by* (2.2), (2.4). *Then,*

$$\phi_{\lambda/\bar{\lambda}}(\theta, p) = |\phi_\lambda(p, \theta)| e^{\pm i \angle \phi_\lambda(\theta, p)} \tag{2.26}$$

with:

$$|\phi_\lambda(\theta, p)| := \lim_{t \to \infty} \frac{1}{t} \int_0^t e^{\sigma\tau} \left(\mathcal{U}^\tau g_1\right)(\theta, p) d\tau \tag{2.27a}$$

$$e^{\pm i \angle \phi_\lambda(\theta, p)} := \lim_{t \to \infty} \frac{1}{t} \int_0^t e^{\pm i\eta\tau} \left(\mathcal{U}^\tau g_2\right)(\theta, p) d\tau \tag{2.27b}$$

are Koopman eigenfunctions at eigenvalues $\lambda/\bar{\lambda} = -\sigma \pm i\eta$.

Proof. The claim follows by showing that the integrals (33) converge (to a non-zero value) for all initial conditions on the basin. If $(\theta, p) \in \mathcal{A}_1$, the dynamics are identical to that of the conventional pendulum, and therefore by Theorem 2.3 in [7], there exists a C^1-diffeomorphism $h : \mathcal{A}_1 \mapsto Y \subset \mathbb{R}^2$ between the flows S^t and R^t. For all other initial

conditions on the basin, one can infer from theorem 2 and corollary 1 that there exists a $T^* > 0$ such that:

$$S^t(\theta, p) \in \mathcal{A}_1, \quad \forall t > T^*$$

A change of variables may be used to prove convergence of the integrals in that case. □

Figure 2.5 shows a contour plot of the eigenfunction in theorem 2.3.1. The functions $|\phi_\lambda(\theta, p)|$ and $e^{i\angle\phi_\lambda(\theta,p)}$ have the following geometric interpretation. The level sets of $|\phi_\lambda(\theta, p)|$ define the so-called isostables [32] and describe the set of points that have the same asymptotic convergence toward the fixed point. It can be observed that the isostables blow up in the region that corresponds to the unstable periodic orbit (associated with the fixed point in theorem 2.2.3). The level sets of $e^{i\angle\phi_\lambda(\theta,p)}$ (or equivalently those of $\angle\phi_\lambda((\theta, p))$, on the other hand, describe the set of points that simultaneously move in phase around the fixed point.

The phase plots indicate that the kicking of the pendulum introduces a high level of phase sensitivity [33] close to the unstable periodic orbit.

Overall, the eigenfunctions of theorem 2.3.1 can be used to describe a *semi-conjugacy* with a linear system. Specifically, the modulus and phase form a map:

$$(\theta, p) \mapsto (|\phi_\lambda(\theta, p)|, \angle\phi_\lambda(\theta, p))$$

such that under the new coordinates, the following simplified dynamics hold true:

$$\begin{aligned} \frac{d}{dt}|\phi_\lambda(\theta, p)| &= -\sigma|\phi_\lambda(\theta, p)| \\ \frac{d}{dt}\angle\phi_\lambda(\theta, p) &= \eta. \end{aligned}$$

Chapter 3

The spectral decomposition of the unitary Koopman operator

This section reviews the relevant spectral decomposition theorems of unitary Koopman operators on a Hilbert space. The theorems are presented in order of increasing complexity. At first, the spectral theory of one-to-one, finite-state dynamical systems is covered. This is followed by a more general account of the spectral theorem applicable to invertible, measure-preserving transformations on a compact state-space. Finally, the results are further generalized to include continuous one-parameter families of unitary operators that arise in the Koopman linearization of measure-preserving flows.

Although the spectral decomposition of finite-state dynamical systems is basic and involves only knowing linear algebra, the theorems related to measure-preserving maps and flows will require the more complex machinery of functional analysis. Nevertheless, the results covered here on unitary operators are well-known and can be found in classical texts such as [34].

3.1 Spectral theory of finite-state systems

Consider a map $T : X \mapsto X$ on a finite state-space $X = \{1, 2, \ldots, N\}$. Observables $g : X \mapsto \mathbb{C}$ associated with such a map are effectively equivalent to a finite-dimensional vector[1] $\mathrm{g} \in \mathbb{C}^n$. Under the assumption that T is one-to-one, the Koopman operator can be expressed as a permutation matrix $\mathrm{U} \in \mathbb{R}^{N \times N}$ given by

$$[U]_{ij} := \begin{cases} 1 & \text{if } T(j) = i \\ 0 & \text{otherwise} \end{cases}. \tag{3.1}$$

Permutation matrices are a special class of unitary matrices and the propogation of an observable $\mathrm{g} \in \mathbb{C}^n$ can be decomposed as:

$$U^l \mathrm{g} = \sum_{k=1}^{N} e^{il\theta_k} v_k (v_k^* \mathrm{g}) \tag{3.2}$$

where $\theta_k \in [\pi, \pi)$ and $v_k \in \mathbb{C}^N$ (with $v_k^T v_l = 1$ if $k = l$ and zero otherwise) are respectively the eigenfrequencies and eigenvectors of the matrix.

Two spectral quantities of interest are defined:

1. The *spectral projection* of an observable $\mathrm{g} \in \mathbb{C}^N$ on a interval $D \subset \mathbb{S}$:

$$S_D \mathrm{g} = \sum_{\theta_k \in D} v_k v_k^* \mathrm{g} \tag{3.3}$$

[1]Notice that the vector quantity is expressed here with an "upright' g in order to distinguish it from the "function" g.

2. The *spectral density function*[2] of an observable $\mathrm{g} \in \mathbb{C}^N$:

$$\rho(\theta; \mathrm{g}) = \sum_{k=1}^{N} \delta(\theta - \theta_k) |v_k^* \mathrm{g}|^2 \tag{3.4}$$

The eigenvectors and eigenvalues of (3.2) are easily found for a permutation matrix. The cycle decomposition, which decouples a permutation matrix into its cycles, plays a critical role here. That is, associated to every permutation $\mathrm{U} \in \mathbb{R}^{N \times N}$ there exists another permutation matrix $\mathrm{P} \in \mathbb{R}^{N \times N}$ such that by a similarity transformation:

$$\mathrm{P}^T \mathrm{U} \mathrm{P} = \mathrm{C}, \tag{3.5}$$

where C is given by:

$$\mathrm{C} = \begin{bmatrix} \mathrm{C}^{(1)} & & \\ & \ddots & \\ & & \mathrm{C}^{(s)} \end{bmatrix}, \qquad \mathrm{C}_n^{(k)} := \begin{bmatrix} 0 & 0 & \cdots & 0 & 1 \\ 1 & 0 & \cdots & 0 & 0 \\ 0 & 1 & \cdots & 0 & 0 \\ \vdots & \vdots & \ddots & \vdots & \vdots \\ 0 & 0 & \cdots & 1 & 0 \end{bmatrix} \in \mathbb{R}^{n^{(k)} \times n^{(k)}},$$

$$n^{(1)} + n^{(2)} + \ldots + n^{(s)} = N.$$

The decomposition of (3.1) into its cyclic subspaces is obtained as follows. Initialize $\mathrm{U}_1 := \mathrm{U}$ and call:

$$\mathrm{P}^{(1)} := \begin{bmatrix} \mathrm{U}_1 e_1 & \cdots & \mathrm{U}_1^{n^{(1)}} e_1 & e_{n^{(1)}+1} & \cdots & e_{q(n)} \end{bmatrix}, \qquad \text{with } \mathrm{U}_1^{n^{(1)}} e_1 = e_1.$$

[2] A slight abuse of language here, given that it really is a distribution!

A similarity transformation yields:

$$U_2 := \mathrm{P}^{(1)^T}\mathrm{U}_1\mathrm{P}^{(1)} = \begin{bmatrix} \mathrm{C}^{(1)} & \\ & \tilde{\mathrm{U}}_1 \end{bmatrix}.$$

Repeating this process for all s cycles should result in $U_s = \mathrm{C}$ and $\mathrm{P} = \mathrm{P}^{(1)} \cdots \mathrm{P}^{(s)}$.

It is well-known that the Discrete Fourier Transform (DFT) matrix diagonalizes any circulant matrix. In particular, for $\mathrm{C}^{(k)} \in \mathbb{R}^{n^{(k)} \times n^{(k)}}$ the decomposition reads:

$$\mathrm{C}^{(k)} = (\mathrm{DFT})^*_{n^{(k)}} \, \Lambda_{n^{(k)}} \, (\mathrm{DFT})_{n^{(k)}}, \tag{3.6}$$

where:

$$(\mathrm{DFT})_{n^{(k)}} = \frac{1}{\sqrt{n^{(k)}}} \begin{bmatrix} 1 & 1 & 1 & \cdots & 1 \\ 1 & \omega & \omega^2 & \cdots & \omega^{n^{(k)}-1} \\ 1 & \omega^2 & \omega^4 & \cdots & \omega^{2(n^{(k)}-1)} \\ \vdots & \vdots & \vdots & \ddots & \vdots \\ 1 & \omega^{1(n^{(k)}-1)} & \omega^{2(n^{(k)}-1)} & \cdots & \omega^{(n^{(k)}-1)(n^{(k)}-1)} \end{bmatrix},$$

$$\Lambda_{n^{(k)}} = \begin{bmatrix} \omega^0 & & \\ & \ddots & \\ & & \omega^{n^{(k)}-1} \end{bmatrix} \quad \text{and} \quad \omega = \exp\left(\frac{2\pi}{n^{(k)}} i\right).$$

By combining (3.5) with (3.6), the following explicit expression for the spectral decomposition of (3.1) is obtained:

$$\mathrm{U} = \mathrm{V}\Lambda\mathrm{V}^*, \tag{3.7}$$

where:

$$\mathrm{V} = \mathrm{P}\begin{bmatrix} (\mathrm{DFT})^*_{n^{(1)}} & & \\ & \ddots & \\ & & (\mathrm{DFT})^*_{n^{(s)}} \end{bmatrix}, \qquad \Lambda = \begin{bmatrix} \Lambda_{n^{(1)}} & & \\ & \ddots & \\ & & \Lambda_{n^{(s)}} \end{bmatrix}.$$

3.2 Spectral theory for iterative maps

Let $T : X \mapsto X$ be a self-map on the compact, norm-induced metric space $X \subseteq \mathbb{R}^m$. Associate with X the measure space $(X, \mathcal{M}, \mu)$, where $\mathcal{M}$ denotes the Borel sigma-algebra and μ is an absolutely continuous measure with its support equaling the state-space, i.e. supp $\mu = X$. The map T is given to be an invertible measure-preserving transformation such that $\mu(B) = \mu(T(B)) = \mu(T^{-1}(B))$ for every $B \in \mathcal{M}$ (also referred to as a measure-preserving *automorphisms*).

The Koopman linearization of T can be defined on the following Hilbert space:

$$L^2(X, \mathcal{M}, \mu) := \{g : X \mapsto \mathbb{C} \quad | \quad \|g\| < \infty\}, \qquad \|g\| := \left(\int_X |g(x)|^2 \mathrm{d}\mu(x)\right)^{\frac{1}{2}}.$$

The Koopman operator $\mathcal{U} : L^2(X, \mathcal{M}, \mu) \mapsto L^2(X, \mathcal{M}, \mu)$, defined by:

$$\mathcal{U}g = g \circ T \tag{3.8}$$

is in this situation again unitary. The generalization of (3.2) requires machinery from functional analysis and is known as the integral form of the spectral theorem [34]. The evolution of an observable can be decomposed as:

$$\mathcal{U}^k g = \int_{\mathbb{S}} e^{i\theta k} \mathrm{d}\mathcal{S}_\theta g, \qquad k \in \mathbb{Z}. \tag{3.9}$$

Here, $\mathcal{S}_\theta$ is a self-adjoint, *projection-valued measure* on the Borel sigma-algebra $\mathcal{B}(\mathbb{S})$ of the circle $\mathbb{S}$ parameterized by $\theta \in [-\pi, \pi)$. The projection-valued measure satifies the following properties:

(i) For every $D \in \mathcal{B}(\mathbb{S})$,

$$\mathcal{S}_D := \int_D \mathrm{d}\mathcal{S}_\theta$$

is an orthogonal projector on $L^2(X, \mathcal{M}, \mu)$.

(ii) $\mathcal{S}_D = 0$ if $D = \emptyset$ and $\mathcal{S}_D = I$ if $D = \mathbb{S}$.

(iii) If $D_1, D_2 \in \mathcal{B}(\mathbb{S})$ and $D_1 \cap D_2 = \emptyset$, then

$$\langle \mathcal{S}_{D_1} g, \mathcal{S}_{D_2} h \rangle := \int_X \left(\mathcal{S}_{D_1} g\right)^* (x) \left(\mathcal{S}_{D_2} h\right)(x) \mathrm{d}\mu(x) = 0$$

for every $g, h \in L^2(X, \mathcal{M}, \mu)$.

(iv) If $\{D_k\}_{k=1}^\infty$ is a sequence of pairwise disjoint sets in $\mathcal{B}(\mathbb{S})$, then

$$\lim_{m\to\infty} \sum_{k=1}^{m} \mathcal{S}_{D_k} g = \mathcal{S}_D g, \qquad D := \bigcup_{k=1}^{\infty} D_k$$

for every $g \in L^2(X, \mathcal{M}, \mu)$.

The quantities (3.3) and (3.4) can be generalized as follows:

- The *spectral projection* of an observable $g \in L^2(X, \mathcal{M}, \mu)$ on a interval $D \subset \mathbb{S}$:

$$\mathcal{S}_D g = \int_D \mathrm{d}\mathcal{S}_\theta g \tag{3.10}$$

- The *spectral density function* of an observable $g \in L^2(X, \mathcal{M}, \mu)$, defined as the

distributional derivative:

$$\int_{\mathbb{S}} \varphi'(\theta) c(\theta; g) \mathrm{d}\theta = -\int_{\mathbb{S}} \varphi(\theta) \rho(\theta; g) \mathrm{d}\theta \tag{3.11}$$

of the so-called spectral cumulative function on $[-\pi, \pi)$:

$$c(\theta; g) := \langle \mathcal{S}_{[-\pi,\theta)} g, g \rangle,$$

where $\varphi(\theta) \in \mathcal{D}(\mathbb{S})$ is some smooth test functions on the circle.

In essence, the Koopman operator still behaves as permutation matrix, albeit an infinite-dimensional one. A method of computing numerical approximations to (3.10) and (3.11) is the main focus of this dissertation, and will be developed in the upcoming chapters.

3.3 Spectral theory for flows

Let $S^t : X \mapsto X$ denote a Lipschitz continuous flow on a compact *norm-induced* metric space $X \subseteq \mathbb{R}^m$, with S^t satisfying the well-known group properties: $S^t \circ S^s(x) = S^{t+s}(x)$ for any $t, s \in \mathbb{R}$, and $S^0(x) = x$. Again, associate with X the measure space $(X, \mathcal{M}, \mu)$, where $\mathcal{M}$ denotes the Borel sigma-algebra, and μ an absolutely continuous measure with full support on the state-space. The flow S^t is invariant with respect to the measure μ, i.e. for every $t \in \mathbb{R}$ and $B \in \mathcal{M}$: $\mu(B) = \mu(S^t(B))$.

The Koopman linearization of a measure-preserving flow is again defined on:

$$L^2(X, \mathcal{M}, \mu) := \{g : X \mapsto \mathbb{C} \quad | \quad \|g\| < \infty\}, \qquad \|g\| := \left(\int_X |g(x)|^2 \mathrm{d}\mu(x) \right)^{\frac{1}{2}}.$$

One now obtains a continuous one-parameter family of Koopman operators:

$$(\mathcal{U}^t g)(x) := g \circ S^t(x), \qquad t \in \mathbb{R}. \tag{3.12}$$

Since S^t is an invertible measure-preserving transformation for every $t \in \mathbb{R}$, the family of operators $\{\mathcal{U}^t\}_{t\in\mathbb{R}}$ forms a continuous one-parameter *unitary* group. In other words, (3.12) is an unitary operator for every fixed $t \in \mathbb{R}$ and satisfies the group properties: $\mathcal{U}^t\mathcal{U}^s = \mathcal{U}^{t+s}$ for $t, s \in \mathbb{R}$, and $\mathcal{U}^0 = I$.

A detailed account on the spectral theorem for continuous one-parameter unitary groups can again be found in [34]. The evolution of an oberservable $g \in L^2(\mathcal{X}, \mathcal{M}, \mu)$ under (3.12) can be decomposed as:

$$\mathcal{U}^t g = \int_{\mathbb{R}} e^{i\omega t} \mathrm{d}\mathcal{S}_\omega g, \qquad t \in \mathbb{R}. \tag{3.13}$$

In comparison to (3.9), notice that the integration is performed over the real line. Here, $\mathcal{S}_\omega$ denotes a self-adjoint, *projection-valued measure* on the Borel sigma-algebra $\mathcal{B}(\mathbb{R})$ of the real line $\mathbb{R}$. The projection-valued measure satifies the following properties:

(i) For every $D \in \mathcal{B}$,

$$\mathcal{S}_D := \int_D \mathrm{d}\mathcal{S}_\theta$$

is an orthogonal projector on $L^2(X, \mathcal{M}, \mu)$.

(ii) $\mathcal{S}_D = 0$ if $D = \emptyset$ and $\mathcal{S}_D = I$ if $D = \mathbb{R}$.

(iii) If $D_1, D_2 \in \mathcal{B}$ and $D_1 \cap D_2 = \emptyset$, then

$$\langle \mathcal{S}_{D_1} g, \mathcal{S}_{D_2} h \rangle := \int_X \left(\mathcal{S}_{D_1} g\right)^* (x) \left(\mathcal{S}_{D_2} h\right)(x) \mathrm{d}\mu(x) = 0$$

for every $g, h \in L^2(X, \mathcal{M}, \mu)$.

(iv) If $\{D_k\}_{k=1}^{\infty}$ is a sequence of pairwise disjoint sets in $\mathcal{B}$, then

$$\lim_{m\to\infty} \sum_{k=1}^{m} \mathcal{S}_{D_k} g = \mathcal{S}_D g, \qquad D := \bigcup_{k=1}^{\infty} D_k$$

for every $g \in L^2(X, \mathcal{M}, \mu)$.

Similar to (3.10) and (3.11), the following quantities may be defined:

- The *spectral projection* of an observable $g \in L^2(X, \mathcal{M}, \mu)$ on a interval $D \subset \mathbb{R}$:

$$\mathcal{S}_D g := \int_D \mathrm{d}\mathcal{S}_\omega g \tag{3.14}$$

- The *spectral density function* of an observable $g \in L^2(X, \mathcal{M}, \mu)$, defined as the distributional derivative:

$$\int_{\mathbb{R}} \varphi'(\omega) c(\omega; g) \mathrm{d}\omega = -\int_{\mathbb{R}} \varphi(\omega) \rho(\omega; g) \mathrm{d}\omega \tag{3.15}$$

of the so-called spectral cumulative function on $\mathbb{R}$:

$$c(\omega; g) := \langle \mathcal{S}_{(-\infty,\omega)} g, g \rangle.$$

where $\varphi(\omega) \in \mathcal{D}(\mathbb{R})$ belongs to the space of smooth test functions (i.e. Schwarz space).

Chapter 4

Periodic approximations - iterative maps

Let $T : X \mapsto X$ be a self-map on the compact, norm-induced metric space $X \subseteq \mathbb{R}^m$. Associate with X the measure space $(X, \mathcal{M}, \mu)$, where $\mathcal{M}$ denotes the Borel sigma-algebra and μ is an absolutely continuous measure with its support equaling the state-space, i.e. supp $\mu = X$. The map T is assumed to be an invertible measure-preserving transformation such that $\mu(B) = \mu(T(B)) = \mu(T^{-1}(B))$ for every $B \in \mathcal{M}$.

In this chapter, the unitary Koopman operator $\mathcal{U} : L^2(X, \mathcal{M}, \mu) \mapsto L^2(X, \mathcal{M}, \mu)$ associated with T is approximated by Koopman operators of one-to-one, finite-state dynamical systems (i.e. permutation operators). This gives rise to the concept of periodic approximations. The main result here is a spectral convergence theorem which relates the spectra of these discrete Koopman operators to their infinite dimensional analogues.

4.1 Discretization of the unitary Koopman operator

4.1.1 Why permutation operators?

The use of permutation operators as a means to approximate Koopman operator is in many ways natural. Just like (3.8), permutation operators are unitary, and therefore, its spectrum is contained on the unit circle. But the Koopman operator also satisfies the following properties:

1. $\mathcal{U}(fg) = (\mathcal{U}f)(\mathcal{U}g)$.
2. $\mathcal{U}$ is Markov, i.e. $\mathcal{U}g > 0$ whenever $g > 0$.
3. The constant function, i.e. $g(x) = 1$ for every $x \in X$, is an invariant of the operator.

Permutation operators are (finite-dimensional) operators which satisfy the aforementioned properties as well.

4.1.2 The discretization procedure

The following discretization of the Koopman operator is proposed. Consider *any* sequence of measurable partitions $\{\mathcal{P}_n\}_{n=1}^{\infty}$, where $\mathcal{P}_n := \{p_{n,1}, p_{n,2}, \ldots, p_{n,q(n)}\}$ such that:

1. Every partition element $p_{n,j}$ is compact, connected, and of equal measure, i.e.

$$\mu(p_{n,j}) = \frac{\mu(X)}{q(n)}, \qquad j \in \{1, 2, \ldots, q(n)\} \tag{4.1}$$

where $q : \mathbb{N} \mapsto \mathbb{N}$ is a strictly, monotonically increasing function. Asking for compactness, one gets that the partition elements intersect. By (4.1), it must follow that these intersections are of zero measure.

2. The diameters of partition elements are bounded by

$$\operatorname{diam}(p_{n,j}) := \sup_{x,y \in p_{n,j}} d(x,y) \leq l(n) \tag{4.2}$$

where $l : \mathbb{N} \mapsto \mathbb{R}$ is a positive, monotonic function decaying to zero in the limit.

3. $\mathcal{P}_n$ is a refinement of $\mathcal{P}_m$ whenever $n > m$. That is, every $p_{m,j} \in \mathcal{P}_m$ is the union of some partition elements in $\mathcal{P}_n$.

The main idea set forth in this chapter is to project observables $g \in L^2(X, \mathcal{M}, \mu)$ onto a finite-dimensional subspace of indicator functions,

$$L^2_n(X, \mathcal{M}, \mu) := \left\{ g_n : X \mapsto \mathbb{C} \quad | \quad \sum_{j=1}^{q(n)} c_j \chi_{p_{n,j}}(x), \quad c_j \in \mathbb{C} \right\}, \quad \chi_{p_{n,j}}(x) = \begin{cases} 1 & x \in p_{n,j} \\ 0 & x \notin p_{n,j} \end{cases}$$

by means of a smoothing/averaging operation:

$$(\mathcal{W}_n g)(x) = g_n(x) := \sum_{j=1}^{q(n)} g_{n,j} \chi_{p_{n,j}}(x), \qquad g_{n,j} = \frac{q(n)}{\mu(X)} \int_X g(x) \chi_{p_{n,j}}(x) \mathrm{d}\mu(x) \tag{4.3}$$

and then replace (3.8) by its discrete analogue $\mathcal{U}_n : L^2_n(X, \mathcal{M}, \mu) \mapsto L^2_n(X, \mathcal{M}, \mu)$ given by

$$\left(\mathcal{U}_n g_n\right)(x) := \sum_{j=1}^{q(n)} g_{n,j} \chi_{T_n^{-1}(p_{n,j})}(x) \tag{4.4}$$

where $T_n : \mathcal{P}_n \mapsto \mathcal{P}_n$ is a *discrete* map on the partition.

The map T_n is chosen such that it "mimics" the dynamics of the continuous map T. The condition is imposed that T_n has to be a bijection. By doing so, a *periodic approximation* is obtained of the dynamics. Since every partition element is of equal measure (4.1) and since T_n is a bijection, the resulting discretization is regarded as one

which preserves the measure-preserving properties of the original map on the subsigma algebra generated by $\mathcal{P}_n$, i.e. $\mu(T^{-1}(p_{n,j})) = \mu(p_{n,j}) = \mu(T_n^{-1}(p_{n,j}))$.

The discrete operators $\{\mathcal{U}_n\}_{n=1}^{\infty}$ are isomorphic to a sequence of finite-dimensional permutation operators. The spectra for these operators simplify to a pure point spectrum, where the eigenvalues correspond to roots of unity. Let $v_{n,k} = \sum(v_{n,k})_j \chi_{p_{n,j}} \in L_n^2(X, \mathcal{M}, \mu)$ denote a normalized eigenvector, i.e.

$$\mathcal{U}_n v_{n,k} = e^{i\theta_{n,k}} v_{n,k}, \qquad \|v_{n,k}\| = 1.$$

The spectral decomposition can be expressed as:

$$\mathcal{U}_n g_n = \sum_{k=1}^{q(n)} e^{i\theta_{n,k}} \mathcal{S}_{n,\theta_{n,k}} g_n \tag{4.5}$$

where $\mathcal{S}_{n,\theta_{n,k}} : L_n^2(X, \mathcal{M}, \mu) \mapsto L_n^2(X, \mathcal{M}, \mu)$ denotes the rank-1 self-adjoint projector:

$$\mathcal{S}_{n,\theta_{n,k}} g_n = v_{n,k} \langle v_{n,k}, g_n \rangle = v_{n,k} \left(\int_X v_{n,k}^*(x) g_n(x) \mathrm{d}\mu \right) = v_{n,k} \left(\frac{\mu(X)}{q(n)} \sum_{j=1}^{q(n)} v_{n,kj}^* g_{n,j} \right). \tag{4.6}$$

The discrete analogue to the spectral projection (3.10) may then be defined as:

$$\mathcal{S}_{n,D} g_n = \int_D \mathrm{d}\mathcal{S}_{n,\theta} g_n = \sum_{\theta_{n,k} \in D} \mathcal{S}_{n,\theta_{n,k}} g_n \tag{4.7}$$

In addition, the discrete analogue to the spectral density function turns out to be:

$$\rho_n(\theta; g_n) = \sum_{k=1}^{q(n)} \left\| \mathcal{S}_{n,\theta_{n,k}} g_n \right\|^2 \delta(\theta - \theta_{n,k}). \tag{4.8}$$

An overview of the discretization process is given in fig. 4.1.

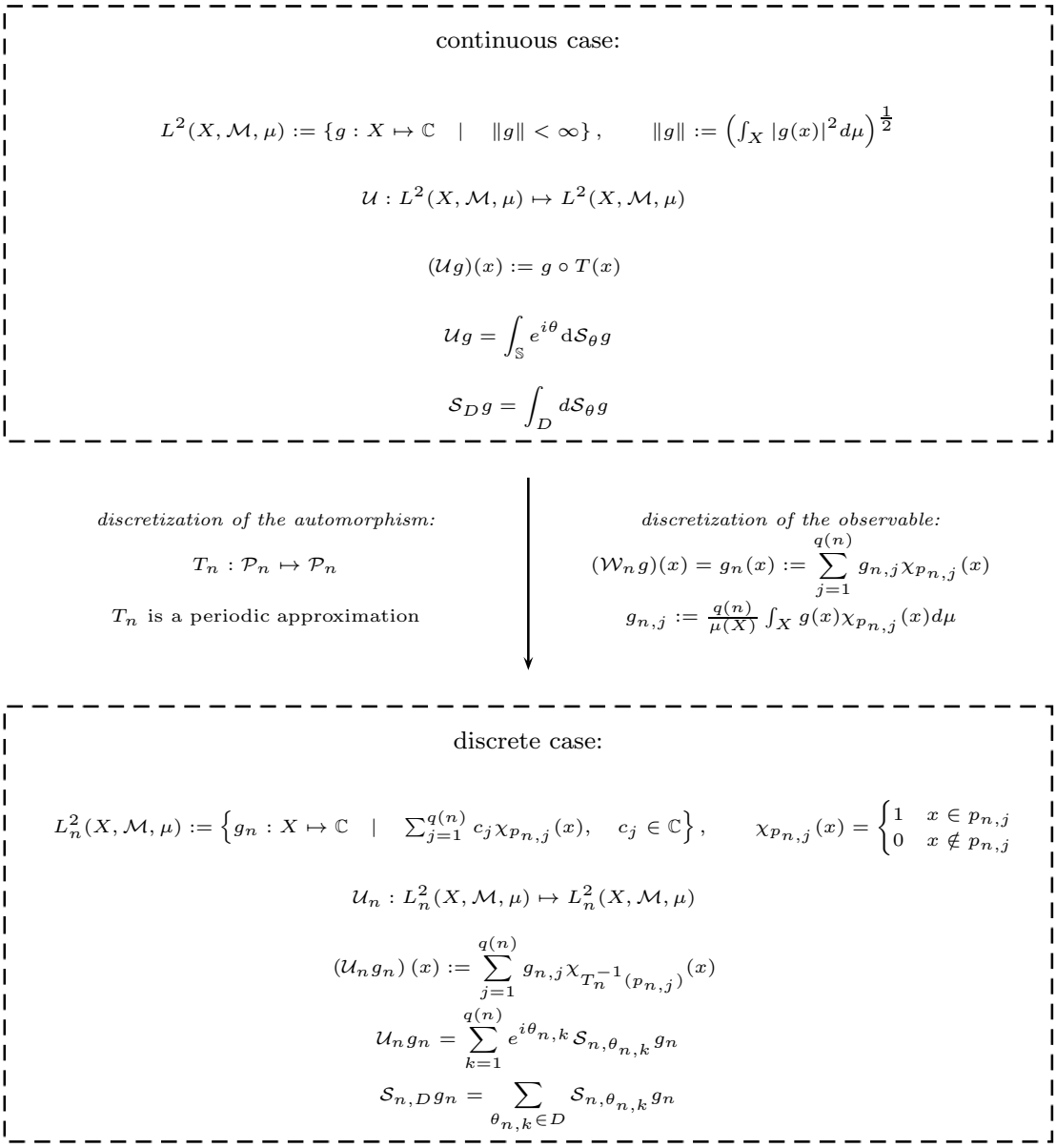

Figure 4.1: An overview of the discretization process.

4.2 Existence of a periodic approximation

It is possible to approximate the map T by a sequence of periodic discrete maps T_n, as the following theorem suggests.

Theorem 4.2.1 (Existence of a periodic approximation)**.** *Let $T : X \mapsto X$ be a con-*

tinuous, measure-preserving automorphism with the invariant measure μ absolutely continuous w.r.t. the Lebesgue measure and $\mathrm{supp}(\mu) = X$. *If $\{\mathcal{P}_n\}_{n=1}^{\infty}$ is a sequence of measurable partitions on X which are refinements and satisfy the conditions* (4.1) *and* (4.2)*, then there exists a sequence of bijective maps $\{T_n : \mathcal{P}_n \mapsto \mathcal{P}_n\}_{n=1}^{\infty}$ that periodically approximates T in an asymptotic sense. More specifically, for every fixed $k \in \mathbb{N}$ and compact set $A \in \mathcal{M}$:*

$$\lim_{n\to\infty} \sum_{l=-k}^{k} d_H(T^l(A), T_n^l(A_n)) = 0 \tag{4.9}$$

where $d_H(A,B) := \max\{\sup_{a\in A} \inf_{b\in B} d(a,b), \sup_{b\in B} \inf_{a\in A} d(a,b)\}$ denotes the Hausdorf metric, and

$$A_n := \bigcup_{p\in\mathcal{P}_n:\ p\cap A\neq\emptyset} p$$

is an over-approximation of A by the partition elements of $\mathcal{P}_n$.

The proof of this result is postponed to the end of this subsection and will involve two intermediate steps. From a numerical analysis standpoint, theorem 4.2.1 claims that one can make the finite-time set evolution of T_n *numerically indistinguishable* from that of the true map in both the forward and backward direction by choosing $n \in \mathbb{N}$ sufficiently large. In fig. 4.2 the situation is sketched for one forward iteration of the map.

Note that the specific formulation of the periodic approximation used in this dissertation is more along the lines of that proposed by Lax [23], and also not equivalent to the ones proposed by Katok and Stepin [25]. There, the quality of the approximation was phrased in the measure-theoretic context, where the proximity of T_n to T is described in terms of the one-iteration cost [25]:

$$\sum_{i=1}^{q(n)} \mu\left(T(p_{n,i}) \Delta T_n(p_{n,i})\right) \tag{4.10}$$

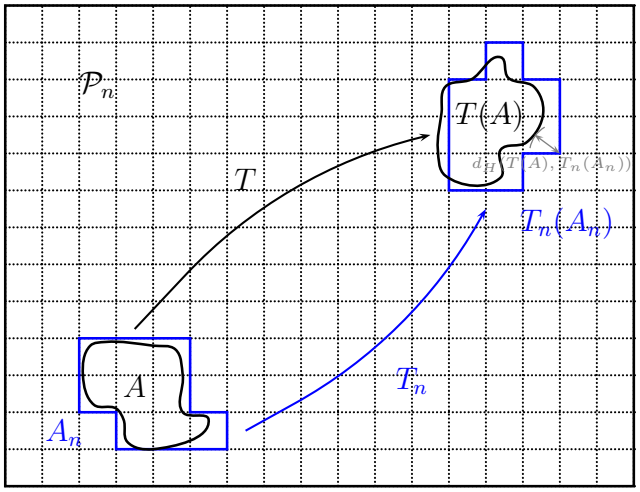

Figure 4.2: Shown is a partition $\mathcal{P}_n$ of a compact domain X into square boxes. The set A is (over-)approximated by the partition elements with A_n. As a consequence of theorem 4.2.1, the distance between the images: $T(A)$ and $T_n(A_n)$, must converge to zero in the Haussdorf metric as the partition is consecutively refined.

with Δ denoting the symmetric set difference, i.e. $A\Delta B := (A\backslash B) \cup (B\backslash A)$. It turns out that a specific sequence of maps $\{T_n : \mathcal{P}_n \mapsto \mathcal{P}_n\}_{n=1}^{\infty}$ may converge in the sense of theorem 4.2.1, while not converging in the sense of (4.10). Relatively simple examples of such sequences may be constructed. Take for example the map $T(x) = (x + \frac{1}{2})$ mod 1 on the unit-length circle and choose a partition $\mathcal{P}_n = \{p_{n,1}, p_{n,2}, \ldots, p_{n,r^n}\}$ with $p_{n,i} = \left[\frac{i-1}{r^n}, \frac{i}{r^n}\right]$ and r being odd. The mapping:

$$T_n(p_{n,j}) = p_{n,j^*}, \qquad j^* = \begin{cases} j + \lfloor \frac{r^n}{2} \rfloor & j + \lfloor \frac{r^n}{2} \rfloor \leq r^n \\ j + \lfloor \frac{r^n}{2} \rfloor - r^n & j + \lfloor \frac{r^n}{2} \rfloor > r^n \end{cases},$$

is the best one can do in terms of the cost (4.10), yet

$$\sum_{i=1}^{q(n)} \mu\left(T(p_{n,i}) \Delta T_n(p_{n,i})\right) = 1, \qquad \forall n \in \mathbb{N}.$$

As further remark, note that the convergence results of the measure-theoretic formulation

(see [21]) were stated for general automorphisms on Lebesgue spaces. Here, the analysis is restricted to just automorphism which are continuous.

Lemma 4.2.2. *Let $T : X \mapsto X$ satisfy the hypothesis stated in theorem 4.2.1. Then, for any partition $\mathcal{P}_n$ that satisfies the condition* (4.1)*, there exists a bijection $T_n : \mathcal{P}_n \mapsto \mathcal{P}_n$ with the property:*

$$T(p_{n,l}) \cap T_n(p_{n,l}) \neq \emptyset \quad \textit{and} \quad T^{-1}(p_{n,l}) \cap T_n^{-1}(p_{n,l}) \neq \emptyset, \qquad \forall l \in \{1, 2, \ldots, q(n)\}\,. \tag{4.11}$$

Proof. It suffices to show that there exists a map $T_n : \mathcal{P}_n \mapsto \mathcal{P}_n$ with the property: $\mu(T(p_{n,l}) \cap T_n(p_{n,l})) > 0$ for all $l \in \{1, 2, \ldots, q(n)\}$. This follows from the fact that $\mu(A \cap B) > 0$ implies $A \cap B \neq \emptyset$ for any $A, B \in \mathcal{M}$, and:

$$\mu(T(p_{n,l}) \cap T_n(p_{n,l})) > 0, \quad \forall l \in \{1, 2, \ldots, q(n)\} \quad \Rightarrow$$
$$\mu(T^{-1}(p_{n,l}) \cap T_n^{-1}(p_{n,l})) > 0, \quad \forall l \in \{1, 2, \ldots, q(n)\}\,.$$

The latter claim is easily verified by contraposition: suppose that $T_n^{-1}(p_{n,k}) = p_{n,s}$ and $\mu(T^{-1}(p_{n,k}) \cap T_n^{-1}(p_{n,k})) = 0$ for some $k \in \{1, 2, \ldots, q(n)\}$, then $\mu(T(p_{n,s}) \cap T_n(p_{n,s})) = 0$.

Let $G_n = (\mathcal{P}_n, \mathcal{P}_n', E)$ denote a bipartite graph where $\mathcal{P}_n'$ is a copy of $\mathcal{P}_n$ and $(p_{n,k}, p_{n,l}) \in E$ if $\mu(T(p_{n,k}) \cap p_{n,l}) > 0$. In order to generate a bijective map so that $\mu(T(p_{n,l}) \cap T_n(p_{n,l})) > 0$ for all $l \in \{1, 2, \ldots, q(n)\}$, every element in $\mathcal{P}_n$ needs to be uniquely paired with one in $\mathcal{P}_n'$ connected by the edges of G_n. Let this new graph be called $\tilde{G}_n = (\mathcal{P}_n, \mathcal{P}_n', \tilde{E})$ (see fig. 4.3). To verify that such a graph assignment is possible, it needs to be confirmed that G_n admits a perfect matching.

To show that this is indeed the case, let $N_G(B) \subset \mathcal{P}_n'$ be the set of all vertices in $\mathcal{P}_n'$ adjacent for some $B \subset \mathcal{P}_n$. By Hall's marriage theorem (see e.g. [35]), G_n has a perfect matching if and only if the cardinality $|B| \leq |N_G(B)|$ for any $B \subset \mathcal{P}_n$. Since T is a

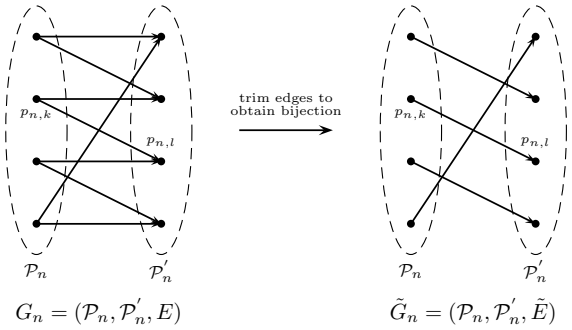

Figure 4.3: Because of the measure-preserving property, the graph G_n satisfies Hall's marriage conditions, and hence admits a perfect matching.

measure-preserving automorphism and because of condition (4.1), it follows that for any $k \in \{1, 2, \ldots, q(n)\}$:

$$\sum_{l=1}^{q(n)} \mu(T(p_{n,k}) \cap p_{n,l}) = \frac{\mu(X)}{q(n)}, \qquad 0 \leq \mu(T(p_{n,k}) \cap p_{n,l}) \leq \frac{\mu(X)}{q(n)}.$$

Because of these properties, it can be deduced that:

$$\begin{aligned} |N_G(B)| &:= \sum_{k \in B} \left(\sum_{l : \mu(T(p_{n,k}) \cap p_{n,l} > 0)} 1 \right) \\ &\geq \sum_{k \in B} \frac{q(n)}{\mu(X)} \sum_{l=1}^{q(n)} \mu(T(p_{n,k}) \cap p_{n,l}) \\ &= \sum_{k \in B} 1 = |B| \end{aligned}$$

for any arbitrary $B \subset \mathcal{P}_n$. Hence, G_n has a perfect matching. □

The value of theorem 4.2.2 is that it can be used as a means to bound the distance between the forward and inverse images of the partition elements in the Hausdorff metric.

Lemma 4.2.3. *Let $T : X \mapsto X$ satisfy the hypothesis stated in theorem 4.2.1 and let $\{\mathcal{P}_n\}_{n=1}^{\infty}$ be a sequence of measurable partitions that satisfy both the conditions* (4.1) *and*

(4.2). *If* $\{T_n : \mathcal{P}_n \mapsto \mathcal{P}_n\}_{n=1}^{\infty}$ *is a sequence of bijective maps which satisfy the property* (4.11) *for each* $n \in \mathbb{N}$*, then*

$$\lim_{n\to\infty} \sum_{l=-k}^{k} \max_{p\in\mathcal{P}_n} d_H(T^l(p), T_n^l(p)) = 0 \tag{4.12}$$

for every $k \in \mathbb{N}$*.*

Proof. This result is proven using induction. Set $k = 1$, if $T_n : \mathcal{P}_n \mapsto \mathcal{P}_n$ is a bijective map satisfying the property (4.11), then:

$$d_H(T(p_{n,j}), T_n(p_{n,j})) \leq \operatorname{diam}(T(p_{n,j})) + \operatorname{diam}(T_n(p_{n,j})) \tag{4.13}$$

and

$$d_H(T^{-1}(p_{n,j}), T_n^{-1}(p_{n,j})) \leq \operatorname{diam}(T^{-1}(p_{n,j})) + \operatorname{diam}(T_n^{-1}(p_{n,j})).$$

Let $\epsilon > 0$ and note that T has a continuous inverse, since the map is a continuous bijection on a compact metric space X. By compactness, there exist a $\delta > 0$ such that:

$$\operatorname{diam}(p_{n,j}) < \delta \qquad \Rightarrow \qquad \operatorname{diam}(T(p_{n,j})) < \epsilon/4, \quad \operatorname{diam}(T^{-1}(p_{n,j})) < \epsilon/4$$

Pick $n \in \mathbb{N}$ so that $l(n) < \min\{\delta, \epsilon/4\}$ to obtain:

$$\begin{aligned} d_H(T^{-1}(p_{n,j}), T_n^{-1}(p_{n,j})) + d_H(T(p_{n,j}), T_n(p_{n,j})) &< \frac{\epsilon}{4} + \min\left\{\delta, \frac{\epsilon}{4}\right\} + \frac{\epsilon}{4} + \min\left\{\delta, \frac{\epsilon}{4}\right\} \\ &\leq \epsilon \end{aligned}$$

Since ϵ and $p_{n,j} \in \mathcal{P}_n$ are both arbitrary, (4.12) is proven for the case where $k = 1$.

Now to prove the result for $k > 1$, note from the triangle inequality that:

$$d_H(T^k(p_{n,j}), T_n^k(p_{n,j})) \leq d_H(T(T^{k-1}(p_{n,j})), T(T_n^{k-1}(p_{n,j}))) + d_H(T(T_n^{k-1}(p_{n,j})), T_n(T_n^{k-1}(p_{n,j})))$$

Using the inductive hypothesis, assume that (4.12) is true for $k-1$ so that the distance $d_H(T^{k-1}(p_{n,j}), T_n^{k-1}(p_{n,j}))$ can be made arbitrarily small by choosing $n \in \mathbb{N}$ sufficiently large. By uniform continuity of T, there exist a $N_a \in \mathbb{N}$ sufficiently large, so that:

$$d_H(T(T^{k-1}(p_{n,j})), T(T_n^{k-1}(p_{n,j}))) \leq \frac{\epsilon}{8} \quad \text{and} \quad d_H(T(T_n^{k-1}(p_{n,j})), T_n(T_n^{k-1}(p_{n,j}))) \leq \frac{\epsilon}{8}$$

for all $n > N_a$. Analogously, there exists a $N_b \in \mathbb{N}$ so that:

$$d_H(T^{-1}(T^{-k+1}(p_{n,j})), T^{-1}(T_n^{-k+1}(p_{n,j}))) \leq \frac{\epsilon}{8}$$

and

$$d_H(T^{-1}(T_n^{-k+1}(p_{n,j})), T^{-1}(T_n^{-k+1}(p_{n,j}))) \leq \frac{\epsilon}{8}$$

for all $n > N_b$. Setting $N_c = \max\{N_a, N_b\}$, one gets:

$$d_H(T^{-k}(p_{n,j}), T_n^{-k}(p_{n,j})) + d_H(T^k(p_{n,j}), T_n^k(p_{n,j})) \leq \frac{\epsilon}{2}$$

for all $n > N_c$. Again, using the inductive hypothesis, there also exists a $N_d \in \mathbb{N}$ so that:

$$\sum_{l=-k+1}^{k-1} d_H(T^l(p_{n,j}), T_n^l(p_{n,j})) \leq \frac{\epsilon}{2}, \qquad \forall n > N_c.$$

By setting $N = \max\{N_c, N_d\}$, one finally obtains:

$$\sum_{l=-k+1}^{k-1} d_H(T^l(p_{n,j}), T_n^l(p_{n,j})) + d_H(T^{-k}(p_{n,j}), T_n^{-k}(p_{n,j})) + d_H(T^k(p_{n,j}), T_n^k(p_{n,j})) \leq \epsilon$$

where $\epsilon > 0$ and $p_{n,j} \in \mathcal{P}_n$ was arbitrary. □

Note that continuity of T plays a critical role in the proof of theorem 4.2.3. Furthermore, observe that T is assumed to have an absolutely continuous invariant measure with $\text{supp}(\mu) = X$, which ensures that both conditions (4.1) and (4.2) are satisfied, simultaneously. With theorems 4.2.2 and 4.2.3, the proof of theorem 4.2.1 can be completed as follows.

Proof of theorem 4.2.1. Let $\{T_n : \mathcal{P}_n \mapsto \mathcal{P}_n\}_{n=1}^{\infty}$ be a sequence of bijective maps that satisfies the property of theorem 4.2.2 for each $n \in \mathbb{N}$. Set $\epsilon > 0$ and note that A_n is compact, since it is a finite union of compact sets. By the triangle inequality, it is known that:

$$\sum_{l=-k}^{k} d_H(T^l(A), T_n^l(A_n)) \leq \sum_{l=-k}^{k} d_H(T^l(A), T^l(A_n)) + \sum_{l=-k}^{k} d_H(T^l(A_n), T_n^l(A_n))$$

It will be shown that each term above can be made arbitrarily small by selecting n sufficiently large. From uniform continuity of T and that $d_H(A, A_n)$ is monotonically decreasing to 0 as $n \to \infty$, it follows that there exists a $N_1 \in \mathbb{N}$ so that the first sum is bounded by $\epsilon/2$ for all $n > N_1$. In order to find also a bound for the second sum, notice

that:

$$\begin{aligned}\sum_{l=-k}^{k} d_H(T^l(A_n), T_n^l(A_n)) &= \sum_{l=-k}^{k} d_H\left(\bigcup_{p\in P_n, p\cap A\neq\emptyset} T^l(p), \bigcup_{p\in P_n, p\cap A\neq\emptyset} T_n^l(p)\right) \\ &\leq \sum_{l=-k}^{k} \max_{p\in P_n, p\cap A\neq\emptyset} d_H(T^l(p), T_n^l(p)) \\ &\leq \sum_{l=-k}^{k} \max_{p\in P_n} d_H(T^l(p), T_n^l(p))\end{aligned}$$

where repetitive use is made of the Haussdorf property:

$$d_H(A\cup B, C\cup D) \leq \max\{d_H(A,C), d_H(B,D)\}$$

in the first inequality. From theorem 4.2.3, it follows that one can choose a $n > N_2$ so that the second sum is also bounded by $\epsilon/2$. Setting $N = \max\{N_1, N_2\}$ completes the proof. □

4.3 Convergence of the operator

Whenever $\{T_n\}_{n=1}^{\infty}$ is a sequence of periodic approximations converging to the T in the sense of theorem 4.2.1, the associated discrete Koopman operators $\{\mathcal{U}_n\}_{n=1}^{\infty}$ approximate the operator (3.8) in some sense as well. To quantify this relationship, the following lemma will be usefull.

Lemma 4.3.1. *Let $\{A_n\}_{n=1}^{\infty}$ be a sequence of compact sets converging monotonically to the compact set A in the Haussdorf metric (i.e. $\lim_{n\to\infty} d_H(A, A_n) = 0$) and suppose that $\mu(A_n) = \mu(A)$ for every $n \in \mathbb{N}$. Then,*

$$\lim_{n\to\infty} \mu(A\Delta A_n) = 0 \tag{4.14}$$

Proof. By definition: $\mu(A\Delta A_n) = \mu(A \setminus A_n) + \mu(A_n \setminus A)$, and hence, to prove (4.14) one must show that both of these terms go to zero in the limit. However, since $\mu(A_n) = \mu(A)$, and:

$$\mu(A_n \setminus A) = \mu(A_n) - \mu(A \cap A_n), \qquad \mu(A \setminus A_n) = \mu(A) - \mu(A \cap A_n)$$

it follows that $\mu(A \setminus A_n) = \mu(A_n \setminus A)$, and therefore it sufficient to show that either $\mu(A \setminus A_n)$ or $\mu(A_n \setminus A)$ tends to zero.

Consider $\mu(A_n \setminus A)$. Let $A_{\epsilon(n)} := \bigcup_{x \in A} B_{\epsilon(n)}(x)$ be the $\epsilon(n)$-fattening of A where $\epsilon(n) := d_H(A, A_n)$. Observe that:

$$(A_n \setminus A) \subset (A_{\epsilon(n)} \setminus A) \qquad \Rightarrow \qquad 0 \leq \mu(A_n \setminus A) \leq \mu(A_{\epsilon(n)} \setminus A)$$

Since $\epsilon(n)$ is a monotonically decreasing sequence, from Theorem 1.19(e) in [36], it is known that:

$$\bigcap_{n=1}^{\infty} A_{\epsilon(n)} = A \quad \text{and} \quad \mu(A_{\epsilon(n)}) \to \mu(A) \text{ as } n \to \infty.$$

Therefore, $\mu(A_{\epsilon(n)} \setminus A) \to 0$ as $n \to \infty$, leading to the desired result. □

In addition to theorem 4.3.1, some properties on the averaging operation (4.3) must also be identified. The operator (4.3) is an *approximation of the identity* and therefore $\|g - g_n\| \to 0$ as $n \to \infty$. This property can be verified by first establishing this fact for continuous observables and then employ the fact that $C(X)$ is dense in $L^2(X, \mathcal{M}, \mu)$. In addition to being an approximation to the identity, (4.3) is an orthogonal projector which maps observables $g \in L^2(X, \mathcal{M}, \mu)$ to their best approximations $g_n \in L^2_n(X, \mathcal{M}, \mu)$. This follows from the fact that $\mathcal{W}_n$ is idempotent and that $\langle g - \mathcal{W}_n g, \mathcal{W}_n g \rangle = 0$.

Lemma 4.3.2. *Let $T : X \mapsto X$ satisfy the hypothesis of theorem 4.2.1 and suppose that $\{T_n : \mathcal{P}_n \mapsto \mathcal{P}_n\}_{n=1}^{\infty}$ is a sequence of discrete maps that periodically approximates T in the*

sense of (4.9). *Define:*

$$g = \sum_{j=1}^{q(m)} c_j \chi_{p_{m,j}} \in L^2_m(X, \mathcal{M}, \mu), \qquad m \in \mathbb{N}$$

Then:

$$\lim_{n\to\infty} \sum_{l=-k}^{k} \left\| \mathcal{U}^l g - \mathcal{U}_n^l g_n \right\|^2 = 0$$

for every $k \in \mathbb{N}$.

Proof. For notational clarity, write $A^{(j)} := p_{m,j}$, $g^{(j)} := \chi_{p_{m,j}}$ and $g_n^{(j)} := \mathcal{W}_n g^{(j)}$. The following can be derived:

$$\begin{aligned}
\sum_{l=-k}^{k} \left\| \mathcal{U}^l g - \mathcal{U}_n^l g_n \right\|^2 &= \sum_{l=-k}^{k} \left\| \sum_{j=1}^{q(m)} c_j (\mathcal{U}^l g^{(j)} - \mathcal{U}_n^l g_n^{(j)}) \right\|^2 \\
&\leq \sum_{l=-k}^{k} \left(\sum_{j=1}^{q(m)} |c_j| \left\| \mathcal{U}^l g^{(j)} - \mathcal{U}_n^l g_n^{(j)} \right\| \right)^2 \\
&\leq M \sum_{j=1}^{q(m)} \left(\sum_{l=-k}^{k} \left\| \mathcal{U}^l g^{(j)} - \mathcal{U}_n^l g_n^{(j)} \right\|^2 \right), \qquad M = \sum_{j=1}^{q(m)} |c_j|^2 \\
&\leq q(m) M \max_{j=1,\ldots,q(m)} \left(\sum_{l=-k}^{k} \left\| \mathcal{U}^l g^{(j)} - \mathcal{U}_n^l g_n^{(j)} \right\|^2 \right)
\end{aligned}$$

Hence, it suffices to show that:

$$\lim_{n\to\infty} \sum_{l=-k}^{k} \left\| \mathcal{U}^l g^{(j)} - \mathcal{U}_n^l g_n^{(j)} \right\|^2 = 0, \qquad j = 1, \ldots, m. \tag{4.15}$$

Since $\{\mathcal{P}_n\}_{n=1}^{\infty}$ are consecutive refinements, observe that $g_n^{(j)} = g^{(j)}$ for $n \geq m$, which

implies:

$$\begin{aligned}\sum_{l=-k}^{k} \left\|\mathcal{U}^l g^j - \mathcal{U}_n^l g_n^{(j)}\right\|^2 &= \sum_{l=-k}^{k} \left\|(\mathcal{U}^l - \mathcal{U}_n^l) g^{(j)}\right\|^2, \qquad \text{if } n \geq m \\ &= \sum_{l=-k}^{k} \mu(T^{-l}(A^{(j)}) \Delta T_n^{-l}(A^{(j)})).\end{aligned}$$

By theorem 4.2.1, $\left\{T_n^{-l}(A^{(j)}))\right\}_{n=m}^{\infty}$ converges to $T^{-l}(A^{(j)})$ in the Haussdorf metric. Also, since $\mu(T^{-l}(A^{(j)})) = \mu(T_n^{-l}(A^{(j)}))$ for $n \geq m$, it follows from theorem 4.3.1 that:

$$\sum_{l=-k}^{k} \mu(T^{-l}(A^{(j)}) \Delta T_n^{-l}(A^{(j)})) \to 0 \qquad \text{as } n \to \infty.$$

□

Theorem 4.3.3 (Operator convergence)**.** *Let $T : X \mapsto X$ satisfy the hypothesis of theorem 4.2.1 and suppose that $\{T_n : \mathcal{P}_n \mapsto \mathcal{P}_n\}_{n=1}^{\infty}$ is a sequence of discrete maps that periodically approximates T in the sense of* (4.9)*. Then, $\{\mathcal{U}_n : L_n^2(X, \mathcal{M}, \mu) \mapsto L_n^2(X, \mathcal{M}, \mu)\}_{n=1}^{\infty}$ converges to $\mathcal{U}$ in the following sense:*

$$\lim_{n\to\infty} \sum_{l=-k}^{k} \left\|\mathcal{U}^l g - \mathcal{U}_n^l g_n\right\|^2 = 0 \tag{4.16}$$

for every fixed $k \in \mathbb{N}$ and $g \in L^2(X, \mathcal{M}, \mu)$.

Proof. Let $\epsilon > 0$ and define:

$$g_m = \sum_{j=1}^{q(m)} c_j \chi_{p_{m,j}} \in L_m^2(X, \mathcal{M}, \mu), \qquad m \in \mathbb{N}.$$

The following manipulations are performed:

$$\begin{aligned}
\sum_{l=-k}^{k} \left\|\mathcal{U}^l g - \mathcal{U}_n^l g_n\right\|^2 &= \sum_{l=-k}^{k} \left\|\mathcal{U}^l(g - g_m + g_m) - \mathcal{U}_n^l(g - g_m + g_m)_n\right\|^2 \\
&\leq \sum_{l=-k}^{k} \left(\|g - g_m\| + \|\mathcal{W}_n(g - g_m)\| + \left\|\mathcal{U}^l g_m - \mathcal{U}_n^l (g_m)_n\right\|\right)^2 \\
&\leq \sum_{l=-k}^{k} \left(2\|g - g_m\| + \left\|\mathcal{U}^l g_m - \mathcal{U}_n^l (g_m)_n\right\|\right)^2 \\
&\leq \left(\left(\sum_{l=-k}^{k} 4\|g - g_m\|^2\right)^{\frac{1}{2}} + \left(\sum_{l=-k}^{k} \left\|\mathcal{U}^l g_m - \mathcal{U}_n^l (g_m)_n\right\|^2\right)^{\frac{1}{2}}\right)^2 \\
&= \left(2\|g - g_m\| + \left(\sum_{l=-k}^{k} \left\|\mathcal{U}^l g_m - \mathcal{U}_n^l (g_m)_n\right\|^2\right)^{\frac{1}{2}}\right)^2
\end{aligned}$$

Since (4.3) is approximation of the identity, one can select a $m \in \mathbb{N}$ so that $\|g - g_m\| \leq \frac{1}{4}\sqrt{\epsilon}$. Using theorem 4.3.2 further establishes that there exists a $N \in \mathbb{N}$ such that:

$$\sum_{l=-k}^{k} \left\|\mathcal{U}^l g_m - \mathcal{U}_n^l (g_m)_n\right\| \leq \frac{\epsilon}{4}, \qquad \forall n \geq N.$$

Overall, the following can be established:

$$\sum_{l=-k}^{k} \left\|\mathcal{U}^l g - \mathcal{U}_n^l g_n\right\|^2 \leq \epsilon,$$

which confirms (4.16). □

4.4 Convergence of spectra

In this section, it will be analyzed how the spectral projectors (4.7) converge to (3.10) in the limit.

4.4.1 An illuminating example

Before proceeding to the general results, it is worthwhile to work out the details of a periodic approximation for a basic example in order to clarify certain subtelties on weak vs. strong convergence of the spectra. In particular, consider the map:

$$T(x) = (x + \frac{1}{2}) \mod 1, \quad x \in [0, 1),$$

which is rotation on the circle by a half.

For the partition $\mathcal{P}_n = \{p_{n,1}, p_{n,2}, \ldots, p_{n,r^n}\}$ with $p_{n,j} = \left(\frac{j-1}{r^n}, \frac{j}{r^n}\right)$, $j = 1, \ldots, r^n$ for some integer $r > 1$, one may define the sequence of maps[1]:

$$T_n(p_{n,j}) = p_{n,j^*}, \qquad j^* = \begin{cases} j + \lfloor \frac{r^n}{2} \rfloor & j + \lfloor \frac{r^n}{2} \rfloor \leq r^n \\ j + \lfloor \frac{r^n}{2} \rfloor - r^n & j + \lfloor \frac{r^n}{2} \rfloor > r^n \end{cases},$$

which clearly is a periodic approximation to the original transformation in the sense of theorem 4.2.1. The discrete Koopman operator associated with this map is isometric to the circulant matrix. That is, the permutation matrices:

$$[\mathrm{U}_n]_{ij} = \langle \mathcal{U}_n \chi_{p_{n,i}}, \chi_{p_{n,j}} \rangle,$$

[1] $\lfloor \cdot \rfloor$ denotes here the floor function.

are equal to the circulant matrices:

$$\mathrm{U}_n = \begin{bmatrix} d_1 & d_{r^n} & \cdots & d_3 & d_2 \\ d_2 & d_1 & d_{r^n} & & d_3 \\ \vdots & d_2 & d_1 & \ddots & \vdots \\ d_{r^n-1} & & \ddots & \ddots & d_{r^n} \\ d_{r^n} & d_{r^n-1} & \cdots & d_2 & d_1 \end{bmatrix}, \quad \text{where } d_{\lfloor \frac{r^n}{2} \rfloor + 1} = 1 \text{ and zero otherwise.}$$

The spectral decomposition of a circulant matrix can be obtained in closed-form using the Discrete Fourier Transform [2]:

$$v_{n,k}(x) = \frac{1}{\sqrt{r^n}} \sum_{j=1}^{r^n} e^{2\pi i \frac{(k-1)(j-1)}{r^n}} \chi_{p_{n,j}}(x), \qquad \theta_{n,k} = \begin{cases} \frac{(-1)^k+1}{2}\pi & r \text{ is even} \\ \frac{(-1)^k+1}{2}\pi - \frac{k-1}{r^n}\pi & r \text{ is odd} \end{cases}. \tag{4.17}$$

Recall that the spectra of the true (i.e. infinite-dimensional) operator consists of only two eigenvalues located at 1 and -1. Yet, from the equations above, it can be seen that this property is maintained for the discrete analogue when r is an even number. For an odd r, the eigenvalues of the discrete Koopman operators seem to densely fill up the unit circle as $n \to \infty$.

At first sight, this fragility of the spectrum in the discretization process appear as a serious problem. However, if one weakens the notion of what it means for the discretizations to converge spectrally, this issue can be largely avoided. The ordering of the eigenvalue-eigenvector pairs $\{\theta_{n,k}, v_{n,k}\}_{k=1}^{r^n}$ in (4.17) provide clues on what approach should be taken. Particularly, notice that the first set of eigenvalues (corresponding to the slower oscillatory modes) are concentrated around the points $\theta = 0$ and $\theta = \pi$. One may then ask which of the eigenvalue-eigenvector pairs actually play a significant role in

[2] The scaling $1/\sqrt{r^n}$ here is required for normalization.

the spectral approximation of a specific *fixed* observable. The following can be observed.

After application of the smoothing operator (4.3), any square-integrable observable $g \in L_n^2(\mathbb{T}, \mathcal{B}(\mathbb{T}), \mu)$ on the circle (with μ being the standard Lebesgue measure in this case), can be written in terms of the eigenvectors:

$$g_n(x) = \sum_{k=1}^{r^n} c_{n,k} v_{n,k}(x),$$

where $v_{n,k} \in L_n^2(\mathbb{T}, \mathcal{B}(\mathbb{T}), \mu)$ are nothing else but the discrete analogues of the Fourier harmonics (see (4.17)). Henceforth, one can show that for any $\epsilon > 0$, there exists an $m = m(\epsilon) \in \mathbb{N}$ and a $N \in \mathbb{N}$ so that:

$$\|g_n\| - \epsilon < \sum_{k \leq m} |c_{n,k}|^2 \leq \|g_n\|, \qquad \forall n \geq N.$$

For this specific m which only depends on ϵ, the set $\{\theta_{n,k} \in \mathbb{S} : k \leq m\}$ is at most a δ-distance separated from the eigenfrequencies $\theta = 0$ and $\theta = \pi$, where $\delta > 0$ can be made arbitrarily small by choosing sufficiently large $n \in \mathbb{N}$.

In other words, as n approaches infinity, most of the "spectral energy" will get concentrated around the eigenvalues. From this perspective, the discrete analogues of the Koopman operator do seem to approximate the infinite analogue spectrally. The situation described here is not something which holds true for only this basic example, but applies more generally.

4.4.2 Approximation of the spectral projectors

Consider any smooth test function $\varphi \in \mathcal{D}(\mathbb{S})$ on the circle, and define:

$$\mathcal{S}_\varphi g = \int_{\mathbb{S}} \varphi(\theta) \mathrm{d}\mathcal{S}_\theta g, \qquad \mathcal{S}_{n,\varphi} g_n = \sum_{\theta_{n,k} \in \mathbb{S}} \varphi(\theta_{n,k}) \mathcal{S}_{n,\theta_{n,k}} g_n.$$

The following can be established.

Theorem 4.4.1. *Let $T : X \mapsto X$ satisfy the hypothesis of theorem 4.2.1 and suppose that $\{T_n : \mathcal{P}_n \mapsto \mathcal{P}_n\}_{n=1}^{\infty}$ is a sequence of discrete maps that periodically approximates T in the sense of (4.9). For any smooth test function $\varphi \in \mathcal{D}(\mathbb{S})$ and observable $g \in L^2(X, \mathcal{M}, \mu)$, the following holds:*

$$\lim_{n\to\infty} \|\mathcal{S}_\varphi g - \mathcal{S}_{n,\varphi} g_n\| = 0.$$

Proof. Expand the smoothed indicator function $\varphi(\theta)$ by its Fourier series: $\varphi(\theta) = \sum_{l=-\infty}^{\infty} b_l e^{il\theta}$, and note that the series is uniformly convergent. Next, observe that:

$$\mathcal{S}_\varphi g = \int_{\mathbb{S}} \left(\sum_{l=-\infty}^{\infty} b_l e^{il\theta} \right) \mathrm{d}\mathcal{S}_\theta g = \sum_{l=-\infty}^{\infty} b_l \left(\int_{\mathbb{S}} e^{il\theta} \mathrm{d}\mathcal{S}_\theta g \right) = \sum_{l=-\infty}^{\infty} b_l \mathcal{U}^l g,$$

where the last equality is a consequence of the spectral theorem of unitary operators [34]. Similarly, it also holds that:

$$\mathcal{S}_{n,\varphi} g_n = \sum_{l=-\infty}^{\infty} b_l \mathcal{U}_n^l g_n$$

Hence,

$$\mathcal{S}_\varphi g - \mathcal{S}_{n,\varphi} g_n = \sum_{l=-\infty}^{\infty} b_l (\mathcal{U}^l g - \mathcal{U}_n^l g_n)$$

Now let $\epsilon > 0$ and choose $k \in \mathbb{N}$ such that:

$$\sum_{|l|>k} |b_l| < \frac{\epsilon}{4\,\|g\|}$$

This is possible, because the Fourier coefficients of $\varphi(\theta)$ are absolutely summable. Write:

$$\begin{aligned}
\|\mathcal{S}_\varphi g - \mathcal{S}_{n,\varphi} g_n\| &\leq \sum_{l=-\infty}^{\infty} |b_l| \left\|\mathcal{U}^l g - \mathcal{U}_n^l g_n\right\| \\
&= \sum_{l=-k}^{k} |b_l| \left\|\mathcal{U}^l g - \mathcal{U}_n^l g_n\right\| + \sum_{|l|>k} |b_l| \left\|\mathcal{U}^l g - \mathcal{U}_n^l g_n\right\| \\
&\leq M \sum_{l=-k}^{k} \left\|\mathcal{U}^l g - \mathcal{U}_n^l g_n\right\| + 2\|g\| \sum_{|l|>k} |b_l| \\
&\leq M \sum_{l=-k}^{k} \left\|\mathcal{U}^l g - \mathcal{U}_n^l g_n\right\| + \frac{\epsilon}{2}
\end{aligned}$$

For a fixed $k \in \mathbb{N}$, it follows from theorem 4.3.3 that there exist an $N \in \mathbb{N}$ so that[3]

$$\sum_{l=-k}^{k} \left\|\mathcal{U}^l g - \mathcal{U}_n^l g_n\right\| \leq \frac{\epsilon}{2M}, \qquad \forall n \geq N.$$

This yields:

$$\|\mathcal{S}_\varphi g - \mathcal{S}_{n,\varphi} g_n\| \leq \epsilon.$$

□

Remark 4.4.2. Note that in the proof of theorem 4.4.1, explicit use is made of the fact that the discrete operators are unitary, which in turn is a consequence of the periodic approximation. Therefore, the arguments in the proof would break down if the periodic approximation was replaced with a many-to-one map.

Recall the spectral projectors (3.10) and (4.7), and notice that they may be re-

[3]Note that the squaring of the norms in theorem 4.3.3 is immatarial for a finite sum.

expressed as:

$$\mathcal{S}_D g = \int_{\mathbb{S}} \chi_D(\theta) \mathrm{d}\mathcal{S}_\theta g, \qquad \mathcal{S}_{n,D} g_n = \sum_{\theta_{n,k} \in \mathbb{S}} \chi_D(\theta_{n,k}) \mathcal{S}_{n,\theta_{n,k}} g_n,$$

where $\chi_D(\theta)$ is an indicator function on the circle for the interval D. To avoid technicalities like having eigenvalues on the boundary of D, a smoothed version of the projectors using summability kernels [37] will be considered. That is, for some $0 < \alpha < 2\pi$, define $\varphi_\alpha : \mathbb{S} \times \mathbb{S} \mapsto \mathbb{R}_+$:

$$\varphi_\alpha(x,y) = \begin{cases} \frac{K}{\alpha} \exp\left(\frac{-1}{1-\left(\frac{d(x,y)}{\alpha}\right)^2} \right) & \frac{d(x,y)}{\alpha} < 1 \\ 0 & \text{otherwise} \end{cases}, \tag{4.18}$$

where $d(x,y)$ is the Euclidian metric on $\mathbb{S}$ and $K = (\int_{-1}^{1} \exp(\frac{-1}{1-x^2}) \mathrm{d}x)^{-1}$. Now replace the indicator function with:

$$\chi_{D_\alpha}(\theta) = \int_{\mathbb{S}} \varphi_\alpha(\theta, \xi) \chi_D(\xi) \mathrm{d}\xi,$$

and define:

$$\mathcal{S}_{D_\alpha} = \int_{\mathbb{S}} \chi_{D_\alpha}(\theta) \mathrm{d}\mathcal{S}_\theta g, \qquad , \qquad \mathcal{S}_{n,D_\alpha} g_n = \sum_{\theta_{n,k} \in \mathbb{S}} \chi_{D_\alpha}(\theta_{n,k}) \mathcal{S}_{n,\theta_{n,k}} g_n. \tag{4.19}$$

The following corollary is obtained.

Corollary 4.4.3 (Convergence of spectral projectors)**.** *Given any* $0 < \alpha < 2\pi$ *and interval* $D \subset \mathbb{S}$*, it follows that:*

$$\lim_{n \to \infty} \| \mathcal{S}_{D_\alpha} g - \mathcal{S}_{n,D_\alpha} g_n \| = 0,$$

where $g \in L^2(X, \mathcal{M}, \mu)$.

4.4.3 Approximation of the spectral density function

Recall the definitions of the spectral density function $\rho(\theta; g) \in \mathcal{D}^*(\mathbb{S})$, along with its discrete analogue (4.8):

$$\rho_n(\theta; g_n) = \sum_{k=1}^{q(n)} \left\| \mathcal{S}_{n,\theta_{n,k}} g_n \right\|^2 \delta(\theta - \theta_{n,k})$$

To assess the convergence of $\rho_n(\theta; g_n)$ to $\rho(\theta; g)$, the summability kernels will again be employed (4.18). The following result may be established.

Theorem 4.4.4 (Approximation of the spectral density function)**.** *Let:*

$$\rho_\alpha(\theta; g) := \int_{\mathbb{S}} \varphi_\alpha(\theta, \xi)\rho(\xi; g)\mathrm{d}\xi, \qquad \rho_{\alpha,n}(\theta; g_n) := \int_{\mathbb{S}} \varphi_\alpha(\theta, \xi)\rho_n(\xi; g_n)\mathrm{d}\xi. \tag{4.20}$$

Then:

$$\lim_{n\to\infty} \rho_{\alpha,n}(\theta; g_n) = \rho_\alpha(\theta; g), \quad \textit{uniformly.}$$

Proof. To prove uniform convergence, two facts will be established: (i) $\rho_\alpha(\theta; g) - \rho_{\alpha,n}(\theta; g_n)$ forms an equicontinuous family, and (ii) $\rho_{\alpha,n}(\theta; g_n)$ converges to $\rho_\alpha(\theta; g)$ in the L^2-norm. Uniform convergence of $\rho_{\alpha,n}(\theta; g_n)$ to $\rho_\alpha(\theta; g)$ is an immediate consequence of these facts. Indeed, if this wasn't the case, there would exist an $\epsilon > 0$ and a subsequence n_k such that $|\rho_\alpha(\theta_k; g) - \rho_{\alpha,n_k}(\theta_k; g_{n_k})| \geq \epsilon$ for all $k \in \mathbb{N}$. But by equicontinuity, one can choose a $\delta > 0$ such that:

$$d\left(\rho_\alpha(\phi; g) - \rho_{\alpha,n}(\phi; g_n), \rho_\alpha(\theta; g) - \rho_{\alpha,n}(\theta; g_n)\right) < \epsilon/2, \quad \text{whenever } d(\phi, \theta) < \delta.$$

This leads to a contradiction to (ii) as $||\rho_\alpha(\cdot; g) - \rho_{\alpha,n_k}(\cdot; g_{n_k})||_2 \geq \epsilon/2\sqrt{\delta}$. What follows

next is a derivation of the claims (i) and (ii):

1. To show that $\rho_\alpha(\theta; g) - \rho_{\alpha,n}(\theta; g_n)$ is an equicontinuous family, it suffices to verify that the derivative $\rho_\alpha^{'}(\theta; g) - \rho_{\alpha,n}^{'}(\theta; g_n)$ is uniformly bounded. Consider the fourier expansion of $\rho_\alpha(\theta; g) - \rho_{\alpha,n}(\theta; g_n)$:

$$\rho_\alpha(\theta; g) - \rho_{\alpha,n}(\theta; g_n) = \frac{1}{2\pi} \sum_{l \in \mathbb{Z}} b_n(l; g) e^{il\theta}$$

where:

$$b_n(l; g) := \int_{\mathbb{S}} e^{-il\theta} \left(\rho_\alpha(\theta; g) - \rho_{\alpha,n}(\theta; g_n)\right) \mathrm{d}\theta$$

According to the spectral theorem of unitary operators [34], it follows that:

$$a(l; g) := \int_{\mathbb{S}} e^{-il\theta} \rho(\theta; g) \mathrm{d}\theta = \langle g, \mathcal{U}^l g \rangle,$$

and

$$a_n(l; g_n) := \int_{\mathbb{S}} e^{-il\theta} \rho_n(\theta; g_n) \mathrm{d}\theta = \langle g_n, \mathcal{U}_n^l g_n \rangle, \qquad l \in \mathbb{Z}.$$

The functions $\rho_\alpha(\theta; g)$ and $\rho_{\alpha,n}(\theta; g_n)$ are defined as convolutions with a C^∞ smooth function, and recognizing that convolutions implies pointwise multiplication in the Fourier domain, it follows that:

$$b_n(l; g) = d_\alpha(l)(a(l; g) - a_n(l; g_n)),$$

where:

$$d_\alpha(l) := \int_{\mathbb{S}} e^{-il\theta} \varphi_\alpha(\theta, 0) \mathrm{d}\theta \quad \text{and} \quad |d_\alpha(l)| \leq \frac{C_\alpha}{1 + |l|^N} \text{ for every } N \in \mathbb{N}.$$

Now examining the derivative $\rho_{\alpha}^{'}(\theta;g)-\rho_{\alpha,n}^{'}(\theta;g_n)$ more closely, it can be seen that:

$$\begin{aligned}\left|\rho_{\alpha}^{'}(\theta;g)-\rho_{\alpha,n}^{'}(\theta;g_n)\right| &= \left|\frac{1}{2\pi}\sum_{l\in\mathbb{Z}} ilb_n(l;g)e^{il\theta}\right| \\ &\leq \frac{1}{2\pi}\sum_{l\in\mathbb{Z}}|l||b_n(l;g)| \\ &= \frac{1}{2\pi}\sum_{l\in\mathbb{Z}}|l||d_{\alpha}(l)|\,|a(l;g)-a_n(l;g_n)| \\ &= \frac{1}{2\pi}\sum_{l\in\mathbb{Z}}|l||d_{\alpha}(l)|\left|\langle g,\mathcal{U}^l g\rangle-\langle g_n,\mathcal{U}_n^l g_n\rangle\right| \\ &\leq \frac{\|g\|^2}{\pi}\sum_{l\in\mathbb{Z}}\frac{C_{\alpha}|l|}{1+|l|^N},\end{aligned}$$

which is a convergent sum for $N\geq 3$. Notice that summability is possible because the constant C_{α} only depends on α and is independent of n.

2. To show that $\rho_{\alpha,n}(\omega;g_n)$ converges to $\rho_{\alpha}(\omega;g)$ in the L^2-norm, Parseval's identity can be used to confirm that the sum: $\sum_{l\in\mathbb{Z}}|b_n(l;g)|^2$ can be made arbitrarily small. At first, note that:

$$a(l;g)-a_n(l;g_n)=\langle g,\mathcal{U}^l g-\mathcal{U}_n^l g_n\rangle-\langle g-g_n,\mathcal{U}_n^l g_n\rangle$$

By the triangle inequality and Cauchy-Schwarz, it follows that:

$$\begin{aligned}|a(l;g)-a_n(l;g_n)| &\leq \|g\|\left\|\mathcal{U}^l g-\mathcal{U}_n^l g_n\right\|+\|g-g_n\|\left\|\mathcal{U}_n^l g_n\right\| \\ &\leq \|g\|\left(\left\|\mathcal{U}^l g-\mathcal{U}_n^l g_n\right\|+\|g-g_n\|\right).\end{aligned}$$

Let $\epsilon>0$, and choose $k\in\mathbb{N}$ such that:

$$\sum_{|l|>k}|d_{\alpha}(l)|^2\leq\epsilon. \tag{4.21}$$

This is always possible, because $\varphi_\alpha(\theta, 0)$ is a C^∞ smooth function, and therefore also square-integrable. The following upper bound can be established:

$$\begin{aligned}
\sum_{l=-\infty}^{\infty} |b_n(l;g)|^2 &= \sum_{l=-\infty}^{\infty} |d_\alpha(l)|^2 |a(l;g) - a_n(l;g_n)|^2 \\
&\leq \sum_{l=-\infty}^{\infty} |d_\alpha(l)|^2 \left(\|g\| \left(\left\| \mathcal{U}^l g - \mathcal{U}_n^l g_n \right\| + \|g - g_n\| \right) \right)^2 \\
&\leq \|g\|^2 \max_{-k \leq l \leq k} |d_\alpha(l)|^2 \sum_{l=-k}^{k} \left\| \mathcal{U}^l g - \mathcal{U}_n^l g_n \right\|^2 + 16 \|g\|^2 \sum_{|l|>k} |d_\alpha(l)|^2 \\
&\quad + \|g\|^2 \|g - g_n\| \sum_{l=-\infty}^{\infty} |d_\alpha(l)|^2 \left(2 \left\| \mathcal{U}^l g - \mathcal{U}_n^l g_n \right\| + \|g - g_n\| \right).
\end{aligned}$$

Now apply (4.21) and theorem 4.3.3 to complete the proof.

□

Chapter 5

Periodic approximations - generalization to flows

Let $S^t : X \mapsto X$ denote a Lipschitz continuous flow on a compact *norm-induced* metric space $X \subseteq \mathbb{R}^m$, with S^t satisfying the well-known group properties: $S^t \circ S^s(x) = S^{t+s}(x)$ for any $t, s \in \mathbb{R}$, and $S^0(x) = x$. Associate with X the measure space $(X, \mathcal{M}, \mu)$, where $\mathcal{M}$ denotes the Borel sigma-algebra, and μ is an absolutely continuous measure with full support on the state-space, i.e. supp $\mu = X$. The flow S^t is assumed to be invariant with respect to the measure μ, i.e. for every $t \in \mathbb{R}$ and $B \in \mathcal{M}$: $\mu(B) = \mu(S^t(B))$.

In this chapter, the concept of periodic approximations is generalized for the unitary Koopman family $\mathcal{U}^t : L^2(X, \mathcal{M}, \mu) \mapsto L^2(X, \mathcal{M}, \mu)$ associated with S^t. A specific condition is derived on the spatial and temporal discretization so that the spectra can be approximated in a similar manner as in chapter 4.

5.1 Discretization of the Koopman operator family

The discretization of the Koopman operator family can be broken-down into two steps: a temporal discretization and a spatial discretization.

5.1.1 The temporal discretization

Let $\{\tau(n)\}_{n=1}^{\infty} \subset \mathbb{R}^+$ denote a monotonically decreasing sequence converging to zero. The first step in the discretization process is to convert the flow to an automorphism by considering $\tau(n)$-map $S^{\tau(n)} : X \mapsto X$. By doing so, one obtain the discrete one-parameter group: $\{S^{k\tau(n)}\}_{k\in\mathbb{Z}}$ along with its Koopman linearization:

$$\left\{\mathcal{U}^{k\tau(n)} : L^2(X, \mathcal{M}, \mu) \mapsto L^2(X, \mathcal{M}, \mu)\right\}_{k\in\mathbb{Z}},$$

where:

$$(\mathcal{U}^{k\tau(n)}g)(x) = g \circ S^{k\tau(n)}(x), \qquad k \in \mathbb{Z}. \tag{5.1}$$

According to the spectral theorem [34], (5.1) admits the decomposition:

$$\mathcal{U}^{k\tau(n)}g = \int_{\mathbb{S}} e^{ik\theta} \mathrm{d}\hat{\mathcal{S}}_{\theta}^{\tau(n)} g, \qquad k \in \mathbb{Z}. \tag{5.2}$$

Here, $\hat{\mathcal{S}}_{\theta}^{\tau(n)}$ is a self-adjoint, projection-valued measure on the Borel sigma-algebra of the circle $\mathcal{B}(\mathbb{S})$, parameterized by $\theta \in [-\pi, \pi)$. The projection-valued measure on the circle can be mapped on the real line by introducing $\mathcal{S}_{\omega}^{\tau(n)}$ such that:

$$\mathcal{S}_{\omega}^{\tau(n)} = \hat{\mathcal{S}}_{\theta}^{\tau(n)}, \qquad \text{whenever } \theta = (\tau(n)\{\omega\}) \cap [-\pi, \pi).$$

By doing so, (5.2) can be rewritten as:

$$\mathcal{U}^{k\tau(n)}g = \int_{\mathbb{R}} e^{ik\omega\tau(n)}\mathrm{d}\mathcal{S}_{\omega}^{\tau(n)}g = \int_{-\hat{\omega}(n)}^{\hat{\omega}(n)} e^{ik\omega\tau(n)}\mathrm{d}\mathcal{S}_{\omega}^{\tau(n)}g, \qquad k \in \mathbb{Z}. \tag{5.3}$$

where $\hat{\omega}(n)$ denotes the *spectral bandwith*:

$$\hat{\omega}(n) = \pi/\tau(n). \tag{5.4}$$

For any interval $D = [a, b) \subset [-\hat{\omega}(n), \hat{\omega}(n))$ contained within the spectral bandwith, consider the spectral projection:

$$\mathcal{S}_{D}^{\tau(n)}g := \int_{D} \mathrm{d}\mathcal{S}_{\omega}^{\tau(n)}g. \tag{5.5}$$

By comparison of (5.3) with (3.13) and using the fact that $e^{i\theta} = e^{i\theta+2\pi}$, the following relationship between (5.5) and (3.14) can be established:

$$\mathcal{S}_{D}^{\tau(n)}g = \mathcal{S}_{D_n}g, \qquad D_n = \bigcup_{l\in\mathbb{Z}} D_n^{(l)}, \quad D_n^{(l)} = \left[a + 2l\hat{\omega}(n), b + 2l\hat{\omega}(n)\right). \tag{5.6}$$

The equality (5.6) is a consequence of *aliasing*. Hence, to approximate the spectral projection (3.14) through the $\tau(n)$-map $S^{\tau(n)}$ will involve taking into account the errors introduced by the sets $D_n^{(l)}$ for $l \neq 0$.

In practical calculations, this implies that $\tau(n)$ has to be chosen small enough, so that the spectral bandwith of the selected observables are suffciently captured. Consequently, observables with high frequency spectral content will require small time-steps. The conditions on the time discretization are very similar to the *Nyquist-Shannon* sampling theorem, which imposes restrictions on the sample rate of a continuous-time signal so that it can be properly reconstructed.

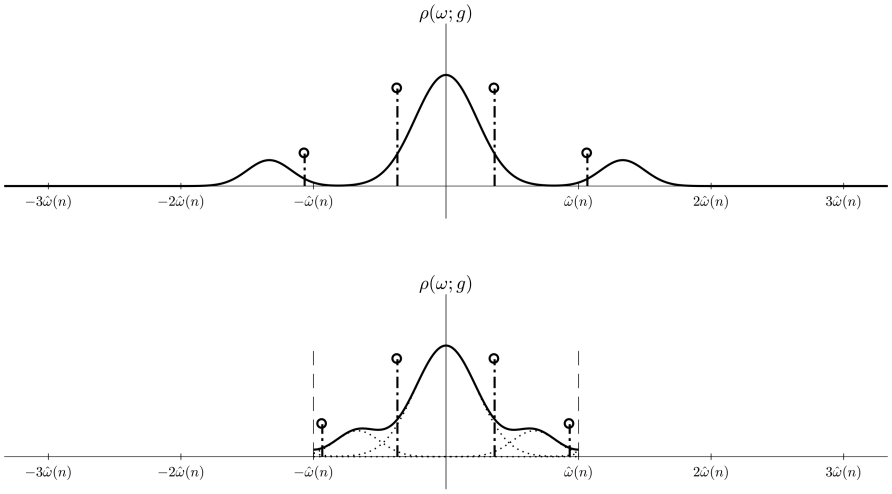

Figure 5.1: The change that the spectral density function undergoes due to aliasing (5.6). The top figure shows the original density plot, the bottom figure shows the density plot after the time discretization.

5.1.2 The spatial discretization

The second step in the discretization process is to convert the map $S^{\tau(n)} : X \mapsto X$ on a "continuous" state-space to a periodic map $S_n^{\tau(n)} : \mathcal{P}_n \mapsto \mathcal{P}_n$ with periodicity $\zeta(n)$ on a "discrete and finite" state-space. The spatial discretization is performed in exactly the same manner as in chapter 4, and the partitions $\{\mathcal{P}_n\}_{n=1}^{\infty}$ satisfy the same properties as in section 4.1.2.

The operators in (5.1) is replaced by the finite group:

$$\left\{\mathcal{U}_n^{k\tau(n)} : L_n^2(X, \mathcal{M}, \mu) \mapsto L_n^2(X, \mathcal{M}, \mu)\right\}_{k\in\mathbb{Z}/\zeta(n)}$$

defined by the permutation operators:

$$\left(\mathcal{U}_n^{k\tau(n)} g_n\right)(x) := \sum_{j=1}^{q(n)} g_{n,j} \chi_{S_n^{-k\tau(n)}(p_{n,j})}(x), \qquad k \in \mathbb{Z}/\zeta(n). \tag{5.7}$$

where $g_n \in L^2_n(X, \mathcal{M}, \mu)$ is obtained from averaging operator (4.3). The eigenfunctions of (5.7) can be expressed in terms of the basis elements of $L^2_n(X, \mathcal{M}, \mu)$, i.e.

$$v_{n,k}(x) = \sum_{j=1}^{q(n)} v_{n,kj} \chi_{p_{n,j}}(x)$$

where $\|v_{n,k}\| = 1$. The associated eigenvalues of (5.7) are roots of unity:

$$\mathcal{U}_n^{k\tau(n)} v_{n,k} = e^{i\omega_{n,k} k\tau(n)} v_{n,k}, \qquad \omega_{n,k} := \theta_{n,k}/\tau(n).$$

Henceforth, the spectral decomposition of an observable $g_n \in L^2_n(X, \mathcal{M}, \mu)$ under the action of (5.7) can be expressed as:

$$\mathcal{U}_n^{k\tau(n)} g_n = \sum_{k=1}^{q(n)} e^{ik\tau(n)\omega_{n,k}} \mathcal{S}^{\tau(n)}_{n,\omega_{n,k}} g_n, \tag{5.8}$$

where $\mathcal{S}^{\tau(n)}_{n,\omega_{n,k}} : L^2_n(X, \mathcal{M}, \mu) \mapsto L^2_n(X, \mathcal{M}, \mu)$ denotes the rank-1 self-adjoint projector:

$$\mathcal{S}^{\tau(n)}_{n,\omega_{n,k}} g_n = v_{n,k} \langle v_{n,k}, g_n \rangle = v_{n,k} \left(\int_X v^*_{n,k}(x) g_n(x) \mathrm{d}\mu \right) = v_{n,k} \left(\frac{\mu(X)}{q(n)} \sum_{j=1}^{q(n)} v^*_{n,kj} g_{n,j} \right). \tag{5.9}$$

Let $D = [a, b] \subset [-\hat{\omega}(n), \hat{\omega}(n))$. The fully discrete analogue to the spectral projection (3.14) (both in time and space) is defined as:

$$\mathcal{S}^{\tau(n)}_{n,D} g_n := \int_D \mathrm{d}\mathcal{S}^{\tau(n)}_{n,\omega} g_n = \sum_{\omega_{n,k} \in D} \mathcal{S}^{\tau(n)}_{n,\omega_{n,k}} g_n. \tag{5.10}$$

Additionally, the discrete analogue of the spectral density function (3.15) is given by:

$$\rho_n(\omega; g_n) = \sum_{k=1}^{q(n)} \left\| \mathcal{S}^{\tau(n)}_{n,\omega_{n,k}} g_n \right\|^2 \delta(\omega - \omega_{n,k}). \tag{5.11}$$

Remark 5.1.1. The periodic approximation $S_n^{\tau(n)} : \mathcal{P}_n \mapsto \mathcal{P}_n$ already inherits the measure-preserving properties of the original flow on the subsigma algebra generated by $\mathcal{P}_n$, i.e. $\mu(S^{-\tau(n)}(p_{n,j})) = \mu(p_{n,j}) = \mu(S^{\tau(n)}(p_{n,j}))$. However, if the underlying flow comes from a Hamiltonian vector field, additional constraints may be imposed so that the periodic approximation also preserves the *symplectic form*.

5.1.3 Overview

The discretization of the Koopman operator of a measure preserving flow is split into stages. In the time-discretization, a continuous one-parameter group is replaced by a discrete one-parameter group:

$$\left\{\mathcal{U}^t : L^2(X,\mathcal{M},\mu) \mapsto L^2(X,\mathcal{M},\mu)\right\}_{t\in\mathbb{R}} \to \left\{\mathcal{U}^{k\tau(n)} : L^2(X,\mathcal{M},\mu) \mapsto L^2(X,\mathcal{M},\mu)\right\}_{k\in\mathbb{Z}}.$$

In the spatial discretization, the discrete one-parameter group is replaced by a finite one-parameter group:

$$\left\{\mathcal{U}^{k\tau(n)} : L^2(X,\mathcal{M},\mu) \mapsto L^2(X,\mathcal{M},\mu)\right\}_{k\in\mathbb{Z}} \to \left\{\mathcal{U}_n^{k\tau(n)} : L_n^2(X,\mathcal{M},\mu) \mapsto L_n^2(X,\mathcal{M},\mu)\right\}_{k\in\mathbb{Z}/\zeta(n)}.$$

An overview of the discretization process is given in fig. 5.2.

5.2 Existence of a periodic approximation for flows

In chapter 4 it was shown that for a measure-preserving automorphism $T : X \mapsto X$, one could construct a sequence of periodic approximations $\{T_n : \mathcal{P}_n \mapsto \mathcal{P}_n\}_{n=1}^{\infty}$ such that the dynamics T is closely mimiced for longer periods of time after each consequtive

refinement. More specifically, given a compact set $A \in \mathcal{M}$ and $k \in \mathbb{N}$, it was shown that the set evolution of A converges in the Haussdorf metric in the following sense:

$$\lim_{n\to\infty} \sum_{l=-k}^{k} d_H(T^l(A), T_n^l(A_n)) = 0, \tag{5.12}$$

where:

$$A_n := \bigcup_{p\in\mathcal{P}_n:\ p\cap A\neq\emptyset} p \qquad \text{and} \qquad d_H(A,B) := \max\left\{ \sup_{a\in A}\inf_{b\in B} d(a,b), \sup_{b\in B}\inf_{a\in A} d(a,b) \right\}.$$

An analogous statement along the lines of (5.12) can also made for measure-preserving flows. In this section, it will be shown that it is possible to construct a sequence of periodic approximations $\{S_n^{\tau(n)} : \mathcal{P}_n \mapsto \mathcal{P}_n\}_{n=1}^{\infty}$ to the flow $S^t : X \mapsto X$, such that for every $t \in \mathbb{R}$:

$$\lim_{n\to\infty} \int_{-t}^{t} d_H\left(S^s(A), S_n^{\xi_n(s)}(A_n)\right) \mathrm{d}s = 0, \tag{5.13}$$

where:

$$\xi_n(t) = \mathrm{sign}(t) \left\lceil \frac{|t|}{\tau(n)} \right\rceil \tau(n). \tag{5.14}$$

In order for (5.13) to hold true, certain conditions on the spatial and temporal discretizations need to be satisfied. Recall that $S_n^{\tau(n)} : \mathcal{P}_n \mapsto \mathcal{P}_n$ is defined as a periodic approximation of the automorphism $S^{\tau(n)} : X \mapsto X$. But since $S^{\tau(n)}$ tends to the identity map as $n \to \infty$, it is necessary that the refinements in $\{\mathcal{P}_n\}_{n=1}^{\infty}$ happen at a sufficiently fast rate, so that the dynamics of the flow are properly captured.

5.2.1 Example: translational flow on the circle

To illustrate this technicality, consider a simple example of a translation flow on the circle:

$$S^t(x) = (x + \Omega t) \mod 1, \qquad \Omega \in \mathbb{R}, \qquad x \in [0, 1).$$

Suppose the following temporal and spatial discretizations are chosen for the flow:

$$\tau(n) = \frac{\gamma}{\Omega w^n}, \qquad \mathcal{P}_n = \{p_{n,1}, p_{n,2}, \ldots, p_{n,r^n}\} \text{ with } p_{n,j} = \left(\frac{j-1}{r^n}, \frac{j}{r^n}\right),$$

where $w, r > 1$ are integers and $\gamma > 0$ a positive real constant. It is not hard to derive that the mapping[1]:

$$S_n^{\tau(n)}(p_{n,j}) = p_{n,j^*}, \qquad j^* = \left\lfloor \left(j - 1 + \gamma \left(\frac{r}{w}\right)^n\right) \mod r^n \right\rceil + 1, \qquad n = 1, 2, \ldots, \tag{5.15}$$

forms a sequence of "optimal" periodic approximations that minimizes the cost:

$$J = \max_{p_{n,j} \in \mathcal{P}_n} d_H(S^{\tau(n)}(p_{n,j}), S_n^{\tau(n)}(p_{n,j})).$$

The sequence of maps (5.15) can be interpreted as an exact discretization of the flow:

$$\hat{S}_n^t(x) = (x + \hat{\Omega}(n)t) \mod 1, \qquad \hat{\Omega}(n) = \left\lfloor \gamma \left(\frac{r}{w}\right)^n \right\rceil \frac{\Omega}{\gamma} \left(\frac{w}{r}\right)^n. \tag{5.16}$$

That is,

$$d_H(\hat{S}_n^{\xi_n(t)}(p_{n,j}), S_n^{\xi_n(t)}(p_{n,j})) = 0, \qquad t \in \mathbb{R}.$$

Whether (5.15) satisfy the convergence criteria (5.13) depends on the ratio of $\frac{r}{w}$. Overall, three different situations can be distinguished:

[1] $\lfloor \cdot \rceil$ denotes nearest integer function, where it was chosen to always round upwards for half-integers.

- *Case* $\frac{r}{w} < 1$. In this scenario, the temporal discretization is refined faster than the spatial discretization. Notice that $S_n^{\tau(n)}$ is matched to the identity map as soon as $n \in \mathbb{N}$ is large enough to make $\gamma \left(\frac{r}{w}\right)^n < \frac{1}{2}$. Henceforth, $\lim_{n\to\infty} \hat{\Omega}(n) = 0$ and convergence in the sense of (5.13) will not occur.

- *Case* $\frac{r}{w} = 1$. In this scenario, the temporal discretization is refined at the same rate as the spatial discretization. The (normalized) frequency mismatch is equal to:

$$\lim_{n\to\infty} \left| \frac{\Omega - \hat{\Omega}(n)}{\Omega} \right| = 1 - \frac{\lfloor \gamma \rceil}{\gamma}.$$

- *Case* $\frac{r}{w} > 1$. In this scenario, the spatial discretization is refined faster than the temporal discretization. In this situation,

$$\lim_{n\to\infty} \left| \frac{\Omega - \hat{\Omega}(n)}{\Omega} \right| = \lim_{n\to\infty} 1 - \left\lfloor \gamma \left(\frac{r}{w}\right)^n \right\rceil \frac{1}{\gamma} \left(\frac{w}{r}\right)^n = 0.$$

  Hence, convergence in the sense of (5.13) must occur.

Since the Koopman operator converges spectrally only when $\lim_{n\to\infty} \hat{\Omega}(n) = \hat{\Omega}$, the conditione $\frac{r}{w} > 1$ is critical in applications of spectral computations.

5.2.2 The general case: an asymptotic requirement on the temporal and spatial discretizations

The analysis of the translation flow on the circle is a specific case of a more general phenomenon that needs to be adressed in the discretization of flows. The following technical result will be used which is a consequence of Grönwall inequality.

Lemma 5.2.1. *Let S^t denote a lipschitz continuous flow on a compact metric space X.*

Then for some $L > 0$,

$$d\left(S^t(x), S^t(y)\right) \leq e^{L|t|} d(x, y), \qquad t \in \mathbb{R} \text{ and } x, y \in X. \tag{5.17}$$

Proof. By compactness and Lipschitz continuity of the flow, it follows that $d\left(S^{t+s}(x), S^t(x)\right) \leq \frac{L}{2}|s|$ and $d\left(S^{t+s}(y), S^t(y)\right) \leq \frac{L}{2}|s|$ for some constant $L > 0$. By combining these facts, one can deduce that:

$$d\left(S^{t+s}(x), S^{t+s}(y)\right) \leq (1 + L|s|) d\left(S^t(x), S^t(y)\right).$$

By repeated application of this inequality, one can show that for any $n \in \mathbb{N}$:

$$d\left(S^{t+s}(x), S^{t+s}(y)\right) \leq \left(1 + \frac{L|s|}{n}\right)^n d\left(S^t(x), S^t(y)\right).$$

Taking limits as $n \to \infty$ yields $d\left(S^{t+s}(x), S^{t+s}(y)\right) \leq \exp(L|s|) d\left(S^t(x), S^t(y)\right)$. □

The following theorem will be proven.

Theorem 5.2.2. *Let $S^t : X \mapsto X$ be a measure-preserving flow on a compact metric space preserving the absolutely continuous measure μ with support* $\operatorname{supp} \mu = X$*. Recall from* (4.2) *that* $\operatorname{diam}(p_{n,j}) \leq l(n)$*. If:*

$$\lim_{n \to \infty} \frac{l(n)}{\tau(n)} = 0, \tag{5.18}$$

then there exists a sequence of periodic approximation $\{S_n^{\tau(n)} : \mathcal{P}_n \mapsto \mathcal{P}_n\}_{n=1}^{\infty}$ such that (5.13) *holds:*

$$\lim_{n \to \infty} \int_{-t}^{t} d_H\left(S^s(A), S_n^{\xi_n(s)}(A_n)\right) \mathrm{d}s = 0$$

for every fixed $t \in \mathbb{R}$ and compact set A.

The asymptotic condition (5.18) is *sufficient* for convergence to occur, although it is not necessary as it was noticable in the example of section 5.2.1.

Proof of theorem 5.2.2. By the triangle inequality:

$$\int_{-t}^{t} d_H\left(S^s(A), S_n^{\xi_n(s)}(A_n)\right) \mathrm{d}s \leq \int_{-t}^{t} d_H\left(S^s(A), S_n^{\xi_n(s)}(A)\right) \mathrm{d}s + \int_{-t}^{t} d_H\left(S^{\xi_n(s)}(A), S_n^{\xi_n(s)}(A_n)\right) \mathrm{d}s$$

Since the first term will tend to zero because of continuity of the flow S^t, it suffices to show that:

$$\lim_{n\to\infty} \int_{-t}^{t} d_H\left(S^{\xi_n(s)}(A), S_n^{\xi_n(s)}(A_n)\right) \mathrm{d}s = 0.$$

The following can be further established:

$$\begin{aligned}
\int_{-t}^{t} d_H\left(S^{\xi_n(s)}(A), S_n^{\xi_n(s)}(A_n)\right) \mathrm{d}s &\leq \epsilon_n(t) + \int_{-t}^{t} d_H\left(S^{\xi_n(s)}(A_n), S_n^{\xi_n(s)}(A_n)\right) \mathrm{d}s \\
&= \epsilon_n(t) + \int_{-t}^{t} d_H\left(S^{\xi_n(s)}(A_n), S_n^{\xi_n(s)}(A_n)\right) \mathrm{d}s \\
&= \epsilon_n(t) + \int_{-t}^{t} \\
&\quad d_H\left(\bigcup_{p\in P_n:\ p\cap A\neq\emptyset} S^{\xi_n(s)}(p), \bigcup_{p\in P_n:\ p\cap A\neq\emptyset} S_n^{\xi_n(s)}(p)\right) \mathrm{d}s \\
&\leq \epsilon_n(t) + \int_{-t}^{t} \max_{p\in P_n:\ p\cap A\neq\emptyset} d_H\left(S^{\xi_n(s)}(p), S_n^{\xi_n(s)}(p)\right) \mathrm{d}s, \\
&\leq \epsilon_n(t) + \int_{-t}^{t} \max_{p\in P_n} d_H\left(S^{\xi_n(s)}(p), S_n^{\xi_n(s)}(p)\right) \mathrm{d}s,
\end{aligned}$$

where:

$$\epsilon_n(t) := \int_{-t}^{t} d_H\left(S^{\xi_n(s)}(A), S^{\xi_n(s)}(A_n)\right) \mathrm{d}s \qquad \text{and} \qquad \lim_{n\to\infty} \epsilon_n(t) = 0.$$

Let $\{S_n^{\tau(n)} : \mathcal{P}_n \mapsto \mathcal{P}_n\}_{n=1}^{\infty}$ denote a sequence of periodic approximations generated from a maximum cardinality matching of the bipartite graphs (which are all perfect matchings as per theorem 4.2.2):

$$G_n = (\mathcal{P}_n, \mathcal{P}_n^{'}, E), \qquad (p_{n,k}, {p'}_{n,l}) \in E \quad \text{if} \quad \mu(S^{\tau(n)}(p_{n,k}) \cap p_{n,l}) > 0. \tag{5.19}$$

To prove the theorem, it will be shown that $\{S_n^{\tau(n)}\}_{n=1}^{\infty}$ satisfies:

$$\lim_{n\to\infty} \int_{-t}^{t} \max_{p\in P_n} d_H\left(S^{\xi_n(s)}(p), S_n^{\xi_n(s)}(p)\right) = 0.$$

First of all, observe that for any $p \in \mathcal{P}_n$, the following bound can be obtained:

$$\begin{aligned} d_H\left(S^{\tau(n)}(p), S_n^{\tau(n)}(p)\right) &\leq \text{diam}\ (S^{\tau(n)}(p)) + \text{diam}\ (S_n^{\tau(n)}(p)) \\ &\leq (e^{L\tau(n)} + 1) l(n) \\ &\leq (e^{L\tau(n)} + 1) \frac{l(n)}{\tau(n)} e^{L\tau(n)} \tau(n). \end{aligned}$$

By employing the inequality:

$$\begin{aligned} d_H\left(S^{l\tau(n)}(p), S_n^{l\tau(n)}(p)\right) \leq d_H\left(S^{\tau(n)}\left(S^{(l-1)\tau(n)}(p)\right), S^{\tau(n)}\left(S_n^{(l-1)\tau(n)}(p)\right)\right) + \\ d_H\left(S^{\tau(n)}\left(S_n^{(l-1)\tau(n)}(p)\right), S_n^{\tau(n)}\left(S_n^{(l-1)\tau(n)}(p)\right)\right), \qquad l \in \mathbb{N}, \end{aligned}$$

and using theorem 5.2.1: $d_H(S^t(A), S^t(B)) \leq e^{L|t|} d_H(A, B)$, the following recursive relation can be derived:

$$d_H\left(S^{l\tau(n)}(p), S_n^{l\tau(n)}(p)\right) \leq e^{L\tau(n)} d_H\left(S^{(l-1)\tau(n)}(p), S_n^{(l-1)\tau(n)}(p)\right) + (e^{L\tau(n)} + 1) \frac{l(n)}{\tau(n)} e^{L\tau(n)} \tau(n).$$

$$d_H\left(S^{l\tau(n)}(p), S^{l\tau(n)}(p)\right) \leq (e^{L\tau(n)}+1)\frac{l(n)}{\tau(n)}\left(e^{L\tau(n)}+\ldots+e^{Ll\tau(n)}\right).$$

Letting $s>0$, this may be conveniently be re-expressed into a Riemann-Stieltjes notation:

$$d_H\left(S^{\xi_n(s)}(p), S_n^{\xi_n(s)}(p)\right)(e^{L\tau(n)}+1)\frac{l(n)}{\tau(n)}\int_0^{\xi_n(s)} e^{L|\xi_n(\sigma)|}\mathrm{d}\sigma.$$

Following an identical procedure for negative time values, one obtains:

$$d_H\left(S^{\xi_n(-s)}(p), S_n^{\xi_n(-s)}(p)\right) \leq (e^{L\tau(n)}+1)\frac{l(n)}{\tau(n)}\int_{\xi_n(-s)}^{0} e^{L|\xi_n(\sigma)|}\mathrm{d}\sigma.$$

Combining the results yields:

$$\int_{-t}^{t}\max_{p\in P_n} d_H\left(S^{\xi_n(s)}(p), S_n^{\xi_n(s)}(p)\right) \leq \left(e^{L\tau(n)}+1\right)\left(\frac{l(n)}{\tau(n)}\right)\left(\int_{-t}^{t}\int_{\xi_n(-s)}^{\xi_n(s)} e^{L|\xi_n(\sigma)|}\mathrm{d}\sigma\mathrm{d}s\right).$$

Indeed, by taking limits:

$$\lim_{n\to\infty}\int_{-t}^{t}\max_{p\in P_n} d_H\left(S^{\xi_n(s)}(p), S_n^{\xi_n(s)}(p)\right) \leq (2)\left(\lim_{n\to\infty}\frac{l(n)}{\tau(n)}\right)\left(\frac{4(-1+e^{Lt}-Lt)}{L^2}\right),$$

and noting the condition (5.18), the desired result has been established. □

Remark 5.2.3. In practice, $S^{\tau(n)}: X\mapsto X$ is typically not known explicitly. Instead, one has access to an order-s integrator $\tilde{S}^{\tau(n)}: X\mapsto X$ which acts as an approximator to the flow. Assuming that the integrator preserves the invariant measure of the flow, the question arises whether replacing $S_n^{\tau(n)}: \mathcal{P}_n\mapsto\mathcal{P}_n$ with $\tilde{S}_n^{\tau(n)}: \mathcal{P}_n\mapsto\mathcal{P}_n$ would still allow theorem 5.2.2 to fall through. The answer to this question is affirmative. This follows from the fact that $d(S^{\tau(n)}(x), \tilde{S}^{\tau(n)}(x)) = \mathcal{O}(\tau^{s+1}(n))$ and the triangle inequality:

$$d_H(S^{\tau(n)}(p), \tilde{S}_n^{\tau(n)}(p)) \leq d_H(S^{\tau(n)}(p), \tilde{S}^{\tau(n)}(p)) + d_H(\tilde{S}^{\tau(n)}(p), \tilde{S}_n^{\tau(n)}(p)).$$

Remark 5.2.4. Notice that the condition on the spatial and temporal discretizations (5.18) is different than, and in some sense opposite to the Courant-Friedrichs-Lewy (CFL) condition which typically arises in finite difference schemes of Hyperbolic PDEs. In section 5.5, this matter will be discussed in greater detail.

5.3 Convergence of the operator for flows

In this section, operator convergence is established for a sequence of periodic approximations to a flow. Since the proofs are very similar to the discrete-time case, most details of the proof are left out.

Lemma 5.3.1. *Suppose that* $\left\{S_n^{\tau(n)} : \mathcal{P}_n \mapsto \mathcal{P}_n\right\}_{n=1}^{\infty}$ *is a sequence of discrete maps that periodically approximates* $S^t : X \mapsto X$ *in the sense of theorem 5.2.2. For some* $m \in \mathbb{N}$*, define:*

$$g = \sum_{j=1}^{q(m)} c_j \chi_{p_{m,j}} \in L_m^2(X, \mathcal{M}, \mu).$$

Then, for any fixed $t \in \mathbb{R}$*:*

$$\lim_{n\to\infty} \int_{-t}^{t} \left\| \mathcal{U}^s g - \mathcal{U}_n^{\xi_n(s)} g_n \right\|^2 \mathrm{d}s = 0.$$

Proof. Again, by continuity it suffices to just show:

$$\lim_{n\to\infty} \int_{-t}^{t} \left\| \mathcal{U}^{\xi_n(s)} g - \mathcal{U}_n^{\xi_n(s)} g_n \right\|^2 \mathrm{d}s = 0.$$

For notational clarity, write $A^{(j)} := p_{m,j}$, $g^{(j)} := \chi_{p_{m,j}}$ and $g_n^{(j)} := \mathcal{W}_n g^{(j)}$.

$$\int_{-t}^{t} \left\| \mathcal{U}^{\xi_n(s)} g - \mathcal{U}_n^{\xi_n(s)} g_n \right\|^2 \mathrm{d}s \leq$$
$$q(m) \left(\sum_{j=1}^{q(m)} |c_j|^2 \right) \max_{j=1,\ldots,q(m)} \left(\int_{-t}^{t} \left\| \mathcal{U}^{\xi_n(s)} g^{(j)} - \mathcal{U}_n^{\xi_n(s)} g_n^{(j)} \right\|^2 \mathrm{d}s \right).$$

Since $\{\mathcal{P}_n\}_{n=1}^{\infty}$ are consecutive refinements, observe that $g_n^{(j)} = g^{(j)}$ for $n \geq m$, which implies:

$$\int_{-t}^{t} \left\| \mathcal{U}^{\xi_n(s)} g^{(j)} - \mathcal{U}_n^{\xi_n(s)} g_n^{(j)} \right\|^2 \mathrm{d}s = \int_{-t}^{t} \mu \left(S^{\xi_n(s)}(A^{(j)}) \Delta S_n^{\xi_n(s)}(A^{(j)}) \mathrm{d}\xi_n(s) \right) \mathrm{d}s, \qquad \text{if } n \geq m.$$

The proof proceeds in a similar way as in the discrete time case. □

Theorem 5.3.2 (Operator convergence)**.** *Suppose that* $\left\{ S_n^{\tau(n)} : \mathcal{P}_n \mapsto \mathcal{P}_n \right\}_{n=1}^{\infty}$ *is a sequence of discrete maps that periodically approximates* $S^t : X \mapsto X$ *in the sense of theorem 5.2.2. Then, for every fixed* $t \in \mathbb{R}$*:*

$$\lim_{n \to \infty} \int_{-t}^{t} \left\| \mathcal{U}^s g - \mathcal{U}_n^{\xi_n(s)} g_n \right\|^2 \mathrm{d}s = 0, \tag{5.20}$$

where $g \in L^2(X, \mathcal{M}, \mu)$ *and* $\xi_n(s)$ *is defined by* (5.14)*.*

Proof. The proof is very similar to discrete time case. One can pick a

$$g_m = \sum_{j=1}^{q(m)} c_j \chi_{p_{m,j}} \in L_m^2(X, \mathcal{M}, \mu)$$

that approximates $g \in L^2(X, \mathcal{M}, \mu)$ arbitrarily well in the norm-wise sense by choosing a sufficiently large $m \in \mathbb{N}$. □

5.4 Convergence of spectra for flows

In this section, results related to spectral convergence are established. In particular, it will be examined how (5.10) converges to (3.14).

5.4.1 Approximation of the spectral projectors

Consider any smooth test function $\varphi \in \mathcal{D}(\mathbb{R})$ on the reals, and define:

$$\mathcal{S}_\varphi g = \int_{\mathbb{R}} \varphi(\omega) \mathrm{d}\mathcal{S}_\omega g, \qquad \mathcal{S}^{\tau(n)}_{n,\varphi} g_n = \sum_{\omega_{n,k} \in \mathbb{R}} \varphi(\omega_{n,k}) \mathcal{S}^{\tau(n)}_{n,\omega_{n,k}} g_n.$$

The following theorem will be proven.

Theorem 5.4.1. *Suppose that* $\left\{ S^{\tau(n)}_n : \mathcal{P}_n \mapsto \mathcal{P}_n \right\}_{n=1}^{\infty}$ *is a sequence of discrete maps that periodically approximates* $S^t : X \mapsto X$ *in the sense of theorem 5.2.2. For any smooth test function* $\varphi \in \mathcal{D}(\mathbb{R})$ *and observable* $g \in L^2(X, \mathcal{M}, \mu)$*:*

$$\lim_{n \to \infty} \left\| \mathcal{S}_\varphi g - \mathcal{S}^{\tau(n)}_{n,\varphi} g_n \right\| = 0.$$

Proof. Express the test function in terms of its Fourier transform: $\varphi(\omega) = \int_{-\infty}^{\infty} b(\tau) e^{i\tau\omega} \mathrm{d}\tau$, and note that $\int_{-\infty}^{\infty} |b(\tau)| \mathrm{d}\tau < \infty$. It can be seen that:

$$\mathcal{S}_\varphi g = \int_{\mathbb{R}} \left(\int_{-\infty}^{\infty} b(\tau) e^{i\tau\omega} \mathrm{d}\tau \right) \mathrm{d}\mathcal{S}_\omega g = \int_{-\infty}^{\infty} b(\tau) \left(\int_{\mathbb{R}} e^{i\tau\omega} \mathrm{d}\mathcal{S}_\omega g \right) \mathrm{d}\tau = \int_{-\infty}^{\infty} b(\tau) \mathcal{U}^\tau g \mathrm{d}\tau,$$

where the last equality follows from the spectral theorem of unitary one-parameter groups [34]. Similarly, it also holds that:

$$\mathcal{S}^{\tau(n)}_{n,\varphi} g_n = \int_{-\infty}^{\infty} b(\tau) \mathcal{U}^{\xi(\tau)}_n g_n \mathrm{d}\tau$$

Hence,

$$\mathcal{S}_\varphi g - \mathcal{S}^{\tau(n)}_{n,\varphi} g_n = \int_{-\infty}^{\infty} b(\tau)(\mathcal{U}^\tau g - \mathcal{U}^{\xi(\tau)}_n g_n)\mathrm{d}\tau$$

Now let $\epsilon > 0$ and choose $t \in \mathbb{R}$ such that:

$$\int_{|\tau|>t} |b(\tau)|\mathrm{d}\tau < \frac{\epsilon}{4\,\|g\|}$$

Noting that:

$$\|\mathcal{S}_\varphi g - \mathcal{S}_{n,\varphi} g_n\| \;\leq\; M \int_{-t}^{t} \left\|\mathcal{U}^\tau g - \mathcal{U}^{\xi(\tau)}_n g_n\right\| \mathrm{d}\tau + \frac{\epsilon}{2},$$

and using theorem 5.3.2 the proof can be completed. □

Just as in the discrete-time case, smoothen the indicator function $\chi_D(\omega)$ using the summability kernel, i.e.

$$\chi_{D_\alpha}(\omega) = \int_{\mathbb{S}} \varphi_\alpha(\theta, \xi)\chi_D(\xi)\mathrm{d}\xi,$$

where $\varphi_\alpha : \mathbb{R} \times \mathbb{R} \mapsto \mathbb{R}_+$:

$$\varphi_\alpha(x, y) = \begin{cases} \frac{K}{\alpha} \exp\left(\frac{-1}{1-\left(\frac{|x-y|}{\alpha}\right)^2}\right) & \frac{|x-y|}{\alpha} < 1 \\ 0 & \text{otherwise} \end{cases}, \tag{5.21}$$

for some $\alpha > 0$ and $K = (\int_{-1}^{1} \exp(\frac{-1}{1-x^2})\mathrm{d}x)^{-1}$. Define:

$$\mathcal{S}_{D_\alpha} g = \int_{\mathbb{R}} \chi_{D_\alpha}(\omega)\mathrm{d}\mathcal{S}_\omega g, \qquad \mathcal{S}^{\tau(n)}_{n,D_\alpha} g_n = \sum_{\omega_{n,k}\in\mathbb{R}} \chi_{D_\alpha}(\omega_{n,k})\mathcal{S}_{n,\omega_{n,k}} g_n. \tag{5.22}$$

The following corollary holds.

Corollary 5.4.2 (Convergence of spectral projectors)**.** *Suppose that* $\left\{S_n^{\tau(n)} : \mathcal{P}_n \mapsto \mathcal{P}_n\right\}_{n=1}^{\infty}$ *is a sequence of discrete maps that periodically approximates* $S^t : X \mapsto X$ *in the sense of theorem 5.2.2. Given any* $\alpha > 0$ *and interval* $D \subset \mathbb{R}$*, it follows that:*

$$\lim_{n\to\infty} \left\| \mathcal{S}_{D_\alpha} g - \mathcal{S}_{n,D_\alpha}^{\tau(n)} g_n \right\| = 0,$$

where $g \in L^2(X, \mathcal{M}, \mu)$*.*

5.4.2 Approximation of the spectral density function

Recall the definition of the spectral density function along with its discrete analogue in (5.11). To assess the convergence of $\rho_n(\omega; g_n)$ to $\rho(\omega; g)$, again use is made of summability kernels (5.21).

Theorem 5.4.3 (Approximation of the spectral density function)**.** *Let:*

$$\rho_\alpha(\omega; g) := \int_{-\infty}^{\infty} \varphi_\alpha(\omega, \xi)\rho(\xi; g)\mathrm{d}\xi, \qquad \rho_{\alpha,n}(\omega; g_n) := \int_{-\infty}^{\infty} \varphi_\alpha(\omega, \xi)\rho_n(\xi; g_n)\mathrm{d}\xi.$$

It follows that:

$$\lim_{n\to\infty} \rho_{\alpha,n}(\omega; g_n) = \rho_\alpha(\omega; g), \quad \textit{uniformly.}$$

Proof. To prove uniform convergence, the following two facts will be established: (i) $\rho_\alpha(\omega; g) - \rho_{\alpha,n}(\omega; g_n)$ forms an equicontinuous family, and (ii) $\rho_{\alpha,n}(\omega; g_n)$ converges to $\rho_\alpha(\omega; g)$ in the L^2-norm.

(i) To show that $\rho_\alpha(\omega; g) - \rho_{\alpha,n}(\omega; g_n)$ is an equicontinuous family, it sufffices to confirm that the derivative $\rho_\alpha^{'}(\omega; g) - \rho_{\alpha,n}^{'}(\omega; g_n)$ is uniformly bounded. Write:

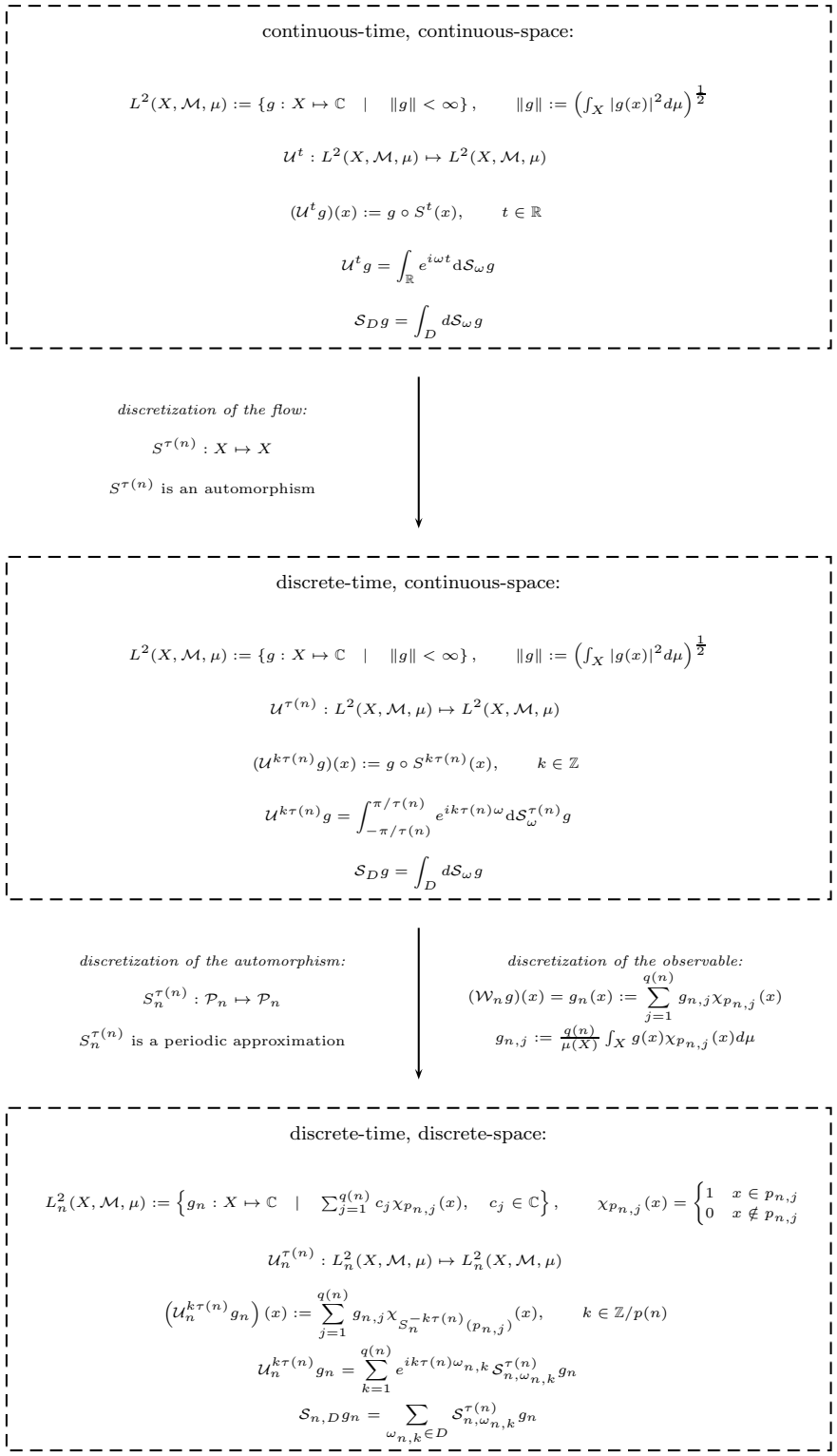

Figure 5.2: An overview of the discretization process.

$$\rho_\alpha(\omega; g) - \rho_{\alpha,n}(\omega; g_n) = \frac{1}{2\pi} \int_{-\infty}^{\infty} b_n(\tau; g) e^{i\tau\omega} \mathrm{d}\tau$$

where:

$$b_n(\tau; g) := \int_{-\infty}^{\infty} e^{-i\tau\omega} \left(\rho_\alpha(\omega; g) - \rho_{\alpha,n}(\omega; g_n)\right) \mathrm{d}\omega.$$

According to the spectral theorem of unitary operators [34], it follows that:

$$a(\tau; g) := \int_{-\infty}^{\infty} e^{-i\tau\omega} \rho(\omega; g) \mathrm{d}\theta = \langle g, \mathcal{U}^\tau g \rangle$$

and

$$a_n(\tau; g_n) := \int_{-\infty}^{\infty} e^{-i\tau\omega} \rho_n(\omega; g_n) \mathrm{d}\omega = \langle g_n, \mathcal{U}_n^{\xi_n(\tau)} g_n \rangle, \quad \tau \in \mathbb{R}.$$

The functions $\rho_\alpha(\omega; g)$ and $\rho_{\alpha,n}(\omega; g_n)$ are defined as convolutions with a function belonging to the *Schwartz space*. Recognizing that convolutions implies pointwise multiplication in Fourier domain, note that:

$$b_n(\tau; g) = d_\alpha(\tau)(a(\tau; g) - a_n(\tau; g_n)),$$

where:

$$d_\alpha(\tau) := \int_{-\infty}^{\infty} e^{-i\tau\omega} \varphi_\alpha(\omega, 0) \mathrm{d}\omega \quad \text{and} \quad |d_\alpha(\tau)| \leq \frac{C_\alpha}{1 + |\tau|^N} \text{ for every } N \in \mathbb{N}.$$

Now examining the derivative $\rho'_\alpha(\omega; g) - \rho'_{\alpha,n}(\omega; g_n)$ more closely, it can be seen

that:

$$\begin{aligned}\left|\rho_{\alpha}^{'}(\omega;g)-\rho_{\alpha,n}^{'}(\omega;g_n)\right| &= \left|\frac{1}{2\pi}\int_{-\infty}^{\infty} itb_n(\tau;g)e^{i\tau\omega}\mathrm{d}\tau\right| \\ &\leq \frac{1}{2\pi}\int_{-\infty}^{\infty}|\tau||d_\alpha(\tau)|\left|\langle g,\mathcal{U}^{\tau}g\rangle-\langle g_n,\mathcal{U}_n^{\xi_n(\tau)}g_n\rangle\right|\mathrm{d}\tau \\ &\leq \frac{\|g\|^2}{\pi}\int_{-\infty}^{\infty}\frac{C_\alpha|\tau|}{1+|\tau|^N}\mathrm{d}\tau,\end{aligned}$$

which is a convergent sum for $N \geq 3$.

(ii) To show that $\rho_{\alpha,n}(\omega;g_n)$ converges to $\rho_\alpha(\omega;g)$ in the L^2-norm, Parseval's identity can be employed to confirm that the integral: $\int_{-\infty}^{\infty}|b_n(\tau;g)|^2\,\mathrm{d}\tau$ can be made arbitrarily small. At first, note that:

$$a(\tau;g)-a_n(\tau;g_n)=\langle g,\mathcal{U}^t g-\mathcal{U}_n^{\xi_n(\tau)}g_n\rangle-\langle g-g_n,\mathcal{U}_n^{\xi_n(\tau)}g_n\rangle$$

By the triangle inequality and Cauchy-Schwarz, one obtains:

$$|a(\tau;g)-a_n(\tau;g_n)| \leq \|g\|\left(\left\|\mathcal{U}^{\tau}g-\mathcal{U}_n^{\xi_n(\tau)}g_n\right\|+\|g-g_n\|\right).$$

Let $\epsilon>0$, and choose $t\in\mathbb{R}_+$ such that:

$$\int_{|\tau|>t}|d_\alpha(\tau)|^2\mathrm{d}\tau\leq\epsilon. \tag{5.23}$$

This is always possible, because $\varphi_\alpha(\theta,0)$ is a C^∞ smooth function, and therefore

also square-integrable. The following upper bound can be established:

$$\begin{aligned}
\int_{-\infty}^{\infty} |b_n(\tau;g)|^2 \tau &= \int_{-\infty}^{\infty} |d_\alpha(\tau)|^2 |a(\tau;g) - a_n(\tau;g_n)|^2 \mathrm{d}\tau \\
&\leq \int_{-\infty}^{\infty} |d_\alpha(\tau)|^2 \left(\|g\| \left(\left\| \mathcal{U}^\tau g - \mathcal{U}_n^{\xi_n(\tau)} g_n \right\| + \|g - g_n\| \right) \right)^2 \mathrm{d}\tau \\
&\leq \|g\|^2 \max_{-t\leq\tau\leq t} |d_\alpha(\tau)|^2 \int_{-t}^{t} \left\| \mathcal{U}^\tau g - \mathcal{U}_n^{\xi_n(\tau)} g_n \right\|^2 \mathrm{d}\tau + \\
&\quad 16 \|g\|^2 \int_{|\tau|>t} |d_\alpha(l)|^2 \mathrm{d}\tau + \\
&\quad \|g\|^2 \|g - g_n\| \int_{-\infty}^{\infty} |d_\alpha(\tau)|^2 \left(2 \left\| \mathcal{U}^\tau g - \mathcal{U}_n^{\xi_n(\tau)} g_n \right\| + \|g - g_n\| \right) \mathrm{d}\tau.
\end{aligned}$$

Now apply (5.23) and theorem 5.3.2 to complete the proof.

□

5.5 Some remarks on the simulation of advection equations

The generator of the associated Koopman unitary group is the operator $f(x)\cdot\nabla$, where $f(x)$ is the vector field that generates the measure-preserving flow $S^t(x)$. Subsequently, the time evolution of an observable under the flow $S^t(x)$ is equivalent to the solution of an advection equation associated with the vector field $f(x)$. Henceforth, the discretization (5.7) is an approximate solution propagator to the advection problem:

$$\left(\left(\frac{\partial}{\partial t} - \mathcal{G} \right) \phi \right) (t,x) = 0 \tag{5.24a}$$

$$(\mathcal{A}\phi)(t,x) = \phi_0(x), \tag{5.24b}$$

where:

$$\mathcal{G}\phi(t,x) := f(x)\cdot\nabla\phi(t,x), \qquad (\mathcal{A}\phi)(t,x) := \phi(t,x)|_{t=0}\,.$$

Within the Computional Fluid Dynamics (CFD) community, there is already some familiarity on the concept of periodic approximation. Specifically, McLachan [38] coined the term "cell rearrangement model" to describe such approximation schemes. In the previous sections, it was shown that these methods are convergent both in a spectral sense and operator sense. That is, if $\phi_n(t,x) := \mathcal{U}_n^{\xi_n(t)}\mathcal{W}_n\phi_0(x)$, then for any fixed $t\in\mathbb{R}$:

$$(i). \quad \lim_{n\to\infty}\|\phi(t,x)-\phi_n(t,x)\| = 0, \qquad (ii). \quad \lim_{n\to\infty}\left\|\mathcal{S}_\varphi\phi(t,x)-\mathcal{S}_{n,\varphi}^{\tau(n)}\phi_n(t,x)\right\| = 0.$$

The advection equation is a hyperbolic PDE which has been heavily studied in the literature. A whole plethora of alternative numerical schemes can be used to solve system (5.24). A simple finite-difference scheme can already exhbibit very different convergence properties than the periodic approximation approach. Consider the *translation flow* on the circle which was examined in section 5.2.1. The generator $\mathcal{G}$ in this case equals $\Omega\frac{\partial}{\partial x}$ and is spatially invariant. Recall the temporal and spatial discretizations which were used in the periodic approximation:

$$l(n) = \frac{1}{r^n}, \quad \tau(n) = \frac{\gamma}{\Omega w^n}.$$

A *first-order upwind* finite-difference scheme yields a sequence of discretizations of the

Koopman operators, whose matrix representation is of the type:

$$\hat{U}_n^{\xi_n(t)} = \begin{bmatrix} 1-\gamma\left(\frac{r}{w}\right)^n & & & \gamma\left(\frac{r}{w}\right)^n \\ \gamma\left(\frac{r}{w}\right)^n & 1-\gamma\left(\frac{r}{w}\right)^n & & \\ & \ddots & \ddots & \\ & & \gamma\left(\frac{r}{w}\right)^n & 1-\gamma\left(\frac{r}{w}\right)^n \end{bmatrix}^{\frac{\xi_n(t)}{\tau(n)}} . \tag{5.25}$$

For a periodic approximation, weak convergence of the spectra was guaranteed when $\frac{r}{w} > 1$ (see again section 5.2.1). For the upwind scheme discretization, this is no longer true:

- *Case* $\frac{r}{w} < 1$. In this situation, (5.25) converges to the identity map. However, unlike the periodic approximation, the limit is never achieved and only holds true in the asymptotic sense. Weak convergence in the spectra is nevertheless not achieved.

- *Case* $\frac{r}{w} = 1$. In this situation, (5.25) is reduced to:

$$\hat{U}_n^{\xi_n(t)} = \begin{bmatrix} 1-\gamma & & & \gamma \\ \gamma & 1-\gamma & & \\ & \ddots & \ddots & \\ & & \gamma & 1-\gamma \end{bmatrix}^{\frac{\xi_n(t)}{\tau(n)}} . \tag{5.26}$$

  In the case when $0 < \gamma \leq 1$, (5.26) is the time evolution of a doubly-stochastic, circulant matrix. In fact, the operator can be interpreted as an Ulam approximation (see e.g. [16]) of the $\tau(n)$-map for the underlying flow:

$$T_n(x) = \left(x + \frac{1}{\gamma w^n}\Omega\right) \mod 1.$$

  As illustrated in fig. 5.3, the parameter $\gamma \in (0, 1]$ signifies the probability of jumping

to next partition interval. For the special $\gamma = 1$, the operator is equivalent to a periodic approximation. Nevertheless, the eigenvalue-eigenfunction pairs of the discretized operator (5.26):

$$\left(\hat{\mathcal{U}}_n^{\xi_n(t)} v_{n,j}\right)(x) = e^{\lambda_{j,n}\xi_n(t)} v_{n,j}(x)$$

for $j = 1, \ldots, r^n$ can be found explicitly,

$$\lambda_{n,j} = (2\pi\kappa_n(j)\Omega)\, i + \frac{\Omega r^n}{\gamma} \log\left(\frac{1-\gamma+\gamma e^{\frac{2\pi\kappa_n(j)}{r^n} i}}{e^{\gamma\frac{2\pi\kappa_n(j)}{r^n} i}}\right)$$

and

$$v_{n,j}(x) = \sum_{k=1}^{r^n} e^{\frac{2\pi\kappa_n(j)(k-1)}{r^n} i} \chi_{p_{n,j}}(x),$$

where:

$$\kappa_n(j) = \left(j - 1 - \frac{r^n}{2}\right) \mod r^n - \frac{r^n}{2}.$$

In fig. 5.4 the location of eigenvalues are plotted for varying $\gamma > 0$ and $n \in \mathbb{N}$. The eigenvalues only remain on the imaginary axis in the special case $\gamma = 1$ when (5.26) reduces to a periodic approximation. If $0 < \gamma \leq 1$ (the CLF condition for the upwind scheme), the eigenvalues deflect off to the left-half plane, whereas for $\gamma > 1$ they deflect off to right-half plane. Although refinements on the partition do push eigenvalues corresponding to slow modes closer to the imaginary axis, the eigenvalues corresponding to fast modes always either get dissipated or amplified.

- *Case* $\frac{r}{w} > 1$. The entries in (5.25) grow unboundedly. Hence, it is impossible to have any operator or weak spectral convergence in this scenario.

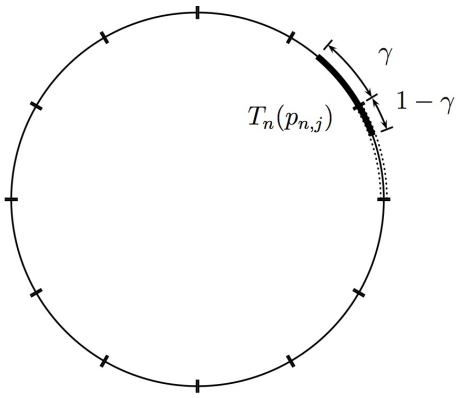

Figure 5.3: The "Ulam interpretation" to the discretized operator (5.26).

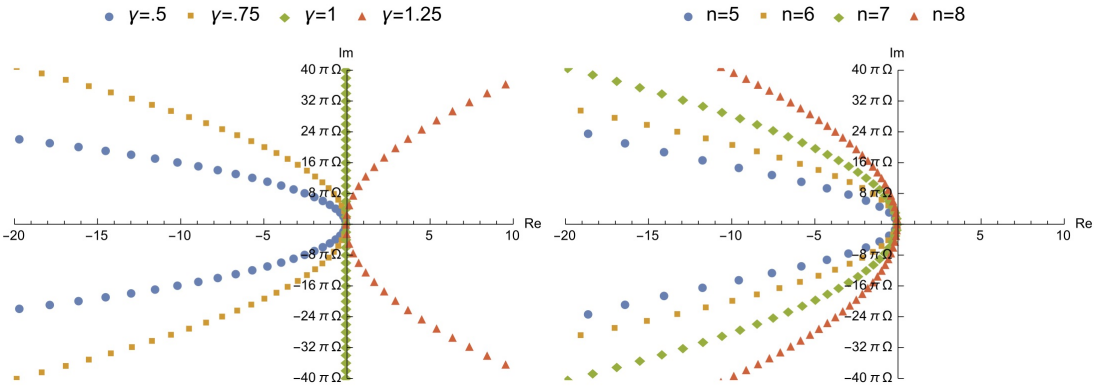

Figure 5.4: Eigenvalues of (5.26) for $r = w = 2$ and varying $\gamma > 0$ and $n \in \mathbb{N}$. Eigenvalues for $n = 7$ and varying $\gamma > 0$ (left). Eigenvalues for $\gamma = 0.75$ and varying $n \in \mathbb{N}$ (right).

In general, statements on the spectral convergence properties of a finite diffference schemes are harder to make. The generator is typically not spatially invariant and there is no longer a specific structure to exploit other than the sparsity. The uniqueness of the periodic approximation is that the discretization preserves the unitary structure of the underlying operator. In [38], McLachan indicated that periodic approximations surpress the formation of spurious oscillations in simulations. The restriction of the spectra to the imaginary axis may play a critical role here, since it prevents instabilities and artificial damping.

Chapter 6

Numerical methods

In the previous two chapters, a procedure was introduced in which the class of measure-preserving maps and flows were approximated using periodic transformations on a discretized state-space. It was shown that the Koopman operators of these periodic maps converge spectrally to that of original operator in a weak-sense. This method of discretization gives rise to a numerical method in which the spectral content of observables can be computed.

In this chapter, the details of the numerical method are broken-down. Overall, the method involves two steps. The first step consists of the actual construction of the periodic approximation. The second step consists of evaluating the spectral projections and density functions. What follows next is a detailed exposition for each of these steps. The emphasis here will be on computing spectra for maps. In the last section, a few pointers are given on how the methods is generalized for flows.

6.1 Constructing the periodic approximation

A periodic approximation can be obtained either through explicit construction or by analytic means. At first, the details of general algorithm will be discussed.

To keep the analysis simple, only volume-preserving maps on the m-torus will be treated. Extensions to other domains and invariant measures are more involved and a topic of further study. Henceforth, unless otherwise stated, in this chapter $X = \mathbb{T}^m$ with:

$$d(x, y) := \max_{k\in\{1,\dots,m\}} \min\{|x_i - y_i|, |1 - x_i - y_i|\} \tag{6.1}$$

and $T : \mathbb{T}^m \mapsto \mathbb{T}^m$ refers to an invertible, continuous Lebesgue measure-preserving transformation on the unit m-torus.

6.1.1 General algorithm for constructing periodic approximations

The algorithm proposed here differs from the method proposed in [39], although in essence they follow the same principle, given that a bipartite matching problem has to be solved one way or the other. In particular, it will be shown that the construction can be done "fast" if the underlying map is Lipschitz continuous.

Discretization of the m-torus Call:

$$p_{n,\hat{\mathbf{j}}} := \left[\frac{\hat{\jmath}_1 - 1}{\tilde{n}}, \frac{\hat{\jmath}_1}{\tilde{n}}\right] \times \left[\frac{\hat{\jmath}_2 - 1}{\tilde{n}}, \frac{\hat{\jmath}_2}{\tilde{n}}\right] \times \ldots \times \left[\frac{\hat{\jmath}_m - 1}{\tilde{n}}, \frac{\hat{\jmath}_m}{\tilde{n}}\right] \tag{6.2}$$

where:

$$\tilde{n} = Ca^n, \qquad C, a \in \mathbb{N}, \tag{6.3}$$

and $\hat{\mathbf{j}} = (\hat{\jmath}_1, \hat{\jmath}_2, \ldots, \hat{\jmath}_m)$ is a multi-index with $\hat{\jmath}_i \in \{1, \ldots, \tilde{n}\}$. To simplify the notation in some cases, it is useful to alternate between the multi-index $\hat{\mathbf{j}}$ and single-index $j \in \{1, 2, \ldots, \tilde{n}^m\}$ through a lexicographic ordering whenever it is convenient. Consider a partitioning of the unit m-torus (with $\mu(\mathbb{T}^m) = 1$) into the m-cubes:

$$\mathcal{P}_n = \{p_{n,j}\}_{j=1}^{q(n)}, \qquad q(n) = \tilde{n}^m$$

and note that this set is isomorphic to $\mathbb{N}_{\tilde{n}}^m := \{\hat{\mathbf{j}} \in \mathbb{N}^m : 0 < \hat{\jmath}_i \leq \tilde{n}, i = 1, \ldots, m\}$.

The sequence of partitions $\{\mathcal{P}_n\}_{n=1}^{\infty}$ of the m-torus form a collection of refinements which satisfy the properties:

$$\mu(p_{n,j}) = \frac{1}{\tilde{n}^m} \quad \text{and} \quad \operatorname{diam}(p_{n,j}) = \frac{\sqrt{m}}{\tilde{n}}, \qquad j \in \{1, 2, \ldots, \tilde{n}^m\},$$

where $\tilde{n}$ is defined as in (6.3). It is clear from these properties that $\{\mathcal{P}_n\}_{n=1}^{\infty}$ is a family of equal-measure partitions which meet the conditions: $\mu(p_{n,j}) \to 0$ and $\operatorname{diam}(p_{n,j}) \to 0$ as $n \to \infty$.

The bipartite matching problem A bipartite graph $G = (X, Y, E)$ is a graph where every edge $e \in E$ has one vertex in X and one in Y. A matching $M \subset E$ is a subset of edges where no two edges share a common vertex (in X or Y). The goal of the bipartite matching problem is to find a maximum cardinality matching, i.e. one with largest number of edges possible. A matching is called perfect if all vertices are matched. A perfect matching is possible if, and only if, the bipartite graph satisfies the so-called Hall's marriage condition:

$$\text{for every } B \subset X \text{ implies } |B| \leq |N_G(B)|$$

where $N_G(B) \subset Y$ is the set of all vertices adjacent to some vertex in A (see e.g. [35]).

Bipartite matching problems belong to the class of combinatorial problems for which well-established polynomial time algorithms exist, e.g. the Ford-Fulkerson algorithm may be used to find a maximum cardinality matching in $\mathcal{O}(|V||E|)$ operations, wheareas the Hopcroft-Karp algorithm does it in $\mathcal{O}(\sqrt{|V|}|E|)$ (see e.g. [40, 41]).

The algorithm In the previous chapters, it was shown that the solution to the bipartite matching problem of the graph[1]:

$$G_n = (\mathcal{P}_n, \mathcal{P}_n, E_n), \qquad (p_{n,s}, p_{n,l}) \in E_n \quad \text{if} \quad \mu(T(p_{n,s}) \cap p_{n,l}) > 0 \tag{6.4}$$

has a perfect matching. This fact played a key role in proving theorem 4.2.1. In practice, it is not advisable to construct this graph explicity since it requires the computation of set images.

Fortunately, a periodic approximation may be obtained from solving a related bipartite matching problem for which set computation are not necessary. Consider the partition $\mathcal{P}_n$ and associate to each partition element $p_{n,\hat{\mathbf{j}}} \in \mathcal{P}_n$ a representative point:

$$x_{n,\hat{\mathbf{j}}} = \psi_n(p_{n,\hat{\mathbf{j}}}) := \left(\frac{\hat{\mathrm{j}}_1 - \frac{1}{2}}{\tilde{n}}, \ldots, \frac{\hat{\mathrm{j}}_m - \frac{1}{2}}{\tilde{n}} \right) \in p_{n,\hat{\mathbf{j}}}. \tag{6.5}$$

Define:

$$\varphi_n(x) = \left(\tilde{n}x_1 + \frac{1}{2}, \ldots, \tilde{n}x_m + \frac{1}{2} \right). \tag{6.6}$$

to be the function that maps the representative points onto the lattice $\mathbb{N}_{\tilde{n}}^m := \{\hat{\mathbf{j}} \in \mathbb{N}^m : 0 < \hat{\mathrm{j}}_i \leq \tilde{n}, i = 1, \ldots, m\}$, i.e. $\hat{\mathbf{j}} = \varphi_n(x_{n,\hat{\mathbf{j}}})$. Let $\lfloor \cdot \rfloor$ ($\lceil \cdot \rceil$) denote the floor (resp. ceil)

[1]Note that the partition elements $p_{n,s} \in \mathcal{P}_n$ are interpreted here as vertices in a bipartite graph.

function, and define the following set-valued map:

$$F^{(t)}(x) = \{\hat{\mathbf{j}} \in \mathbb{N}_{\tilde{n}}^m : \lfloor \varphi_n(x_i) \rfloor - t + 1 \leq \hat{\jmath}_i \leq \lceil \varphi_n(x_i) \rceil + t - 1, \quad i = 1, \ldots, m\} \tag{6.7}$$

to introduce the family of neighborhood graphs:

$$\hat{G}_n^{(t)} := (\mathcal{P}_n, \mathcal{P}_n, \hat{E}_n^{(t)}), \qquad (p_{n,\hat{\mathbf{s}}}, p_{n,\hat{\mathbf{l}}}) \in \hat{E}_n^{(t)} \quad \text{if} \quad \hat{\mathbf{l}} \in F^{(t)}(T(x_{n,\hat{\mathbf{s}}})) \tag{6.8}$$

The proposal is to find a maximum cardinality matching for the bipartite graph $\hat{G}_n^{(t)}$. Notice that $\hat{E}_n^{(t)} \subseteq \hat{E}_n^{(s)}$ whenever $s \geq t$. Hence, if no perfect matching is obtained for some value of t, repeated dilations of the graph eventually will. The algorithm is summarized below.

Algorithm 6.1.1. To obtain a periodic approximation, do the following:

1. Initialize $t = 1$.
2. Find the maximum cardinality maching of $\hat{G}_n^{(t)}$.
3. If the matching is perfect, assign matching to be T_n. Otherwise set $t \leftarrow t + 1$ and repeat step 2.

Theorem 6.1.1 (Algorithmic correctness)**.** *Algorithm 6.1.1 terminates in a finite number of steps and yields a map $T_n : \mathcal{P}_n \mapsto \mathcal{P}_n$ with the desired asymptotic property described in* (5.12)*.*

Proof. For large enough t, the graph $\hat{G}_n^{(t)}$ eventually becomes the complete graph. Hence, the algorithm will terminate in a finite number of steps. However, one needs to show that the algorithm terminates way before that, yielding a map with the asymptotic property (5.12).

In [42], it was proven that for any Lebesgue measure-preserving map $T : \mathbb{T}^d \mapsto \mathbb{T}^d$, there exists a periodic map for which:

$$\sup_{p_{n,\mathbf{j}} \in \mathcal{P}_n} \inf_{x \in \mathbb{T}^d} \max\{d(x, \psi_n(p_{n,\mathbf{j}})), d(T(x), \psi_n(T_n(p_{n,\mathbf{j}})))\} \leq \frac{1}{2\tilde{n}}, \tag{6.9}$$

where $d(\cdot, \cdot)$ refers to the metric defined in (6.1). By virtue of this fact, if one is able to construct a bipartite graph $\tilde{G}_n = (\mathcal{P}_n, \mathcal{P}_n, \tilde{E}_n)$ for which:

$$(p_{n,\hat{\mathbf{s}}}, p_{n,\hat{\mathbf{l}}}) \in \tilde{E}_n \quad \text{if} \quad \inf_{x \in p_{n,\hat{\mathbf{s}}}} d(T(x), \psi_n(p_{n,\hat{\mathbf{l}}})) \leq \frac{1}{2\tilde{n}},$$

then this bipartite graph, or any super-graph, should admit a perfect matching. Indeed, if one were to assume the contrary, then this would imply that one is required to construct a periodic approximation T_n for which $d(T(x), \psi_n(T_n(p_{n,\hat{\mathbf{j}}}))) \geq \frac{1}{2\tilde{n}}$, an immediate contradiction of (6.9).

This fact has implications on the graph $\hat{G}_n^{(t)}$. As soon as t hits a value for which $\hat{E}_n^{(t)} \supseteq \tilde{E}_n$, the graph $\hat{G}_n^{(t)}$ is gauranteed to have a perfect matching (although it may occur even before that). Notice that by compactness of the m-torus, T admits a modulus of continuity $\omega : [0, \infty) \mapsto [0, \infty)$ with $d(T(x), T(y)) \leq \omega(d(x, y))$. An upper bound on the value of t for which $\hat{G}_n^{(t)}$ becomes a supergraph of $\tilde{G}_n$ is given by:

$$t^* = \lceil \tilde{n}\omega(1/\tilde{n}) + \frac{1}{2} \rceil \leq (\tilde{n} + 1) \left(\omega(1/\tilde{n}) + \frac{1}{2\tilde{n}} \right).$$

That is, the algorithm should terminate for $t \leq t^*$.

By assuming that the algorithm terminates at t^*, a worst-case error bound can be

established for any map generated from the bipartite graphs. It can be seen that:

$$\sup_{p_{n,\hat{\mathbf{j}}}\in\mathcal{P}_n} d(\psi_n(T_n(p_{n,\hat{\mathbf{j}}})), T(\psi_n(p_{n,\hat{\mathbf{j}}}))) \leq \frac{t^*}{\tilde{n}} \leq \frac{\tilde{n}+1}{\tilde{n}}\left(\omega(1/\tilde{n}) + \frac{1}{2\tilde{n}}\right).$$

Next, using the inequality:

$$d_H(T(p_{n,\hat{\mathbf{j}}}), T_n(p_{n,\hat{\mathbf{j}}})) \leq \operatorname{diam}(T_n(p_{n,j})) + d(\psi_n(T_n(p_{n,\hat{\mathbf{j}}})), T(\psi_n(p_{n,\hat{\mathbf{j}}}))) + \operatorname{diam}(T(p_{n,j})),$$

it follows that:

$$\lim_{n\to\infty} d_H(T(p_{n,\hat{\mathbf{j}}}), T_n(p_{n,\hat{\mathbf{j}}})) \leq \lim_{n\to\infty} \frac{1}{\tilde{n}} + \frac{\tilde{n}+1}{\tilde{n}}\left(\omega(1/\tilde{n}) + \frac{1}{2\tilde{n}}\right) + \omega(1/\tilde{n}) = 0.$$

From here onwards, one can proceed in the same fashion as the proofs of he proofs of theorem 4.2.3 and theorem 4.2.1 to show that $\{T_n\}_{n=1}^{\infty}$ indeed satisfies the convergence property (5.12). □

Complexity of Algorithm 6.1.1 Since the number of edges in $\hat{G}_n^{(t)}$ is proportional to the number of nodes for small t-values, the Hopcroft-Karp algorithm will solve a matching problem in $\mathcal{O}(\tilde{n}^{\frac{3m}{2}})$ operations. If additionally, the map T is assumed to be Lipschitz, i.e. $\omega(d(x,y)) = Kd(x,y)$, the algorithm terminates before $t^* = \lceil K + \frac{1}{2} \rceil$, i.e. independently of the discretization level $\tilde{n}$. Hence, $\mathcal{O}(\tilde{n}^{\frac{3m}{2}})$ is also the overall time-complexity of algorithm. Note that memory storage of a periodic map has $\mathcal{O}(\tilde{n}^m)$ in complexity. Ideally, it is desirable to obtain a formulaic expression for T_n.

6.1.2 Analytic constructions of periodic approximations

With the boxed partition of the m-torus (6.2), a sub-class of maps may be periodically aproximated analytically through simple algebraic manipulations (see e.g. [43]). In

addition to some purely mathematical transformations, this also includes maps which arise in physical problems. In fact, any perturbed Hamiltonian twist map like Chirikov's Standard Map [44], or certain kinds of volume preserving maps such as Feingold's ABC map [45] belong to this category.

A key observation is that these Lebesgue measure-preserving transformations consists of compositions of the following basic operations:

1. A signed permutation:

$$T(x) = \begin{bmatrix} \xi(1)x_{\sigma(1)} \\ \vdots \\ \xi(m)x_{\sigma(m)} \end{bmatrix}, \quad \text{with } \sigma(\cdot) \text{ a permutation and } \xi(\cdot) \in \{-1, 1\}. \tag{6.10}$$

which is periodically approximated by:

$$T_n(p_{n,\hat{\jmath}}) = \psi_n^{-1} \circ \varphi_n^{-1} \circ \left(\begin{bmatrix} \xi(1)\hat{\jmath}_{\sigma(1)} \\ \vdots \\ \xi(m)\hat{\jmath}_{\sigma(m)} \end{bmatrix} \mod \tilde{n} \right) \circ \varphi_n \circ \psi_n(p_{n,\hat{\jmath}}).$$

2. A translation:

$$T(x) = \begin{bmatrix} x_1 + \omega_1 \\ \vdots \\ x_m + \omega_m \end{bmatrix} \mod 1. \tag{6.11}$$

which is periodically approximated by:

$$T_n(p_{n,\hat{\jmath}}) = \psi_n^{-1} \circ \varphi_n^{-1} \circ \left(\begin{bmatrix} \hat{\jmath}_1 + \lfloor \varphi_n(\omega_1) \rceil \\ \vdots \\ \hat{\jmath}_m + \lfloor \varphi_n(\omega_m) \rceil \end{bmatrix} \mod \tilde{n} \right) \circ \varphi_n \circ \psi_n(p_{n,\hat{\jmath}}).$$

where $\lfloor \cdot \rceil$ denotes the nearest-integer function.

3. A shear:

$$T(x) = \begin{bmatrix} x_1 \\ \vdots \\ x_i + f(x_1, \ldots, x_{i-1}, x_{i+1}, \ldots, x_m) \\ \vdots \\ x_m \end{bmatrix} \tag{6.12}$$

which is periodicaly approximated by:

$$T_n(p_{n,\hat{\jmath}}) = \psi_n^{-1} \circ \varphi_n^{-1} \circ \left(\begin{bmatrix} \hat{\jmath}_1 \\ \vdots \\ \hat{\jmath}_i + \lfloor \varphi_n(f(\varphi_n^{-1}(\hat{\jmath}_1), \ldots, \varphi_n^{-1}(\hat{\jmath}_{i-1}), \varphi_n^{-1}(\hat{\jmath}_{i+1}), \ldots, \varphi_n^{-1}(\hat{\jmath}_m))) \rceil \\ \vdots \\ \hat{\jmath}_m \end{bmatrix} \mod \tilde{n} \right) \circ \varphi_n \circ \psi_n(p_{n,\hat{\jmath}})$$

Any map which is expressable as a finite composition of these operations can be periodically aproximated through approximation of each its component That is, the $T(x) = T_s \circ \cdots \circ T_1(x)$ is approximated by $T_n(x) = T_{s,n} \circ \cdots \circ T_{1,n}(x)$. It is not hard to show that this would lead to a sequence of approximations that satisfy (5.12). Examples of maps which may be approximated in this manner are:

- Arnold's Cat map [46]:

$$T(x) = \begin{bmatrix} 2 & 1 \\ 1 & 1 \end{bmatrix} \begin{bmatrix} x_1 \\ x_2 \end{bmatrix} \mod 1, \tag{6.13}$$

which is the composition of a permutation and shear map:

$$T(x) = T_2 \circ T_1 \circ T_2 \circ T_1(x)$$

where:

$$T_1(x) = \begin{bmatrix} 0 & 1 \\ 1 & 0 \end{bmatrix} \begin{bmatrix} x_1 \\ x_2 \end{bmatrix}, \quad T_2(x) = \begin{bmatrix} 1 & 0 \\ 1 & 1 \end{bmatrix} \begin{bmatrix} x_1 \\ x_2 \end{bmatrix}.$$

- Anzai's example [47] of a skew product transformation:

$$T(x) = \begin{bmatrix} x_1 + \gamma \\ x_1 + x_2 \end{bmatrix} \mod 1, \tag{6.14}$$

which is the composition of a shear map and a translation:

$$T(x) = T_2 \circ T_1(x)$$

where:

$$T_1(x) = \begin{bmatrix} 1 & 0 \\ 1 & 1 \end{bmatrix} \begin{bmatrix} x_1 \\ x_2 \end{bmatrix}, \quad T_2(x) = \begin{bmatrix} x_1 + \gamma \\ x_2 \end{bmatrix}.$$

- Chirikov Standard map [44]:

$$T(x) = \begin{bmatrix} x_1 + x_2 + K\sin(2\pi x_1) \\ x_2 + K\sin(2\pi x_1) \end{bmatrix} \mod 1, \tag{6.15}$$

which is the composition of two distinct shear maps in orthogonal directions:

$$T(x) = T_2 \circ T_1(x)$$

where:

$$T_1(x) = \begin{bmatrix} x_1 \\ x_2 + K\sin(2\pi x_1) \end{bmatrix} \mod 1, \quad T_2(x) = \begin{bmatrix} 1 & 1 \\ 1 & 0 \end{bmatrix} \begin{bmatrix} x_1 \\ x_2 \end{bmatrix} \mod 1.$$

- The ABC-map of Feingold [45] which is the composition of 3 shear maps:

$$T(x) = T_3 \circ T_2 \circ T_1(x),$$

where:

$$T_1(x) = \begin{bmatrix} x_1 + A\sin(2\pi x_1) + C\cos(2\pi x_3) \\ x_2 \\ x_3 \end{bmatrix},$$

$$T_2(x) = \begin{bmatrix} x_1 \\ x_2 + B\sin(2\pi x_1) + A\cos(2\pi x_3) \\ x_3 \end{bmatrix},$$

$$T_3(x) = \begin{bmatrix} x_1 \\ x_2 \\ x_3 + C\sin(2\pi x_2) + B\cos(2\pi x_1) \end{bmatrix}.$$

6.2 Evaluating the spectral projections and density functions

Once a periodic approximation is obtained of a map, it may be used to compute spectral projections and spectral density plots of observables. First the observable needs to discretized as well.

6.2.1 Discretizating the observable

The operator (4.3) is an orthogonal projector which maps observables in $L^2(\mathbb{T}^m, \mathcal{B}(\mathbb{T}^m), \mu)$ onto their best approximations in $L^2_n(\mathbb{T}^m, \mathcal{B}(\mathbb{T}^m), \mu)$. In practice, it makes no sense to explicitly evaluate this projection since typically one is only interested in computing the spectra of well-behaved functions. A discrete representation of the observable may also be obtain by simply sampling the function at the representative points (6.5). The averaging operator (4.3) is replaced with:

$$(\tilde{\mathcal{W}}_n g)(x) = \tilde{g}_n(x) := \sum_{j=1}^{q(n)} g(x_{n,j})\chi_{p_{n,j}}(x).$$

Indeed, for observables that are continuous, it is not hard to show that $\|g_n - \tilde{g}_n\| \to 0$ as $n \to \infty$.

6.2.2 Computing the spectral projection

Let $\mathrm{g}_n \in \mathbb{C}^{q(n)}$ and $\mathrm{S}_{n,D_\alpha} \in \mathbb{C}^{q(n)\times q(n)}$ respectively denote:

$$[g_n]_j = \left\langle \chi_{p_{n,i}}, g_n \right\rangle, \qquad [\mathrm{S}_{n,D_\alpha}]_{ij} := \left\langle \chi_{p_{n,i}}, \mathcal{S}_{n,D_\alpha} \chi_{p_{n,j}} \right\rangle,$$

then from (3.7) it is straightforward to show that:

$$\mathrm{S}_{n,D_\alpha}\mathrm{g}_n = \mathrm{V}_n \chi_{D_\alpha}(\log \Lambda_n)\mathrm{V}_n^* \mathrm{g}_n, \tag{6.16}$$

where:

$$\chi_{D_\alpha}(\theta) = \int_{\mathbb{S}} \varphi_\alpha(\theta,\xi)\chi_D(\xi)\mathrm{d}\xi.$$

The evaluation of (6.16) will involve finding the cycle decomposition (3.5), which in turn requires traversing the cycles of the permutation matrix $\mathrm{U}_n \in \mathbb{R}^{q(n)\times q(n)}$. This requirement is equivalent to traversing the trajectories of the discrete map $T_n : \mathcal{P}_n \mapsto \mathcal{P}_n$. The following algorithm is obtained.

Algorithm 6.2.1. To compute the spectral projection, do the following:

1. Initialize a vector $f \in \mathbb{R}^{q(n)}$ of all zeros and set $j = 1$ and $k = 1$.

2. Given some $j \in \{1, \ldots, q(n)\}$, if $[f]_j = 1$ move on to step 4 directly. Otherwise, traverse the trajectories of the discrete map until it has completed a cycle, i.e.

$$p_{n,j(l)} = T_n^l(p_{n,j(1)}), \qquad l = 1, 2, \ldots, n^{(k)},$$

   where:

$$j(1) = j \quad \text{and} \quad p_{n,j(1)} = T_n^{n^{(k)}}(p_{n,j(1)}).$$

   To demarcate visited partition elements, set $[f]_{j(l)} = 1$ for $l = 1, 2, \ldots, n^{(k)}$.

3. Denote by $\omega = \exp\left(\frac{2\pi}{n^{(k)}} i\right)$. Apply the FFT and inverse-FFT algorithms to evaluate:

$$[\mathrm{S}_{n,D_\alpha} \mathrm{g}_n]_{j(l)} = \frac{1}{n} \sum_{t=1}^{n^{(k)}} \chi_{D_\alpha}\left(\frac{2\pi(t-1)}{n^{(k)}}\right) \omega^{(l-1)(t-1)} \left(\sum_{r=1}^{n^{(k)}} \omega^{(t-1)(r-1)} g(\psi(p_{n,j(r)}))\right)$$

   for $l = 1, 2, \ldots, n^{(k)}$. Increment $k \leftarrow k + 1$.

4. Move on to the next partition element $p_{n,j} \in \mathcal{P}_n$, i.e. $j \leftarrow j + 1$, and repeat step 2 until all partition elements have been visited.

Complexity of Algorithm 6.2.1 The most dominant part of the computation is the application of the FFT and inverse-FFT algorithms on the cycles. Hence, the time-complexity of the algorithm is $\mathcal{O}(\sum_{l=1}^{s} n^{(l)} \log n^{(l)})$. In the worst-case scenario, it may occur that the permutation (3.1) consist of one single large cycle (possible for ergodic systems). In that case, the conservative estimate $\mathcal{O}(\tilde{n}^d \log \tilde{n})$ is obtained. Note that the evaluation of the spectral projections may be further accelerated using sparse FFT techniques. This is true especially for projections wherein the interval $D \subset \mathbb{S}$ is small, leading to a highly rank-deficient $\mathrm{S}_{n,D_\alpha} \in \mathbb{C}^{q(n)\times q(n)}$.

6.2.3 Step 3b: Computing the spectral density function

By modifying step 3 of the previous algorithm, one may proceed to compute an approximation of the spectral density function (4.20):

$$\rho_{\alpha,n}(\theta; g_n) := \int_{\mathbb{S}} \varphi_\alpha(\xi, \theta) \rho_n(\xi; g_n) \mathrm{d}\xi,$$

where:

$$\varphi_\alpha(x,y) = \begin{cases} \frac{K}{\alpha}\exp\left(\frac{-1}{1-\left(\frac{d(x,y)}{\alpha}\right)^2}\right) & \frac{d(x,y)}{\alpha} < 1 \\ 0 & \text{otherwise} \end{cases}, \qquad \rho_n(\theta; g_n) = \sum_{k=1}^{q(n)} \left\|\mathcal{S}_{n,\theta_{n,k}} g_n\right\|^2 \delta(\theta - \theta_{n,k}).$$

If (4.20) needs to evaluated at some collection of points $\{\theta_r\}_{r=1}^R \subset \mathbb{S}$, the algorithm would look as follows:

Algorithm 6.2.2. To evaluate the spectral density function on $\{\theta_r\}_{r=1}^R \subset \mathbb{S}$, do the following:

1. Initialize a vector $f \in \mathbb{R}^{q(n)}$ of all zeros and also initialize $\rho_{\alpha,n}(\theta_r; g_n) = 0$ for $r = 1, \ldots, R$. Furthermore, set $j = 1$ and $k = 1$.

2. Given some $j \in \{1, \ldots, q(n)\}$, if $[f]_j = 1$ move on to step 4 directly. Otherwise, traverse the trajectories of the discrete map until it has completed a cycle, i.e.

$$p_{n,j(l)} = T_n^l(p_{n,j(1)}), \qquad l = 1, 2, \ldots, n^{(k)},$$

   where:

$$j(1) = j \quad \text{and} \quad p_{n,j(1)} = T_n^{n^{(k)}}(p_{n,j(1)}).$$

   To demarcate visited partition elements, set $[f]_{j(l)} = 1$ for $l = 1, 2, \ldots, n^{(k)}$.

3. Denote by $\omega = \exp\left(\frac{2\pi}{n^{(k)}}i\right)$. Apply the FFT algorithms to update:

$$\rho_{\alpha,n}(\theta_r; g_n) \leftarrow \rho_{\alpha,n}(\theta_r; g_n) + \frac{K}{n\alpha}\sum_{t=1}^{n^{(k)}} \exp\left(\frac{-1}{1-\left(\frac{d\left(\frac{2\pi(t-1)}{n^{(k)}},\theta_r\right)}{\alpha}\right)^2}\right)\left|\sum_{l=1}^{n^{(k)}}\omega^{(t-1)(l-1)}g(\psi(p_{n,j(l)}))\right|^2 \quad (6.17)$$

for $r = 1, 2, \ldots, R$. Increment $k \leftarrow k+1$.

4. Move on to the next partition element $p_{n,j} \in \mathcal{P}_n$, i.e. $j \leftarrow j+1$, and repeat step 2 until all partition elements have been visited.

Complexity of Algorithm 6.2.2 Since $\alpha > 0$ is typically small, the most dominant part of the computation wil again be the application of the FFT algorithm in step 3. Assuming that $R << n^{(k)}$, the time-complexity of the algorithm will be $\mathcal{O}(\sum_{l=1}^{s} n^{(l)} \log n^{(l)})$, reducing to $\mathcal{O}(\tilde{n}^d \log \tilde{n})$ in the worst-case scenario of a cyclic permutation.

6.3 Extending the numerical method for flows

The numerical methods described in this section are easily extended for flows. A periodic approximation is obtained in almost the same manner. In the case of a brute force construction, one of course needs to keep in mind the consequences of condition (5.18) in theorem 5.2.2. Analytic constructions of periodic approximations can be obtained in some cases using symplectic lattice maps [48]. Symplectic lattice maps are integer arithmetic implementation of symplectic integrators that leave a lattice in the state-space invariant. It can shown that these integer dynamics are related to a symplectomorphism

of a nearby time-dependent Hamiltonian of the original system. If the trajectories of this nearby Hamiltonian are bounded for a given domain, then a periodic approximation is also obtained for that region. For a planar hamilonian system with bounded energy curves this is always the case: a small time-dependent pertubation of the Hamiltonian will not destroy these energy curves. For higher dimensional Hamiltonians, time-dependent perturbations may introduce Arnold diffusion causing the trajectories not to return to their starting points.

Chapter 7

Examples

In this chapter, the numerical method of the previous chapter is demonstrated on a set of examples. At first, the method is tested on three canonical examples of Lebesgue measure-preserving transformations: the translation map, Arnold's cat map, and Anzai's skew-product transformation. These examples permit an easy closed form expression of both the spectral projectors and density functions, making them a good test bed to illustrate the workings of the numerical method. Next, the method is applied on the Chirikov standard map which is a classical example of a perturbed twist map. After this, the spectra is computed of two planar Hamiltonian systems: the simple pendulum and the Duffing oscillator. This is followed by an analysis of the spectra of a quadruple gyre which is contructed from a stream function with periodic forcing. The final example considered is the volume-preserving Arnold-Beltrami-Childress flow.

7.1 Canonical examples on the 2-torus

In this section, the spectra is analyzed of the translation map (6.11), Arnold's cat map (6.13), and Anzai's skew-product transformation (6.14). The examples cover the

full range of possible "spectral scenario's" that one may encounter in practice: the first map has a fully discrete spectrum, the second one has a fully continuous spectrum[1], and the third map has a mixed spectrum.

7.1.1 Translation on the m-torus

Consider a translation on the torus (6.11):

$$T(x) = \begin{bmatrix} x_1 + \omega_1 \\ \vdots \\ x_m + \omega_m \end{bmatrix} \mod 1.$$

This is the type of map one would typically obtain from a Poincare section of an integrable Hamiltonian expressed in action-angle coordinates. Denote by $k = (k_1, \ldots, k_m) \in \mathbb{Z}^m$ and $\omega = (\omega_1, \ldots, \omega_m) \in \mathbb{R}^m$. The map (6.11) is ergodic if and only if $k \cdot \omega \notin \mathbb{Z}$ for all $k \in \mathbb{Z}^m$ and $k \neq 0$.

Singular and regular subspaces

The Koopman operator associated with (6.11) has a fully discrete spectrum. Moreover, the Fourier basis elements turn out to be eigenfunctions for the operator, i.e.

$$\mathcal{U} e^{2\pi i(k\cdot x)} = e^{2\pi i(k\cdot\omega)} e^{2\pi i(k\cdot x)}.$$

The singular and regular subspaces are respectively:

$$H_s = \overline{\text{span}\{e^{2\pi i(k\cdot x)}, \quad k \in \mathbb{Z}^m\}}, \qquad H_r = \emptyset.$$

[1]Expect for the trivial eigenvalue at 1

Spectral density function

The spectral density function for observables in the form:

$$g = \sum_{k \in \mathbb{Z}^m} a_k e^{2\pi i (k \cdot x)} \in L^m(\mathbb{T}^m, \mathcal{B}(\mathbb{T}^m), \mu),$$

is given by the expression:

$$\rho(\theta; g) = \sum_{k \in \mathbb{Z}^m} |a_k|^2 \delta(\theta - 2\pi(k \cdot \omega) \mod 2\pi). \tag{7.1}$$

Noteworthy to mention is that the spectra of the operator for the map (6.11) can switch from isolated to dense with arbitrarily small perturbations to $\omega \in \mathbb{R}^m$.

Spectral projectors

Given an interval $D = [a, b) \subset \mathbb{S}$, the spectral projectors can be expressed as:

$$\mathcal{S}_D g = \sum_{2\pi(k\cdot\omega) \mod 2\pi \in D} a_k e^{2\pi i (k \cdot x)}.$$

Numerical results

In fig. 7.1, the spectral density function (3.11) is plotted for the case when $d = 1$, $\omega_1 = 1/3$, and:

$$g(x) = \frac{\sin(4\pi x)}{1 + \cos^2(2\pi x) + \sin(7\pi x)}. \tag{7.2}$$

As the partitions are refined, it is evident from fig. 7.1 that the energy becomes progressively more concentrated around the eigenvalues of the true spectra at $e^{i\frac{2\pi(k-1)}{3}}$, with $k = 1, 2, 3$.

In fig. 7.2, the case when $d = 2$ and $(\omega_1, \omega_2) = (\frac{1}{2}, \frac{1}{3})$ is examined. The trajectories

of this map are all 6-periodic, and eigenvalues are also located 6th roots of unity (i.e. $e^{i\frac{2\pi(k-1)}{6}}$, with $k = 1, 2, \ldots, 6$). Shown are spectral projections (5.10) of the observable:

$$g(x) = \sin(2\pi x_1)\cos(2\pi x_2) + \sin(\pi x_2) + \frac{1}{\sin^2(\pi x_1) + 1} - 1 \tag{7.3}$$

around narrow intervals of these eigenvalues.

7.1.2 Arnold's cat map

Consider the area-preserving map $T : \mathbb{T}^2 \mapsto \mathbb{T}^2$, defined in (6.13):

$$T(x) = \begin{bmatrix} 2 & 1 \\ 1 & 1 \end{bmatrix} \begin{bmatrix} x_1 \\ x_2 \end{bmatrix} \mod 1.$$

Arnold's cat map (6.13) is a well-known example of a Anosov diffeomorphism, in which the dynamics are locally characterizable by expansive and contractive directions. The map (6.13) has positive Kolmogorov entropy, is strongly mixing, and therefore also ergodic.

Singular and regular subspaces

The Koopman operator associated with Arnold's cat map is known to have a "Lebesgue spectrum" (see e.g. [46]). A Lebesgue spectrum implies the existence of an orthonormal basis for $L^2(\mathbb{T}^2, \mathcal{B}(\mathbb{T}^2), \mu)$ consisting of the constant function and $\{\varphi_{s,t}\}_{s\in I, t\in\mathbb{Z}}$, $I \subseteq \mathbb{N}$, such that:

$$\mathcal{U}^l \varphi_{s,t} = \varphi_{s,t+l}, \quad l \in \mathbb{Z}.$$

It follows from such a basis that the eigenspace at $\lambda = 1$ is simple, i.e. consisting only the constant function, with the remaining part of the spectrum absolutely continuous. In

the case of the Cat map, the basis $\{\varphi_{s,t}\}_{s\in I,t\in\mathbb{Z}}$ is just a specific re-ordering of the Fourier elements $\{e^{2\pi i(k_1x_1+k_2x_2)}\}_{(k_1,k_2)\in\mathbb{Z}^2}$. Indeed, by applying the Koopman operator (3.8) onto a Fourier element, the following transformation is observed:

$$\mathcal{U}e^{2\pi i(k_1x_1+k_2x_2)} = e^{i2\pi(k'_1x_1+k'_2x_2)}, \qquad \begin{array}{rcl} k'_1 &=& 2k_1+k_2 \\ k'_2 &=& k_1+k_2 \end{array}, \qquad (k_1,k_2)\in\mathbb{Z}^2. \tag{7.4}$$

Partitioning $\mathbb{Z}^2$ into the orbits of (7.4), i.e. $\mathbb{Z}^2 = \xi_0\cup\xi_1\cup\xi_2\cup\xi_3\ldots$, notice that all orbits, except for $\xi_0=\{(0,0)\}$, consists of countable number of elements. The singular and regular subspaces are respectively:

$$H_s = \text{span}\{1\}, \qquad H_r = \overline{\text{span}\{e^{i2\pi(k_1x_1+k_2x_2)}: \quad (k_1,k_2)\neq 0\}}.$$

Spectral density function

The spectral density function (4.20) of a generic observable is found by solving the trigonometric moment problem [34]:

$$d_l := \langle \mathcal{U}^l g, g\rangle = \int_{\mathbb{T}^2} \left(\mathcal{U}^l g\right)^*(x) g(x) \mathrm{d}\mu = \int_{\mathbb{S}} e^{il\theta}\rho(\theta;g)\mathrm{d}\theta, \quad l\in\mathbb{Z}.$$

If the observable consists of a single Fourier element, note that: (i) $(k_1,k_2)=(0,0)$ implies $d_l=1$, $\forall l\in\mathbb{Z}$ which leads to $\rho(\theta;1)=\delta(\theta)$ (i.e. Dirac delta distribution), (ii) $(k_1,k_2)\neq(0,0)$ implies $d_l=0$ $\forall l\neq 0$ and $d_0=1$, leading to $\rho(\theta;e^{i2\pi(k_1x_1+k_2x_2)})=\frac{1}{2\pi}$ (i.e. a uniform density). By virtue of these properties, the spectral density function (4.20) of a generic observable in the form:

$$g = a_0 + \sum_{s\in\mathbb{N}}\sum_{t\in\mathbb{Z}} a_{s,t}\varphi_{s,t} \in L^2(\mathbb{T}^2,\mathcal{B}(\mathbb{T}^2),\mu), \qquad |a_0|^2 + \sum_{s\in\mathbb{N}}\sum_{t\in\mathbb{Z}}|a_{s,t}|^2<\infty, \tag{7.5}$$

can be expressed as:

$$\rho(\theta; g) = |a_0|^2\delta(\theta) + \frac{1}{2\pi}\sum_{l\in\mathbb{Z}}\left(\sum_{s\in\mathbb{N}}\sum_{t\in\mathbb{Z}} a^*_{s,t-l}a_{s,t}\right)e^{il\theta}. \tag{7.6}$$

Spectral projectors

For an interval $D = [c-\delta, c+\delta) \subset \mathbb{S}$, one can use the Fourier series expansions of the indicator function:

$$\chi_D = \sum_{l\in\mathbb{Z}} b_l(D)e^{il\theta}, \qquad b_l(D) := \tfrac{1}{2\pi}\int_{\mathbb{S}} e^{-il\theta}\chi_D(\theta)\mathrm{d}\theta = \frac{1}{2\pi}\begin{cases} \frac{i}{l}e^{-icl}(e^{-i\delta l} - e^{i\delta l}) & l \neq 0 \\ 2\delta & l = 0 \end{cases}. \tag{7.7}$$

to obtain an approximation of the spectral projector with the help of functional calculus. Using the Lebesgue basis in (7.5), the following expression for the spectral projection can be obtained:

$$\mathcal{S}_D g = \sum_{l\in\mathbb{Z}} b_l(D)\mathcal{U}^l g = a_0\nu(D) + \sum_{l\in\mathbb{Z}} b_l(D)\left(\sum_{s\in\mathbb{N}}\sum_{t\in\mathbb{Z}} a_{s,t}\varphi_{s,t+l}\right)$$

where the singular measure $\nu(D) = 1$ whenever $0 \in D$. The frequency content of the projection increases drastically as the width of the interval is shrinked. This is because the Lebesgue basis functions $\varphi_{s,t}$ become increasingly oscillatory for larger values of t, and reducing the width of the interval places more weight on these higher frequency components.

Numerical results

For observables that consist of only a finite number of Fourier components, a closed-form expression of the spectral density function can be obtained. For example:

$$\begin{aligned} g_1(x) &= e^{2\pi i(2x_1+x_2)} \\ g_2(x) &= e^{2\pi i(2x_1+x_2)} + \frac{1}{2}e^{(2\pi i(5x_1+3x_2))} \\ g_3(x) &= e^{2\pi i(2x_1+x_2)} + \frac{1}{2}e^{(2\pi i(5x_1+3x_2))} + \frac{1}{4}e^{2\pi i(13x_1+8x_2)} \end{aligned}$$

yields

$$\begin{aligned} \rho(\theta; g_1) &= \frac{1}{2\pi} \\ \rho(\theta; g_2) &= \frac{1}{2\pi}\left(\frac{5}{4} + \cos\theta\right) \\ \rho(\theta; g_3) &= \frac{1}{2\pi}\left(\frac{21}{16} + \frac{10}{8}\cos\theta + \frac{1}{2}\cos 2\theta\right) \end{aligned} \tag{7.8}$$

In fig. 7.3, the spectral densities of these observables are approximated with (4.20) using the proposed method. Clearly, the result indicate that better approximations are obtained by increasing the discretization level. In fig. 7.4, the spectral projections for the first observable are plotted. As expected, shrinkage of the interval leads to more noisy figures.

7.1.3 Anzai's skew-product transformation

One can use skew-products of dynamical systems to construct examples of maps that have mixed spectra [47]. An example of such a transformation is the map (6.14):

$$T(x_1, x_2) = (x_1 + \gamma, x_1 + x_2) \mod 1, \tag{7.9}$$

for which $\gamma \in [0, 1)$. The map (6.14) is the composition of a translation and a shear. The transformation is ergodic whenever $\gamma \in \mathbb{R}$ is irrational.

Singular and regular subspaces

The mixed spectrum of the operator is recognized by examining the cyclic subspaces generated by the Fourier basis elements. Essentially, Fourier elements that solely depend on the coordinate x_1 behave as if the dynamics of the map are that of a pure translation, whereas the remaining Fourier elements do observe a shear and belong to a cyclic subspace of infinite length. The singular and regular subspaces of the operator are respectively given by:

$$H_s = \overline{\text{span}\{\sigma_t := e^{2\pi i(tx_1)}, \quad t \in \mathbb{Z}\}}$$

and

$$H_r = \overline{\text{span}\{\varphi_{s,t,w} := e^{2\pi i((t+sw)x_1+sx_2)}, \quad s, w \in \mathbb{Z}, t \in \mathbb{N} \text{ with } s \neq 0, t < |s|\}}.$$

Spectral density function

Application of the Koopman operator yields:

$$\mathcal{U}^l \sigma_t = e^{2\pi i l t\gamma}\sigma_t \qquad \text{and} \qquad \mathcal{U}^l \varphi_{s,t,w} = e^{2\pi i l\left(t+s\left(w+\frac{l-1}{2}\right)\right)\gamma}\varphi_{s,t,w+l}.$$

Solving the trigonometric moment problem for observables expressed in the form:

$$g = \sum_{t\in\mathbb{Z}} a_t\sigma_t + \sum_{s\in\mathbb{Z},s\neq 0}\sum_{t\in\mathbb{N},t<|s|}\sum_{w\in\mathbb{Z}} c_{s,t,w}\varphi_{s,t,w} \in L^2(\mathbb{T}^2, \mathcal{B}(\mathbb{T}^2), \mu),$$

yield the density function:

$$\rho(\theta;g) = \sum_{t\in\mathbb{Z}} |a_t|^2 \delta(\theta - 2\pi\gamma t \mod 2\pi) + \frac{1}{2\pi}\sum_{l\in\mathbb{Z}}\left(\sum_{s\in\mathbb{Z},s\neq 0}\sum_{t\in\mathbb{N},t<|s|}\left(\sum_{w\in\mathbb{Z}} e^{-2\pi i l\left(t+s\left(w+\frac{l-1}{2}\right)\right)\gamma} c^*_{s,t,w-l}c_{s,t,w}\right)\right)e^{il\theta}. \quad (7.10)$$

Spectral projectors

For the interval $D = [c-\delta, c+\delta) \subset \mathbb{S}$, an expression for the spectral projection is given by:

$$\mathcal{S}_D g = \sum_{2\pi t\gamma \mod 2\pi\in D} a_t\sigma_t + \sum_{l\in\mathbb{Z}} b_l(D)\left(\sum_{s\in\mathbb{Z},s\neq 0}\sum_{t\in\mathbb{N},t<|s|}\sum_{w\in\mathbb{Z}} e^{2\pi i l\left(t+s\left(w+\frac{l-1}{2}\right)\right)\gamma} c_{s,t,w}\varphi_{s,t,w+l}\right),$$

where the coefficients $b_l(D)$ are defined as in (7.7).

Numerical results

Now set $\gamma = 1/3$ and consider the observable:

$$g(x_1,x_2) = \frac{1}{20}e^{2\pi i x_1} + \frac{1}{20}e^{4\pi i x_1} + \frac{1}{5}e^{6\pi i x_1} + e^{2\pi i x_2} + \frac{1}{2}e^{(2\pi i(x_1+x_2))} \quad (7.11)$$

The spectral decomposition is given by:

$$\rho(\theta;g) = \frac{1}{400}\left(\delta(\theta) + \delta(\theta - \frac{2\pi}{3})\right) + \frac{1}{25}\delta(\theta - \frac{4\pi}{3}) + \frac{1}{2\pi}\left(\frac{5}{4} + \cos\theta\right)$$

In section 7.5, the spectral density function is plotted for different discretization levels. Convergence of the spectra is observed by refinement of the grid. In section 7.5, spectral projections of the observable are shown for small intervals centered around the eigenvalues

$e^{i\frac{2\pi(k-1)}{3}}$, with $k = 1, 2, 3$. Note that the exact eigenfunctions are not recovered due to the presence of continuous spectra which is interleaved in the projection. In section 7.5, projections are shown in a region where only continuous spectrum is present.

7.2 The Chirikov standard map

In this section, the Koopman spectra is analyzed for the family of area-preserving maps introduced by *Chirikov* (6.15):

$$T(x) = \begin{bmatrix} x_1 + x_2 + K\sin(2\pi x_1) \\ x_2 + K\sin(2\pi x_1) \end{bmatrix} \mod 1$$

Unlike the examples of the previous section, finding an explicit expression of the spectra is highly non-trivial (except for the case when $K = 0$). In figs. 7.6 to 7.10 the spectral properties of the standard map are examined for K-values ranging between 0 and 0.35. In fig. 7.6, approximations of the spectral density functions (4.20) are plotted for the observable:

$$g(x) = e^{i4\pi x_1} + e^{i3\pi x_1} + 0.01e^{i2\pi x_2} \tag{7.12}$$

It can be seen that sharp peaks form at locations other than eigen-frequency $\theta = 0$. These peaks illustrate that the purely continuous spectra disintegrate, with the rise of discrete spectra for the operator. Eigenfunctions of (3.8) may be recovered from the spectral projections by means of centering the projection on narrow intervals around the respective eigenfrequency. In figs. 7.7 to 7.10, this is done for respectively $\theta = 0, \pi, 2\pi/3, \pi/2$. The eigenfunction at $\theta = 0$ yields an invariant partition of the state-space, the eigenfunctions of the other frequencies $\theta = \pi, 2\pi/3, \pi/2$ provide periodic partitions of period 2,3 and 4, respectively (see also [9, 10]).

7.3 Planar Hamiltonian systems

Hamiltonian systems are defined on unbounded domains. But in many situations, the trajectories belonging to a sub-level set of energy surfaces are bounded. Hence, for that subdomain of the state-space, periodic approximations may be constructed to compute spectra. For a separable, one degree-of-freedom Hamiltonian systems, periodic approximations can be obtained readily from a symplectic lattice map (see discussion in section 6.3). What follows next is an analysis of the spectra of the simple pendulum and the duffing oscillator.

7.3.1 Simple pendulum

Consider the simple pendulum:

$$\begin{bmatrix} \dot{x}_1 \\ \dot{x}_2 \end{bmatrix} = \begin{bmatrix} x_2 \\ -\sin x_1 \end{bmatrix}, \tag{7.13}$$

restricted to the domain:

$$X = \left\{ x_1 \in [0, 2\pi), x_2 \in \mathbb{R} : \quad \tfrac{1}{2}x_2^2 - \cos(x_1) \leq \tfrac{1}{2}\pi^2 + 1 \right\}.$$

Apart from the single eigenvalue at $\lambda = 0$, it was shown in [49] that the spectra of (7.13) is fully continuous. In fig. 7.11, the spectra is plotted of the observable:

$$g(x_1, x_2) = \frac{1}{2}x_2^2 - (\cos x_1). \tag{7.14}$$

In fig. 7.12, spectral projections are shown for various intervals.

7.3.2 Duffing oscillator

Consider the duffing oscillator:

$$\begin{bmatrix} \dot{x}_1 \\ \dot{x}_2 \end{bmatrix} = \begin{bmatrix} x_2 \\ -bx_1 - ax_1^3 \end{bmatrix}, \tag{7.15}$$

restricted to the domain:

$$X = \left\{ x_1 \in \mathbb{R}, x_2 \in \mathbb{R} : \quad \tfrac{1}{2}x_2^2 + \tfrac{1}{2}bx_1^2 + \tfrac{1}{4}ax_1^4 \leq \tfrac{1}{2}\pi^2 + \tfrac{1}{2}b\pi^2 + \tfrac{1}{4}a\pi^4 \right\}.$$

Set $b = -1$, $a = 1$ and consider the observable:

$$g(x_1, x_2) = \frac{1}{2}x_2^2 - \frac{1}{2}x_1^2 + \frac{1}{4}x_1^4 \tag{7.16}$$

In fig. 7.13 the spectra is plotted and in fig. 7.14 projections are shown.

Let us fix $a = 1$ and vary the coefficient b from negative to positive values. In figs. 7.15 and 7.16, the spectral density is plotted of the observable:

$$g(x_1, x_2) = \frac{1}{2}x_2^2 + i\left(\frac{1}{2}x_1^2\right). \tag{7.17}$$

When $b = 0$, the system undergoes a pitch-fork bifurcation. In fig. 7.15, the spectral density is plotted for small perturbations of b, i.e. around the bifurcation point. From a topological point of view, the duffing oscillator clearly undergoes a sudden transition with the birth of two new fixed points. But from a spectral sense, this transition is however smooth and unnoticable. The smooth transitation can be clarifed by the close proximity of the new fixed points during the bifurcation. Noticable changes in the spectra occur only when b is modified signifanctly, as evident in fig. 7.16. Since the bifurcation does not

induce immediate global topological changes, from a spectral point of view, the transition will remain smooth as the Koopman framework inherently incorporates finite resolution in measurement and observation.

7.4 The quadruple gyre

Next, consider a variation to the double gyre dynamics introduced in [50]. The quadruple gyre dynamics are described by the differential equations:

$$\begin{bmatrix} \dot{x}_1 \\ \dot{x}_2 \\ \dot{x}_3 \end{bmatrix} = \begin{bmatrix} \pi A \sin(\pi f_1(x_1, x_3)) \cos(\pi f_2(x_2, x_3)) \frac{\mathrm{d}f_1(x_1, x_3)}{\mathrm{d}x_1} \\ -\pi A \cos(\pi f_1(x_1, x_3)) \sin(\pi f_2(x_2, x_3)) \frac{\mathrm{d}f_2(x_2, x_3)}{\mathrm{d}x_2} \\ 1 \end{bmatrix} \tag{7.18}$$

on the domain $X = [0, 1] \times [0, 1] \times [0, 1)$, with:

$$f_1(x_1, x_3) = 4\epsilon \sin(2\pi x_3) x_1^2 + (2 - 4\epsilon \sin(2\pi x_3)) x_1,$$

and

$$f_2(x_2, x_3) = 4\epsilon \sin(2\pi x_3) x_2^2 + (2 - 4\epsilon \sin(2\pi x_3)) x_2.$$

The system (7.18) arises from a time-periodic stream function. In fact, the variable x_3 is periodic and equal to the time (modulo the period).

In fig. 7.18, the spectral density function is plotted for the observable:

$$g(x_1, x_2, x_3) = i(\sin(4\pi x_1) \sin(4\pi x_2)) + 4\psi(x_1, x_2), \tag{7.19}$$

where:

$$\psi(x_1, x_2) = \begin{cases} \exp\left(\frac{-1}{1-\frac{1}{2}\sqrt{(x_1-\frac{1}{2})^2+(x_2-\frac{1}{2})^2}}\right) & (x_1-\frac{1}{2})^2+(x_2-\frac{1}{2})^2 \leq \frac{1}{4} \\ 0 & (x_1-\frac{1}{2})^2+(x_2-\frac{1}{2})^2 \leq \frac{1}{4} \end{cases}.$$

The computations are performed for $A = 1/(2\pi)$ and $\epsilon = 0.05$. A spatial partition of $700 \times 700 \times 100$ was used and the time step was set to $\tau = 0.01$. As evident from fig. 7.18, it appears that the quadruple gyre has a mixed spectrum for these parameters. The location of the discrete spectra correspond to resonant frequencies of the KAM tori islands shown in fig. 7.17. This is also noticable in figs. 7.19 to 7.21, where spectral projections are shown for certain intervals of interest.

7.5 The Arnold-Beltrami-Childress flow

Finally, consider the Arnold-Beltrami-Childress (ABC) flow on the unit 3-torus, i.e. $X = [0, 1)^3$. The motion is described by the differential equations:

$$\begin{bmatrix} \dot{x}_1 \\ \dot{x}_2 \\ \dot{x}_3 \end{bmatrix} = \begin{bmatrix} A\sin x_3 + C\cos x_2 \\ B\sin x_1 + A\cos x_3 \\ C\sin x_2 + B\cos x_1 \end{bmatrix}. \tag{7.20}$$

For small τ-values, the flow S^τ of (7.20) can be approximated by:

$$\tilde{S}^\tau(x) = \tilde{S}_1^{\tau/3} \circ \tilde{S}_2^{\tau/3} \circ \tilde{S}_3^{\tau/3}(x) \tag{7.21}$$

where:

$$\tilde{S}_1^{\tau/3}(x) = \begin{bmatrix} x_1 + \frac{\tau}{3}(A\sin x_3 + C\cos x_2) \\ x_2 \\ x_3 \end{bmatrix}, \quad \tilde{S}_1^{\tau/3}(x) = \begin{bmatrix} x_1 \\ x_2 + \frac{\tau}{3}(B\sin x_1 + A\cos x_3) \\ x_3 \end{bmatrix},$$

$$\tilde{S}_1^{\tau/3}(x) = \begin{bmatrix} x_1 \\ x_2 \\ x_3 + \frac{\tau}{3}(C\sin x_2 + B\cos x_1) \end{bmatrix}.$$

This approximate volume-preserving τ-map is called the ABC map [45] and is the composition of three shear maps. A periodic approximation of (7.21) is obtained readily by periodically approximating each of the shear maps separately. In fig. 7.22, the spectral density function is plotted for the observable:

$$g(x_1, x_2, x_3) = \exp(4\pi i x_2) + 2\exp(6\pi i x_1) + \exp(2\pi i x_3) \tag{7.22}$$

The computations are performed for $A = \sqrt{3}/(2\pi)$, $B = \sqrt{2}/(2\pi)$, $C = 1/(2\pi)$. A spatial partition of $400 \times 400 \times 400$ was used and the time step was set to $\tau = 0.025$. In figs. 7.23 and 7.24, spectral projection are shown onto various intervals.

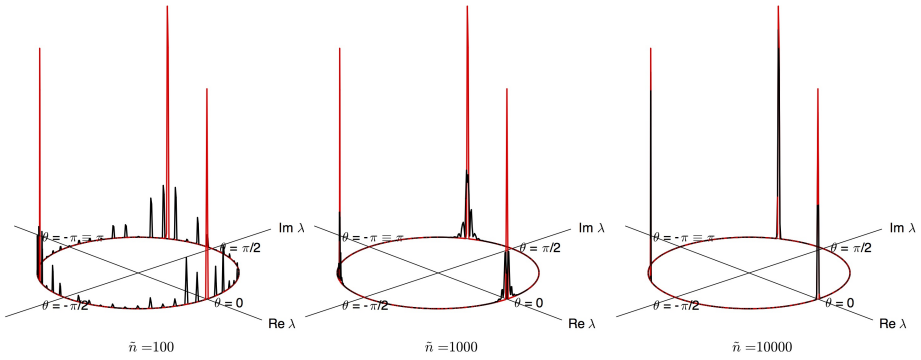

Figure 7.1: Approximations of the spectral density function (3.11) for the translation map (6.11) with $m = 1$ and $\omega_1 = 1/3$. Spectra is approximated for the observable (7.2) with $\alpha = 2\pi/500$. The black curve is approximation and the red curve is the true density.

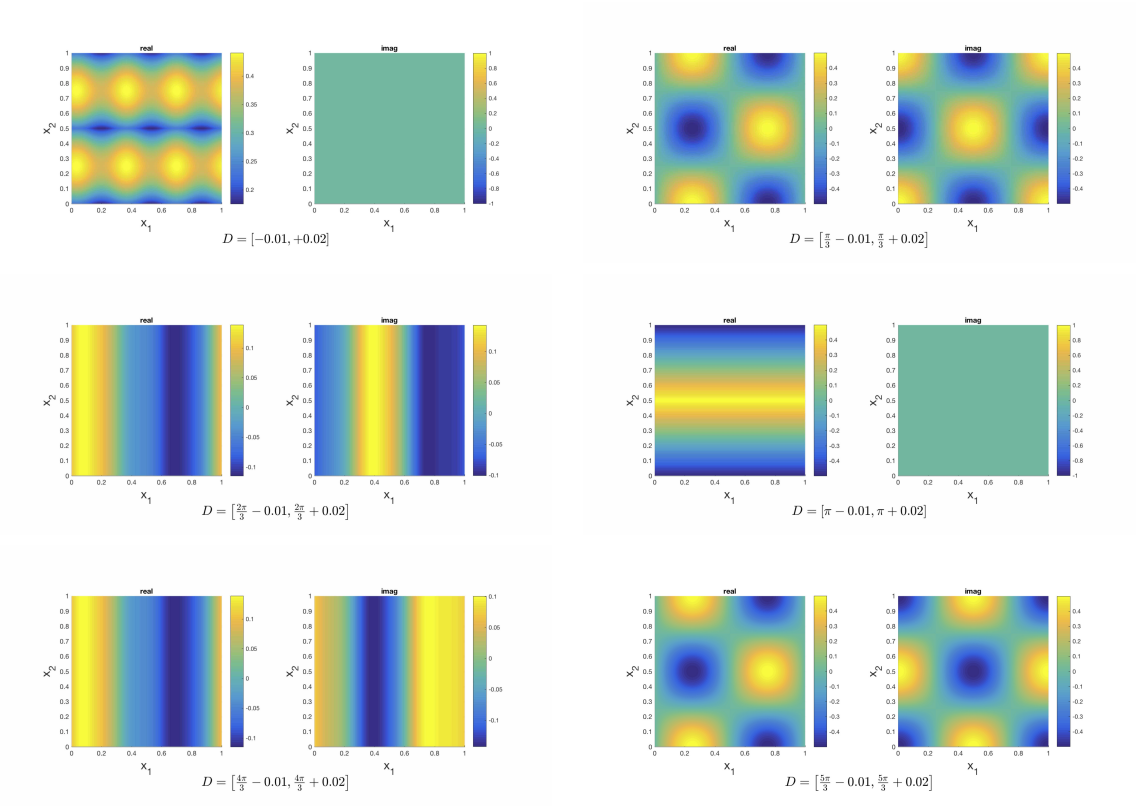

Figure 7.2: Results obtained for the translation map (6.11) with $m = 2$ and $(\omega_1, \omega_2) = (\frac{1}{2}, \frac{1}{3})$. Computations were performed for the observable (7.3) at a spatial discretization of $\tilde{n} = 1000$. Shown are spectral projections of the observable at narrow interval around the eigenvalues $\theta_k = \frac{2\pi(k-1)}{6}$.

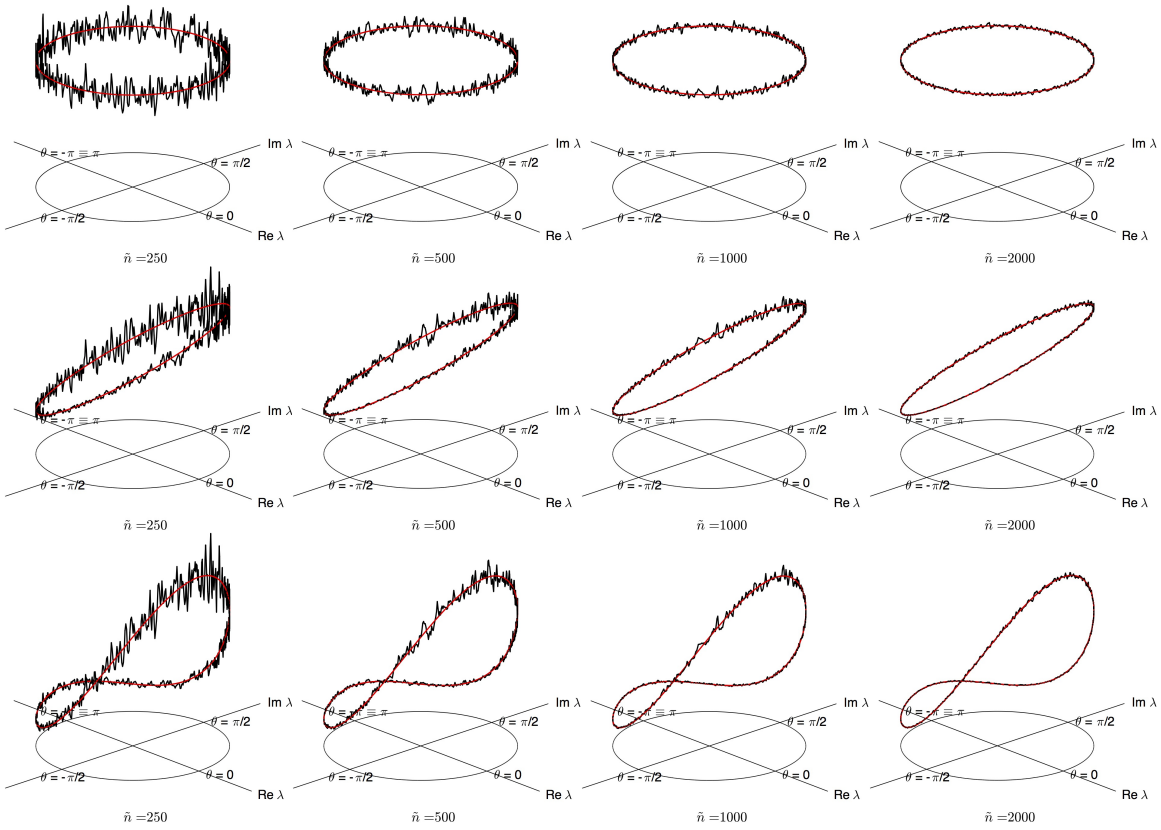

Figure 7.3: Approximations of the spectral density function of the cat map (6.13) for the observables in (7.8). The spectral resolution is set to $\alpha = 2\pi/500$. The black curves denote the approximations and the red curve is the true density. The first row shows approximations of $\rho(\theta; g_1)$, the second row shows $\rho(\theta; g_2)$ and the third row shows $\rho(\theta; g_3)$.

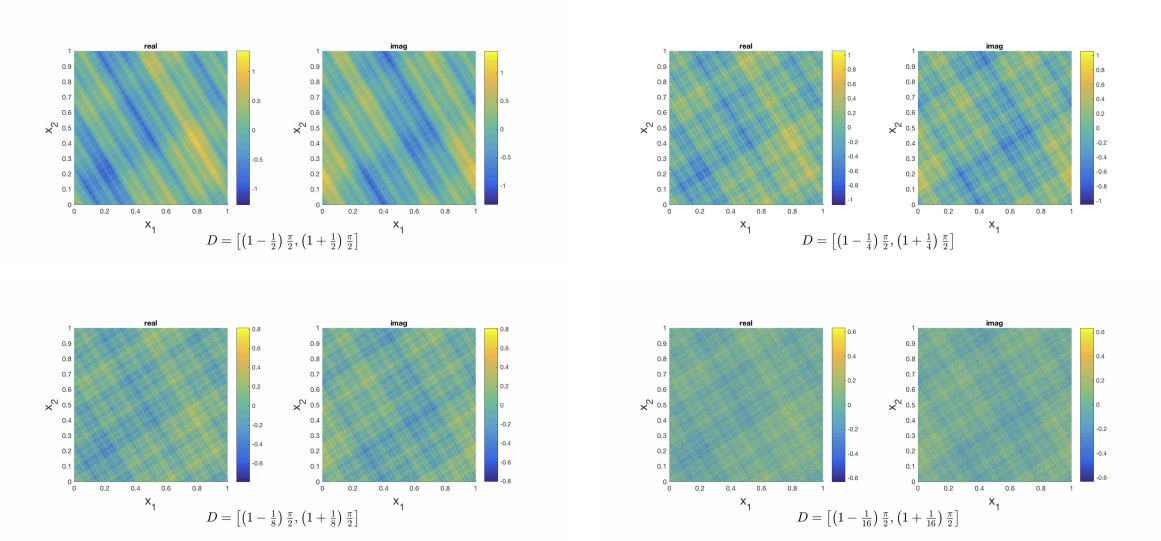

Figure 7.4: The spectral projections of cat map (6.13) for the first observable in (7.8). Projections were computed at the discretization level $\tilde{n} = 2000$.

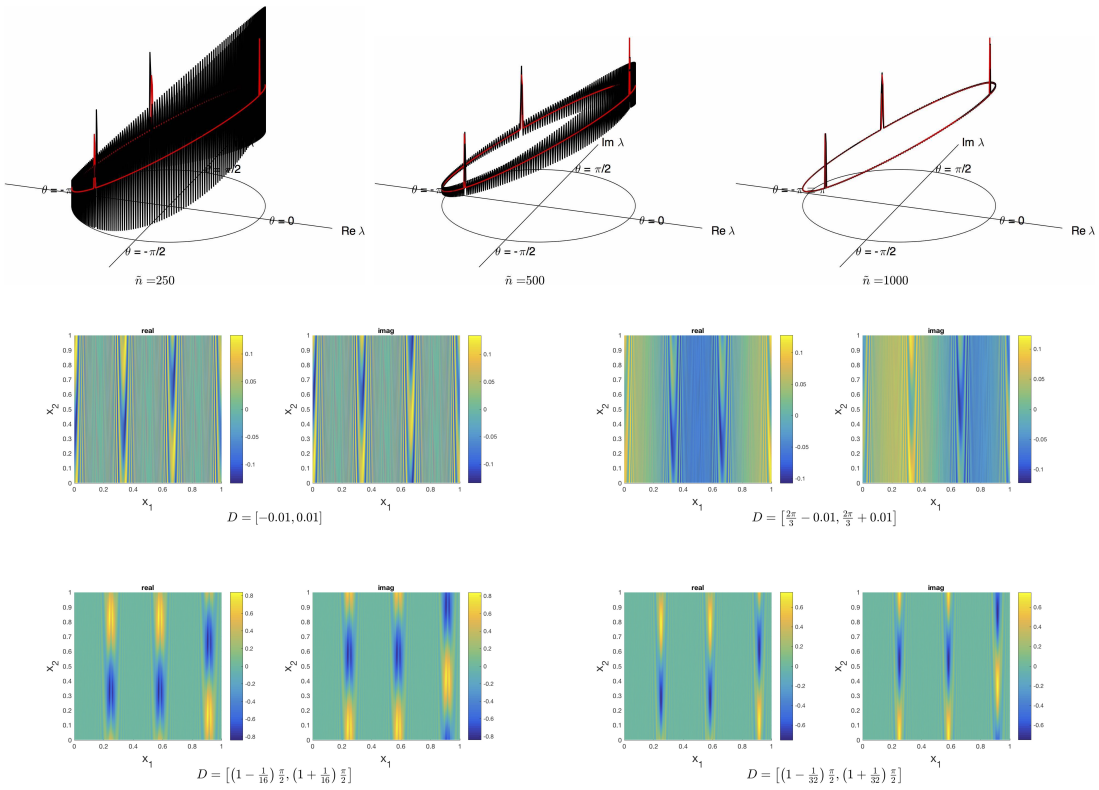

Figure 7.5: Results obtained for Anzai's skew product transformation (6.14) with $\gamma = 1/3$ and observable (7.11). Spectral projections were computed at a discretization level $\tilde{n} = 2000$. The top row shows approximations of the spectral density function at different discretization levels. The spectral resolution is set to $\alpha = 2\pi/500$. The black curves denote the approximations and the red curves are the true density. The middle row shows spectral projections computed at narrow intervals around the eigenfrequencies $\theta = 0, 2\pi/3$. The bottom row shows spectral projections computed at intervals that contain only continuous spectra.

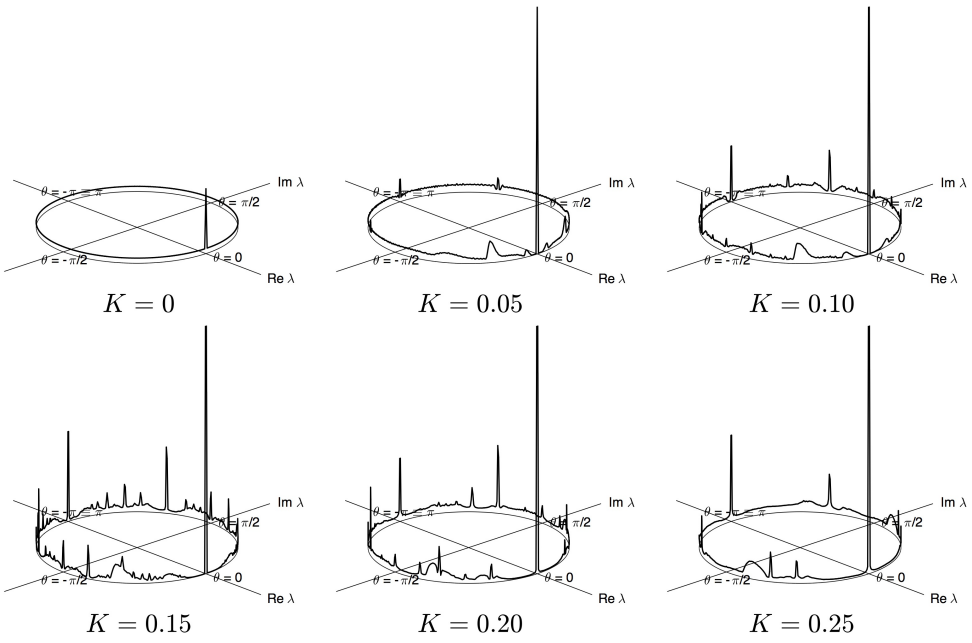

Figure 7.6: Evolution of the spectral density function of the Chirikov map (6.15) for the observable (7.12). Results for $\tilde{n} = 2000$ and $\alpha = 2\pi/500$.

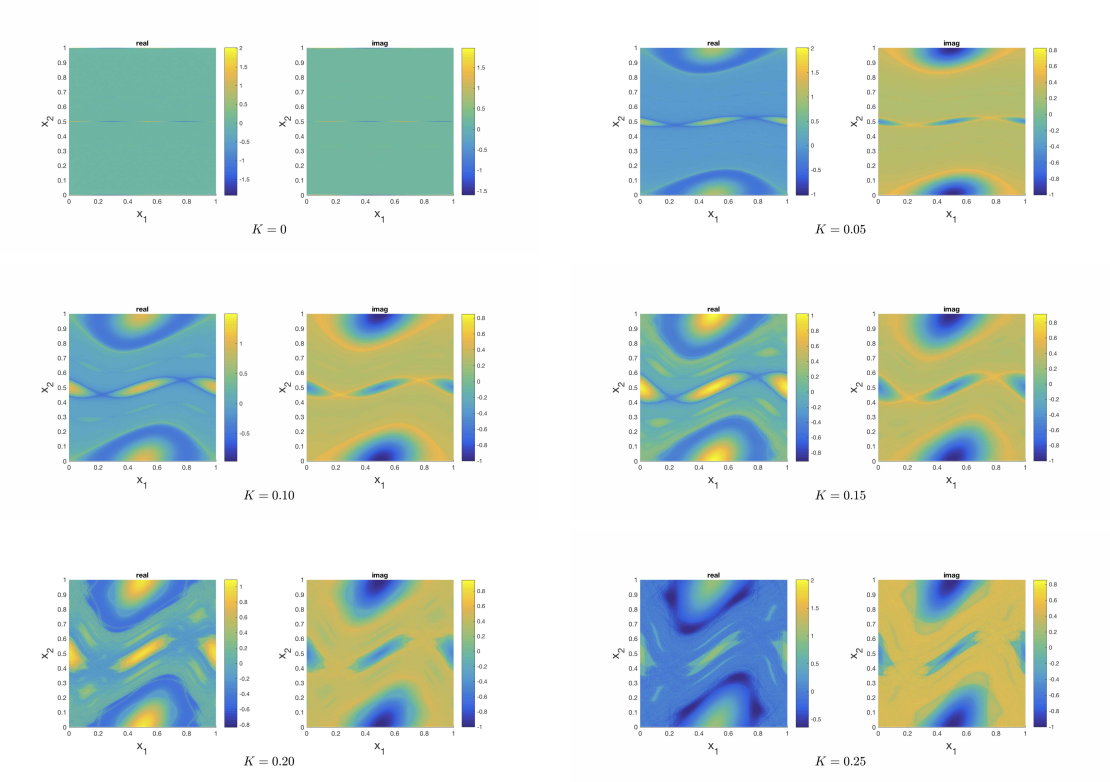

Figure 7.7: Spectral projections computed for the Chirikov map (6.15) at the interval $D = [-0.02, 0.02]$ with $\tilde{n} = 2000$. The depicted projection approximates the eigenfuncions at $\theta = 0$, which generates an invariant partition of the state-space.

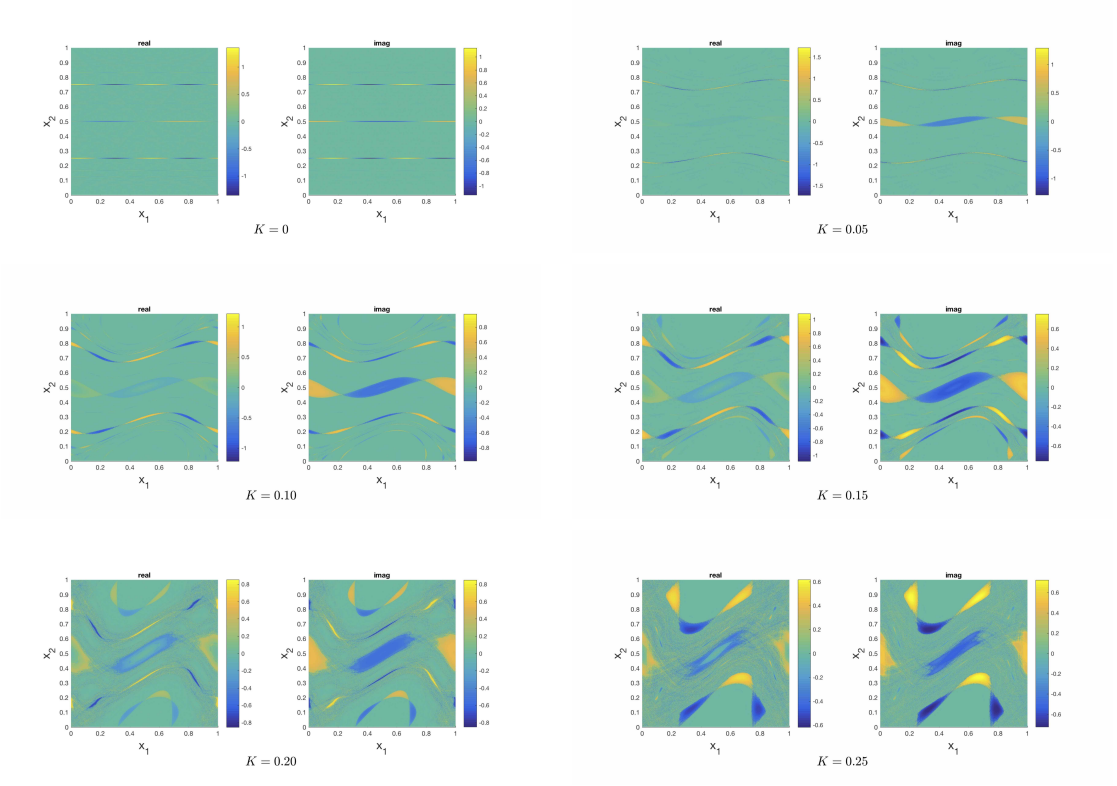

Figure 7.8: Spectral projections computed for the Chirikov map (6.15) at the interval $D = [\pi - 0.02, \pi + 0.02]$ with $\tilde{n} = 2000$. The depicted projection approximates the eigenfuncions at $\theta = \pi$, which generates an period-2 partition of the state-space.

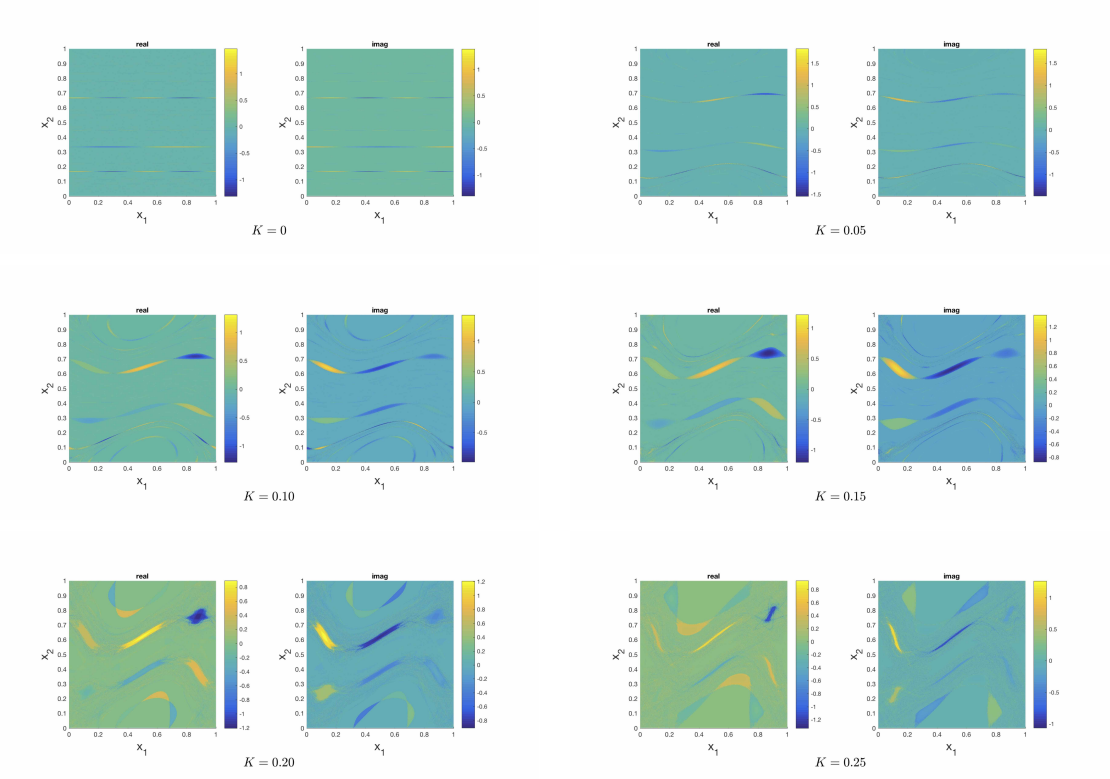

Figure 7.9: Spectral projections computed for the Chirikov map (6.15) at the interval $D = [2\pi/3 - 0.02, 2\pi/3 + 0.02]$ with $\tilde{n} = 2000$. The depicted projection approximates the eigenfuncions at $\theta = 2\pi/3$, which generates an period-3 partition of the state-space.

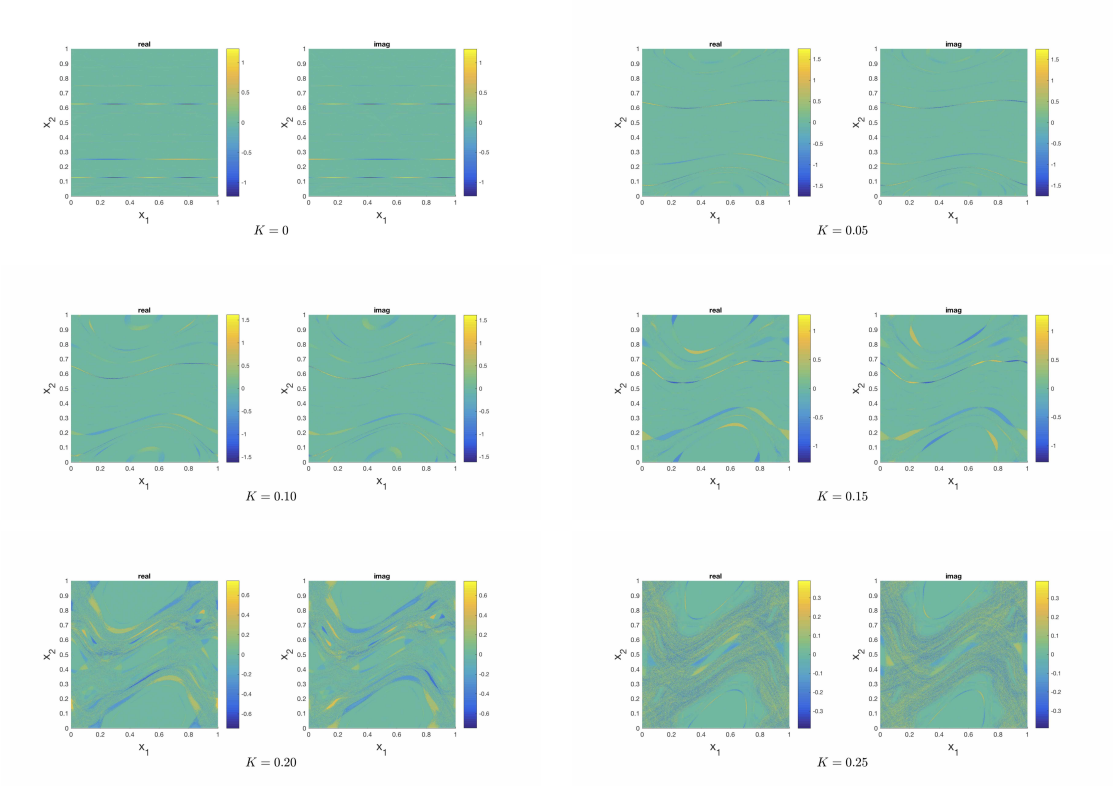

Figure 7.10: Spectral projections computed for the Chirikov map (6.15) at the interval $D = [\pi/2 - 0.02, \pi/2 + 0.02]$ with $\tilde{n} = 2000$. The depicted projection approximates the eigenfuncions at $\theta = 2\pi/3$, which generates an period-3 partition of the state-space.

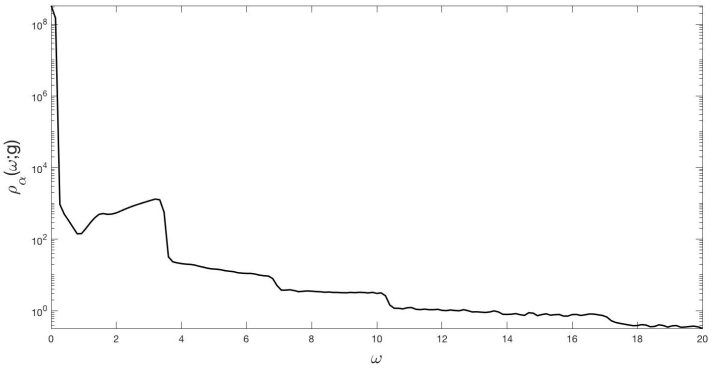

S

Figure 7.11: The spectral density function ($\alpha = 0.1$) for the observable (7.14).

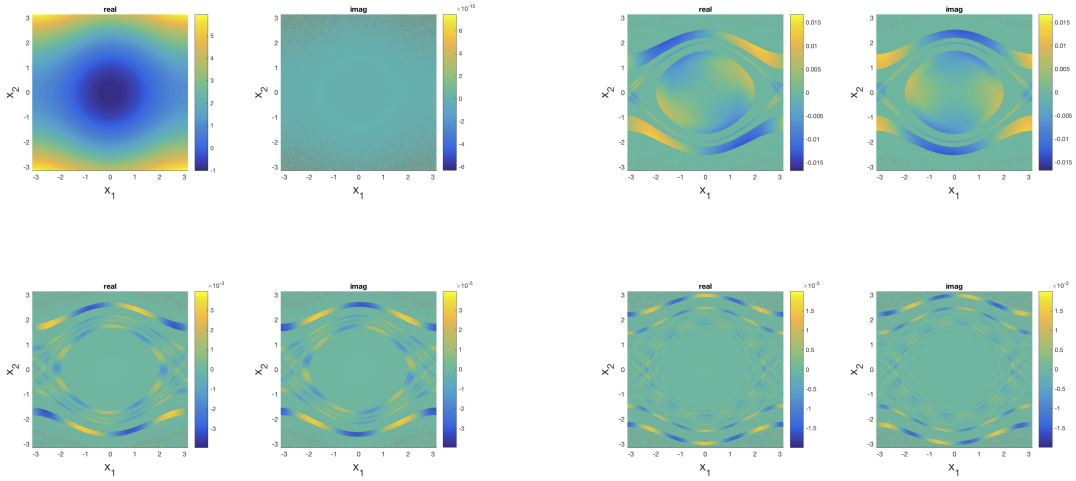

Figure 7.12: Spectral projections for the observable (7.14) on the invervals $D = [-0.3, 0.3)$ (top-left), $D = [1.5, 2.0)$ (top-right), $D = [4.0, 4.5)$ (bottom-left), and $D = [7.5, 8.0)$ (bottom-right).

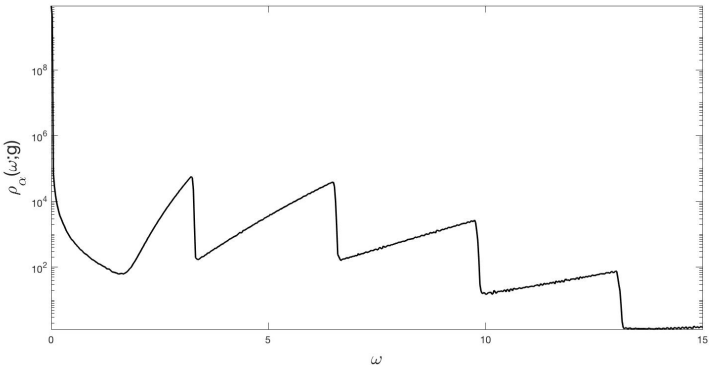

Figure 7.13: The spectral density function ($\alpha = 0.1$) for the observable (7.16).

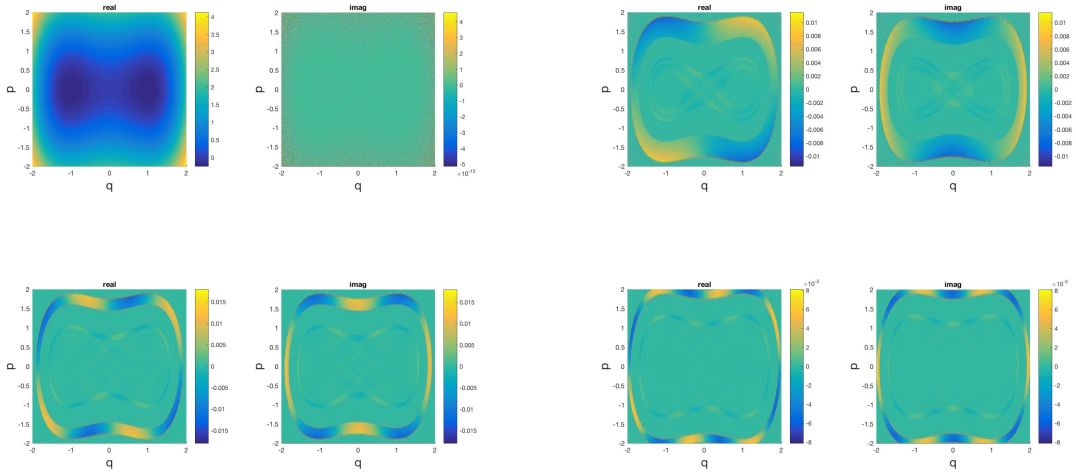

Figure 7.14: Spectral projections for the observable (7.16) on the invervals $D = [-0.3, 0.3)$ (top-left), $D = [2, 2.5)$ (top-right), $D = [4.5, 5)$ (bottom-left), and $D = [7.5, 8.0)$ (bottom-right).

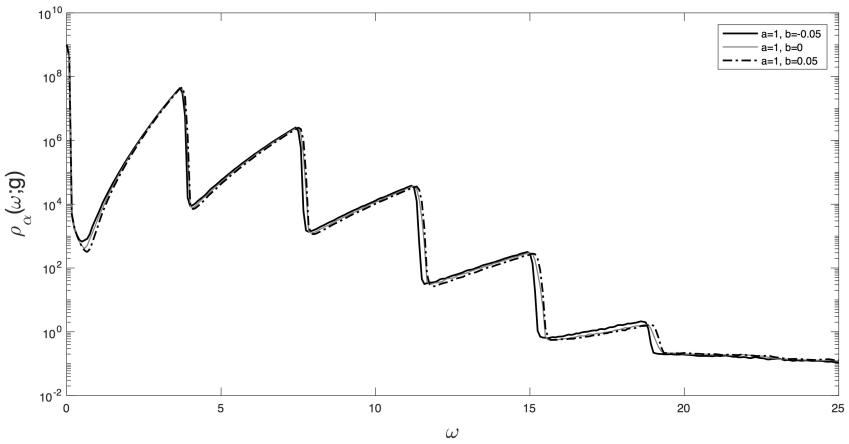

Figure 7.15: The spectral density function ($\alpha = 0.1$) for the observable (7.17).

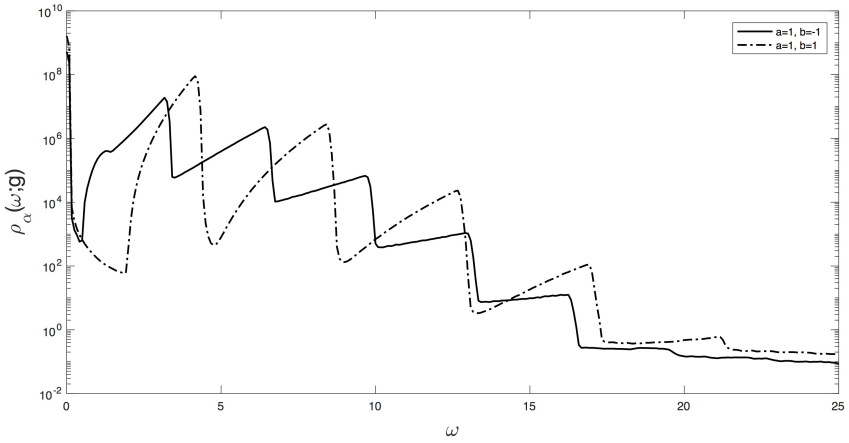

Figure 7.16: The spectral density function ($\alpha = 0.1$) for the observable (7.17).

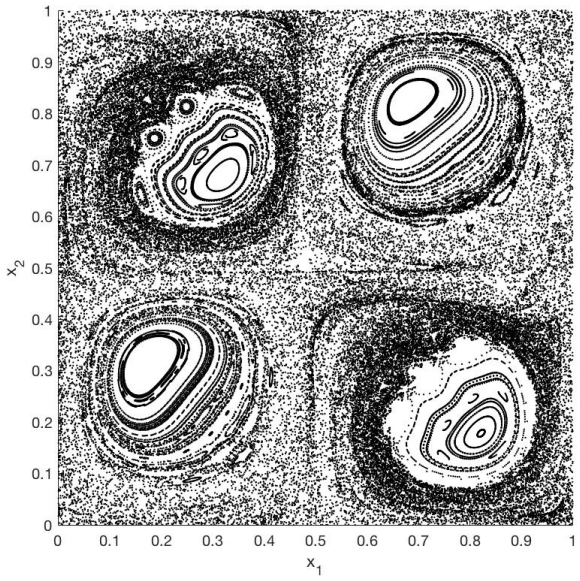

Figure 7.17: Cross-section of trajectories at $x_3 = 0$ for the quadruple gyre with $A = 1/(2\pi)$ and $\epsilon = 0.05$. Clearly noticable in the plot are the KAM tori islands aong with the chaotic region.

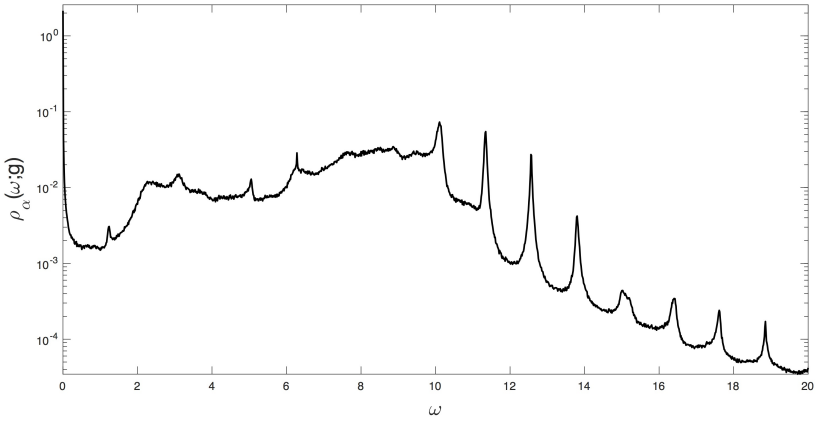

Figure 7.18: The spectral density function ($\alpha = 0.01$) for the observable (7.19).

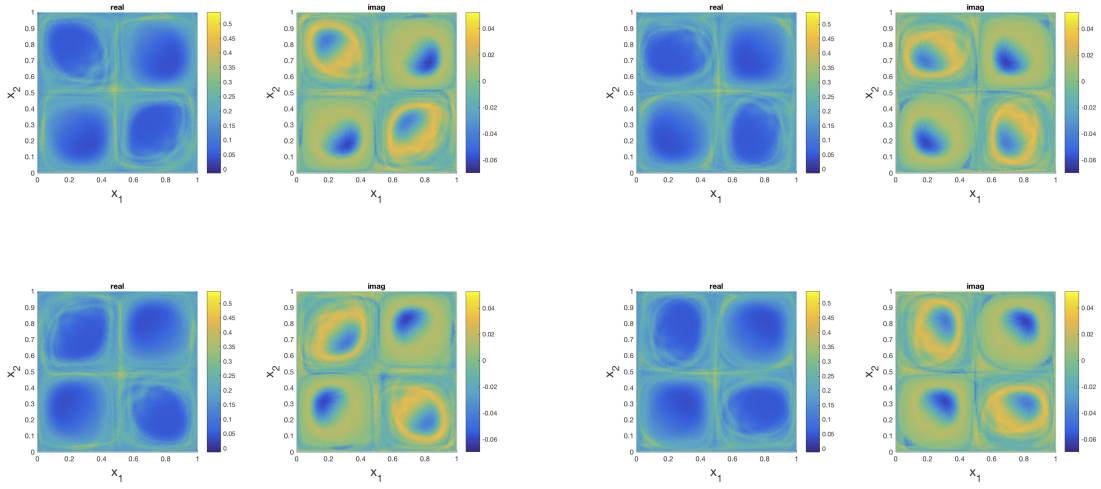

Figure 7.19: Spectral projection of the observable (7.19) onto the interval $D = [-0.4, 0.4)$. Top-left: $x_3 = 0$, top-right $x_3 = 0.25$, bottom-left: $x_3 = 0.5$, bottom-right: $x_3 = 0.75$.

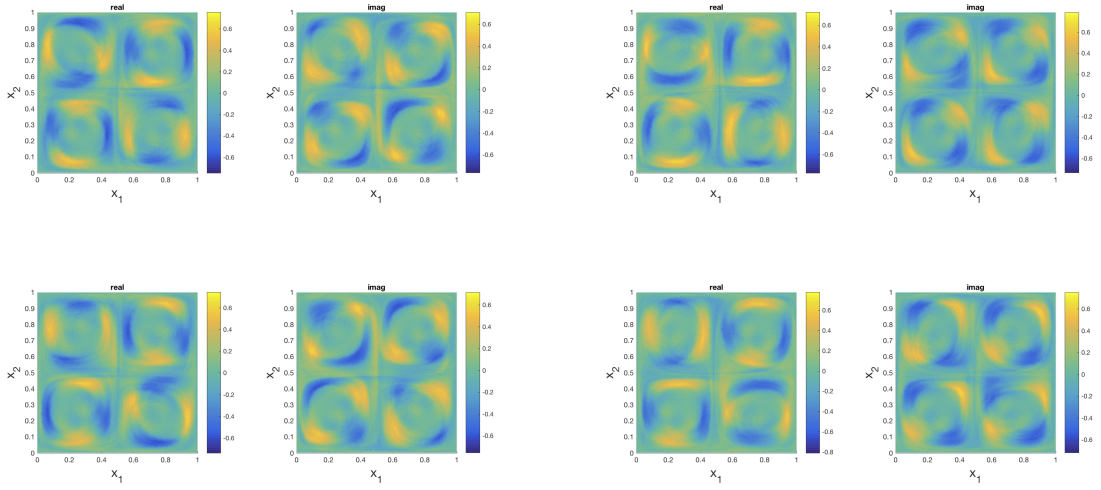

Figure 7.20: Spectral projection of the observable (7.19) onto the interval $D = [6.5, 10.0)$. Top-left: $x_3 = 0$, top-right $x_3 = 0.25$, bottom-left: $x_3 = 0.5$, bottom-right: $x_3 = 0.75$.

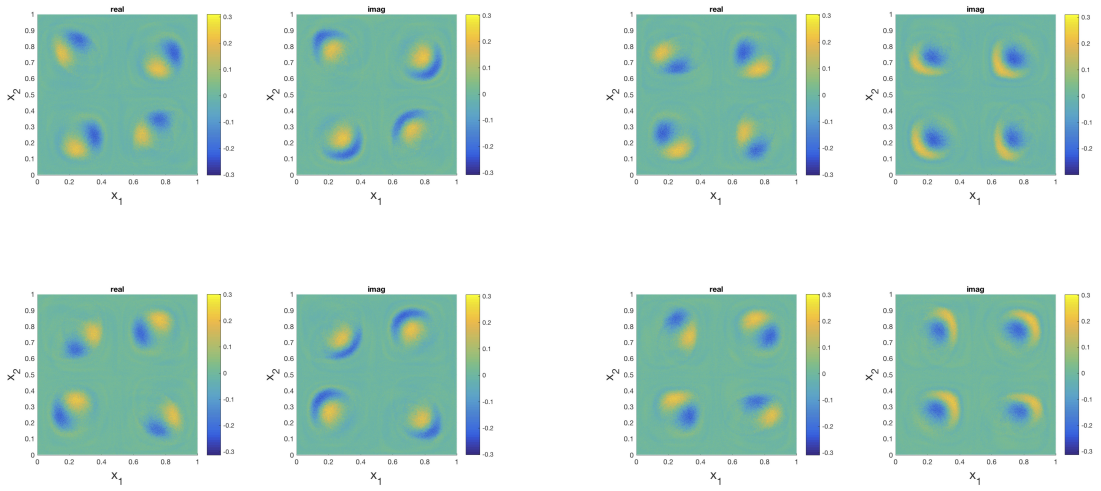

Figure 7.21: Spectral projection of the observable (7.19) onto the interval $D = [11.1, 11.4)$. Top-left: $x_3 = 0$, top-right $x_3 = 0.25$, bottom-left: $x_3 = 0.5$, bottom-right: $x_3 = 0.75$.

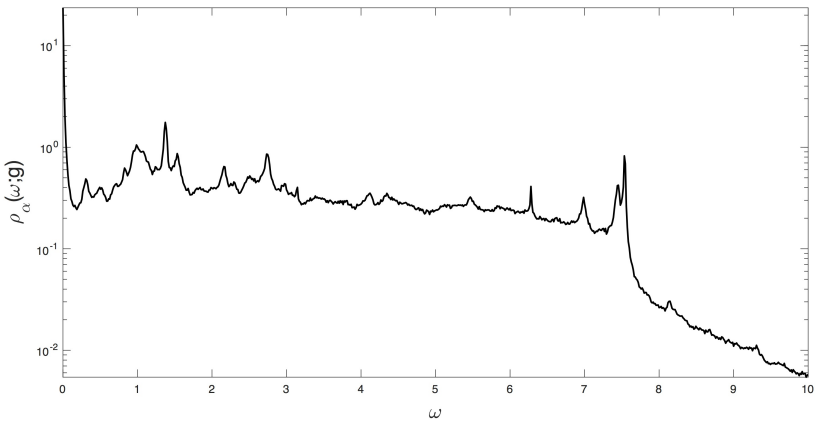

Figure 7.22: The spectral density function ($\alpha = 0.01$) for the observable (7.22).

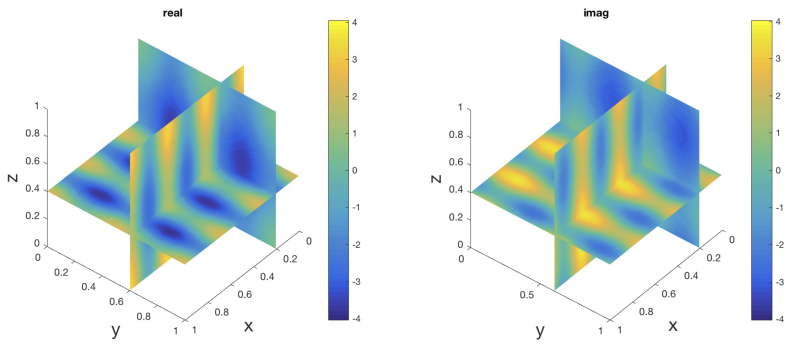

Figure 7.23: Spectral projection of the observable (7.22) onto the interval $D = [-0.3, 0.3)$.

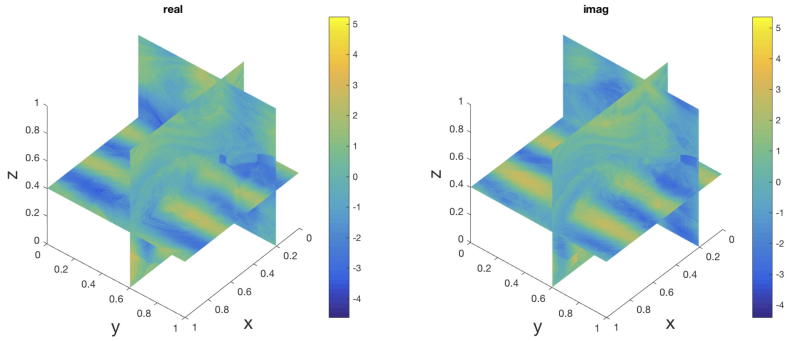

Figure 7.24: Spectral projection of the observable (7.22) onto the interval $D = [7.36, 7.56)$.

Chapter 8

Conclusions

The spectral properties of the Koopman operator are closely related to the geometric properties of a dynamical system in the state-space. In this dissertation, these relationships were specifically explored for a nonsmooth dynamical system characterized by discontinuous orbits. By considering an example of a kicked pendulum, it was illustrated that many of the geometric concepts associated with Koopman eigenfunctions (e.g. isostables, isochrons, invariant partitions, conjugacies, etc.) apply to nonsmooth systems as well. While the fixed space of the operator gave a description of the ergodic partition, the eigenfunctions associated with eigenvalues in the left-half complex plane established a (semi-)conjugacy to a linear system.

Given the central role of the spectral decomposition in Koopman-based analysis of dynamical systems, the focus of this dissertation was to advance the development of numerical methods to compute them. The emphasis was placed on computing spectral decompositions directly from a discretization of the dynamics. Herein, it was recognized that any computer simulation of a dynamical system would always involve some type of a reduction to a finite-state model. Given this observation, it was explored how these models can be used to approximate spectral quantities.

As a result, a new procedure was introduced to discretize the unitary Koopman operator of an invertible, measure-preserving transformation on a compact metric space. The method relied on the construction of a periodic approximation of the dynamics, wherein the measure-preserving system was approximated by a one-to-one map on a partitioning of the state-space. The action of the Koopman operator was thereby reduced to a permutation, yielding a discretization of the operator that preserved its unitary structure.

The unitary discretizations were shown to approximate the spectral decomposition of the Koopman operator in a weak sense. These weak convergence results showed that the individual eigenvalues and spectral projectors of a finite dimensional approximation may have very little to do with the original infinite-dimensional operator. However, when smooth weighted sums of these projectors were applied on some fixed observable, control on the approximation error was achieved in the average sense under the L^2-norm. This convergence results did not require any specific assumptions on the spectral type of the operator and treated systems with continuous or discrete spectra all under same the lens, i.e. measure-preserving transformations with continuous spectra can be approximated arbitrarily well by periodic systems with a fully discrete spectrum.

The concept of periodic approximations was generalized to measure-preserving flows. In order for weak convergence of the spectra to still occur, it was shown that a condition must be satisfied requiring the spatial refinements to happen at a faster rate than the temporal refinements in the discretization process. It was observed that this condition is somewhat opposite to the CLF condition required for finite difference schemes. This was however expected, given that the periodic approximation more closely resembles a semi-Lagrangian scheme.

The entire discretization procedure was constructive and allowed for the development of numerical methods to compute spectra. It was shown that a periodic approximation

can generally be obtained from solving a bipartite matching problem, although in special cases, a direct analytic construction was also possible. The general algorithm did not require the evaluation of set propagations (i.e. as in the Ulam approximation) and was shown to have roughly $O(n^{3m/2})$ complexity, where m is the dimension of the state-space and n the size of the partition in each dimension. Once a periodic approximation was obtained, the computation of the spectral projections and density functions become straightforward. The permutation structure of the discretization gave way for a fast evaluation (i.e. with $O(mn^m \log n)$ complexity) of these spectral quantities using the FFT algorithm.

In reflection, the proposed numerical method turns out to be very closely related to taking harmonic averages of observable traces. Instead of approximating the harmonic averages of a generic (hence typically aperiodic) system, the averages were computed of a "near-by" periodic system. For periodic systems, these averages are effectively reducible to the Discrete Fourier Transform. In the end, only smooth weighted sums of these averages turn out to have any "spectral meaning". It is generally hard to assess how a finite-state model approximation of a dynamical system, in combination with an infinite series truncation, may affect the computation of time averages. This dissertation has shown that, in the special case of measure-preserving systems, these concerns are fully addressed if one uses a periodic approximation.

There are still several open questions which remain. The most important question is how the current method can be generalized to include dissipative dynamical systems. One approach would be to extend the notion of periodic approximation with an "eventually periodic" approximation: whereas the attractor is discretized by a union of cycles, the basin is approximated by a union of trees. It is not immediately clear how to obtain such an approximation correctly in practice, neither is it clear how the Jordan blocks of the transient dynamics are spectrally related to the infinite-dimensional operator.

Bibliography

[1] M. Budišić, R. Mohr, and I. Mezić, *Applied Koopmanism*, *Chaos* **22** (2012), no. 4 [1206.3164].

[2] I. Mezić, *Analysis of Fluid Flows via Spectral Properties of the Koopman Operator*, *Annual Review of Fluid Mechanics* **45** (2012).

[3] C. W. Rowley, I. Mezić, S. Bagheri, P. Schlatter, and D. S. Henningson, *Spectral analysis of nonlinear flows*, *Journal of Fluid Mechanics* **641** (2009), no. Rowley 2005 115.

[4] Y. Susuki and I. Mezic, *Nonlinear Koopman Modes and Coherency Identification of Coupled Swing Dynamics*, *IEEE Transactions on Power Systems* **26** (2011), no. 4 1894–1904.

[5] M. Georgescu and I. Mezić, *Building energy modeling : A systematic approach to zoning and model reduction using Koopman Mode Analysis*, .

[6] R. Mohr and I. Mezić, *Construction of eigenfunctions for scalar-type operators via Laplace averages with connections to the Koopman operator*, arXiv:1403.6559.

[7] Y. Lan and I. Mezić, *Linearization in the large of nonlinear systems and Koopman operator spectrum*, *Physica D: Nonlinear Phenomena* **242** (2013), no. 1 42–53.

[8] I. Mezić and S. Wiggins, *A method for visualization of invariant sets of dynamical systems based on the ergodic partition*, *Chaos: An Interdisciplinary Journal of Nonlinear Science* **9** (1999), no. 1 213–218.

[9] Z. Levnajić and I. Mezić, *Ergodic theory and visualization. i. mesochronic plots for visualization of ergodic partition and invariant sets*, *Chaos: An Interdisciplinary Journal of Nonlinear Science* **20** (2010), no. 3 033114.

[10] Z. Levnajić and I. Mezić, *Ergodic theory and visualization. ii. fourier mesochronic plots visualize (quasi) periodic sets*, *Chaos: An Interdisciplinary Journal of Nonlinear Science* **25** (2015), no. 5 053105.

[11] A. Mauroy and I. Mezić, *On the use of fourier averages to compute the global isochrons of (quasi) periodic dynamics*, *Chaos: An Interdisciplinary Journal of Nonlinear Science* **22** (2012), no. 3 033112.

[12] P. J. Schmid, *Dynamic mode decomposition of numerical and experimental data*, *Journal of fluid mechanics* **656** (2010) 5–28.

[13] H. Arbabi and I. Mezić, *Ergodic theory, dynamic mode decomposition and computation of spectral properties of the koopman operator*, *arXiv preprint arXiv:1611.06664* (2016).

[14] M. O. Williams, I. G. Kevrekidis, and C. W. Rowley, *A data–driven approximation of the koopman operator: Extending dynamic mode decomposition*, *Journal of Nonlinear Science* **25** (2015), no. 6 1307–1346.

[15] M. Korda and I. Mezić, *On convergence of extended dynamic mode decomposition to the koopman operator*, *arXiv preprint arXiv:1703.04680* (2017).

[16] M. Dellnitz and O. Junge, *On the approximation of complicated dynamical behavior*, *SIAM Journal on Numerical Analysis* **36** (1999), no. 2 491–515.

[17] G. Froyland, *On ulam approximation of the isolated spectrum and eigenfunctions of hyperbolic maps*, *Discrete and Continuous Dynamical Systems-Series A (DCDS-A)* **17** (2007), no. 3 671.

[18] M. Korda, M. Putinar, and I. Mezić, *Data-driven spectral analysis of the koopman operator*, *arXiv preprint arXiv:1710.06532* (2017).

[19] D. Gottlieb and S. A. Orszag, *Numerical analysis of spectral methods: theory and applications*, vol. 26. Siam, 1977.

[20] I. Mezić, *Koopman operator spectrum and data analysis*, *arXiv preprint arXiv:1702.07597* (2017).

[21] P. Halmos, *Approximation theories for measure preserving transformations*, *Transactions of the American Mathematical Society* (1944) 1–18.

[22] P. Halmos, *In General a Measure Preserving Transformation is Mixing*, *Annals of Mathematics* **45** (1944), no. 4 786–792.

[23] P. D. Lax, *Approximation of measure preserving transformations*, *Communications on Pure and Applied Mathematics* **24** (1971), no. 2 133–135.

[24] J. C. Oxtboby and S. M. Ulam, *Measure-Preserving Homeomorphisms and Metrical Transitivity*, *Annals of Mathematics* **42** (1941), no. 4 874–920.

[25] A. B. Katok and A. M. Stepin, *Approximations in ergodic theory*, *UspekhiMat. Nauk* **22** (1967), no. 5 81–106.

[26] V. A. Rokhlin, *Selected topics from the metric theory of dynamical systems*, *Uspekhi Mat. Naul* **4** (1949), no. 2 57–128.

[27] T. Schwartzbauer, *Entropy and Approximation of Measure Preserving Tranformations*, *Pacific J. Math* **43** (1972), no. 3 753–764.

[28] I. Mezić and A. Banaszuk, *Comparison of systems with complex behavior*, *Physica D-Nonlinear Phenomena* **197** (2004), no. 1-2 101–133.

[29] I. Mezić, *Spectral properties of dynamical systems, model reduction and decompositions*, *Nonlinear Dynamics* **41** (2005), no. 1-3 309–325.

[30] I. Mezić and S. Wiggins, *A method for visualization of invariant sets of dynamical systems based on the ergodic partition.*, *Chaos* **9** (1999), no. 1 213–218.

[31] I. Mezić, *On the geometrical and statistical properties of dynamical systems: theory and applications*. PhD thesis, California Institute of Technology.

[32] A. Mauroy, I. Mezić, and J. Moehlis, *Isostables, isochrons, and Koopman spectrum for the action-angle representation of stable fixed point dynamics*, *Physica D: Nonlinear Phenomena* **261** (2013) 19–30, [1302.0032].

[33] A. Mauroy and I. Mezić, *Extreme phase sensitivity in systems with fractal isochrons*, *Physica D: Nonlinear Phenomena* **308** (2015) 40–51.

[34] N. I. Akhiezer and I. M. Glazman, *Theory of Linear Operators in Hilbert Space - vol II*. Frederick Ungar Publishing Co., New York, 1963.

[35] P. Cameron, *Combinatorics: Topics, Techniques, Algorithms*. Cambridge University Press, 1994.

[36] W. Rudin, *Real and Complex Analysis*. McGraw-Hil Book Co., New York, third ed., 1987.

[37] Y. Katznelson, *An introduction to harmonic analysis*. Cambridge University Press, 2004.

[38] R. I. McLachlan, *Area preservation in computational fluid dynamics*, *Physics Letters A* **264** (1999), no. 1 36–44.

[39] P. E. Kloeden and J. Mustard, *Constructing permutations that approximate lebesgue measure preserving dynamical systems under spatial discretization*, *International Journal of Bifurcation and Chaos* **7** (1997), no. 02 401–406.

[40] R. K. Ahuja, T. L. Magnanti, and J. B. Orlin, *Network flows: theory, algorithms and applications*. 1993.

[41] T. H. Cormen, C. E. Leiserson, R. L. Rivest, and C. Stein, *Introduction to algorithms*. MIT press, 3rd editio ed., 2009.

[42] P. Diamond, P. Kloeden, and A. Pokrovskii, *Numerical modeling of toroidal dynamical systems with invariant lebesgue measure*, *Complex Systems* **7** (1993), no. 6 415–422.

[43] D. Earn and S. Tremaine, *Exact numerical studies of hamiltonian maps: iterating without roundoff error*, *Physica D: Nonlinear Phenomena* **56** (1992), no. 1 1–22.

[44] B. V. Chirikov, *A universal instability of many-dimensional oscillator systems*, *Physics Reports* **52** (1979), no. 5 263–379.

[45] M. Feingold, L. P. Kadanoff, and O. Piro, *Passive Scalars, 3D Volume Preserving Maps and Chaos*, *J. Stat. Phys.* **50** (1988), no. 1900 529.

[46] V. Arnold and A. Avez, *Ergodic Problems of Classical Mechanics*, .

[47] H. Anzai, *Ergodic skew product transformations on the torus*, *Osaka mathematical journal* **3** (1951), no. 1.

[48] C. Scovel, *On symplectic lattice maps*, *Physics Letters A* **159** (1991), no. 8-9 396–400.

[49] I. Mezić, *Spectral Operator Methods in Dynamical Systems : Theory and Applications*, DRAFT manuscript UCSB, 2016.

[50] S. C. Shadden, F. Lekien, and J. E. Marsden, *Definition and properties of lagrangian coherent structures from finite-time lyapunov exponents in two-dimensional aperiodic flows*, *Physica D: Nonlinear Phenomena* **212** (2005), no. 3 271–304.